VS-FMDF AND EPVS-FMDF FOR LARGE EDDY SIMULATION OF TURBULENT FLOWS

by

Mehdi B. Nik

Submitted to the Graduate Faculty of

the Swanson School of Engineering in partial fulfillment

of the requirements for the degree of

Doctor of Philosophy

University of Pittsburgh

2012

UNIVERSITY OF PITTSBURGH

SWANSON SCHOOL OF ENGINEERING

This dissertation was presented

by

Mehdi B. Nik

It was defended on

July 20, 2012

and approved by

Peyman Givi, Ph.D., James T. MacLeod Professor of Mechanical Engineering and

Materials Science

Sung Kwon Cho, Ph.D., Associate Professor of Mechanical Engineering and Materials

Science

Laura A. Schaefer, Ph.D., Associate Professor of Mechanical Engineering and Materials

Science

Shi-Chune Yao, Ph.D., Professor of Mechanical Engineering, Carnegie Mellon University

Dissertation Director: Peyman Givi, Ph.D., James T. MacLeod Professor of Mechanical

Engineering and Materials Science

VS-FMDF AND EPVS-FMDF FOR LARGE EDDY SIMULATION OF TURBULENT FLOWS

Mehdi B. Nik, PhD

University of Pittsburgh, 2012

The first part of this dissertation is concerned with implementation of the joint "velocity-scalar filtered mass density function" (VS-FMDF) methodology for large eddy simulation (LES) of Sandia Flame D. This is a turbulent piloted non-premixed methane jet flame. In VS-FMDF, the effects of the subgrid scale chemical reaction and convection appear in closed forms. The modeled transport equation for the VS-FMDF is solved by a hybrid finite-difference/Monte Carlo scheme. For this flame (which exhibits little local extinction), a flamelet model is employed to relate the instantaneous composition to the mixture fraction. The LES predictions are compared with experimental data. It is shown that the methodology captures important features of the flame as observed experimentally.

In the second part of this dissertation, the joint "energy-pressure-velocity-scalar filtered mass density function" (EPVS-FMDF) is developed as a new subgrid scale (SGS) model for LES of high-speed turbulent flows. In this model, the effects of compressibility are taken into account by including two additional thermodynamic variables: the pressure and the internal energy. The EPVS-FMDF is obtained by solving its modeled transport equation, in which the effect of convection appears in a closed form. The modeled EPVS-FMDF is employed for LES of a temporally developing mixing layer.

Keywords: Large eddy simulation, filtered density function, turbulent reacting flows.

TABLE OF CONTENTS

LIST OF TABLES

LIST OF FIGURES

ACKNOWLEDGMENTS

I would like to express my sincere gratitude to my advisor, Professor Peyman Givi for his support and guidance through the course of my graduate studies. I am grateful to the members of my doctoral committee, Professors Sung Kwon Cho, Laura Schaefer and Schi-Chune Yao (Carnegie Mellon University). My appreciation also goes to Professor Reza H. Sheikhi (Northeastern University) for his friendship and his collaboration on many technical aspects of my research. I owe special thanks to Professor Stephen B. Pope (Cornell University) whose insights and collaborations contributed greatly to the success of this work. I would like to acknowledge Professor Cyrus K. Madnia (University at Buffalo) for his collaboration on several technical issues of this dissertation.

I am indebted to my colleagues and friends at the Laboratory for Computational Transport Phenomena at the University of Pittsburgh, Dr. Naseem Ansari, Mr. Mahdi Mohebbi, Mr. Collin Otis, Mr. Patrick Pisciuneri, Mr. Sasan Salkhordeh and Dr. Server Levent Yilmaz (Center for Simulation and Modeling). I am also thankful to Dr. Tomasz Drozda (NASA Langley) for his friendship and collaboration during my earlier years in graduate school. I would like to thank Dr. Bertrand Delarue (BNP Paribas) for his great help on the technical aspects of this dissertation. I also would like to thank Mr. Vaghefi (University at Buffalo) whose collaboration was quite helpful in this work.

My deepest gratitude goes to my parents for devoting their lives to me and to my sisters. Their support, encouragement and hard work had a significant influence in my life. I dedicate this thesis to my parents.

MEHDI B. NIK

UNIVERSITY OF PITTSBURGH, 2012

1.0 INTRODUCTION

The filtered density function (FDF)[1–3] is now regarded as one of the most effective means of conducting large eddy simulation (LES) in turbulent combustion. In its initial form, the marginal "scalar" FDF (S-FDF);[4] and its mass weighted scalar filtered mass density function (S-FMDF)[5] provided the first demonstration of a "transported" FDF in reacting flows. The primary advantage of S-FDF (S-FMDF) over conventional (non-FDF) methods is that it accounts for the effects of subgrid scale (SGS) chemical reactions in a closed form. This closure is the primary reason for S-FMDF's popularity and its widespread applications within the past decade.[6–25] See Ref.[26] for a recent review.

Inclusion of the "velocity" in the FDF accounts for the effects of "convection" in a closed form as well. This is demonstrated in the velocity-FDF (V-FDF),[27] the joint velocity-scalar FDF (VS-FDF),[11] and its density weighted VS-FMDF[28] formulations. In its most rudimentary form, the VS-FDF is equivalent to, at the least, a "second-order" SGS model. It is to noted that the majority of conventional hydrodynamic SGS closures are "zero-order."[29–32] This higher accuracy yields a better predictive capability of the FDF in capturing more intricate physics of SGS transport.[33]

The first objective of this work is to assess the capability of the VS-FMDF for prediction of hydrocarbon flames. For that, we consider the piloted non-premixed methane jet flame, as studied in the experiments of the Combustion Research Facility (CRF) at the Sandia National Laboratories,[34,35] and at TU-Darmstadt.[36] Sheikhi *et al.*[37] report the first results of S-FMDF predictions for this flame. Their encouraging results motivated significant subsequent S-FMDF simulations by many others.[12,13,18–23] The contributions are ongoing; the CRF web site maintains an updated bibliography of the growing literature in this field. In the experiments, three flames are considered: flames D, E and F. The geometrical configuration in these flames

is the same, but the jet inlet velocity is varied. In Flame D, the fuel jet velocity is the lowest. The jet velocity increases from flames D to E to F, with noticeable non-equilibrium effects in the latter two. Flame D is considered in this thesis. The objective is to assess the predictive capability of the VS-FMDF in capturing the flow field and the scalar mixing. This is the first application of the VS-FMDF for prediction of a hydrocarbon flame.

The second objective of this work is to extend the VS-FMDF for LES of high speed flows. This is accomplished by considering the joint "energy-pressure-velocity-scalar filtered mass density function" (EPVS-FMDF). This is an extension to VS-FMDF methodology and provides the most comprehensive form of the FDF formulation to date. With the definition of the EPVS-FMDF, the mathematical framework for its implementation in LES is established. A transport equation is developed for the EPVS-FMDF in which the effect of SGS convection appears in a closed form. The unclosed terms in this equation are modeled in a fashion similar to that in the Reynolds-averaged procedures. A Lagrangian Monte Carlo procedure is developed and implemented for numerical solution of the modeled EPVS-FMDF transport equation. Simulations are conducted of a non-reacting temporally developing mixing layer.

1.1   SCOPE

This dissertation is organized as follows. In Chapter 2, the joint velocity-scalar filtered mass density function (VS-FMDF) for LES of Sandia Flame-D is considered. The work described in this chapter has been presented at *APS-DFD*;[38] and is published in *AIAA Journal*,[39] and *Flow, Turbulence and Combustion*.[40] In Chapter 3, the joint energy-pressure-velocity-scalar filtered mass density function (EPVS-FMDF) methodology is developed. Parts of this chapter has been presented at *APS-DFD*,[41,42] and *AIAA-ASM*.[43,44] In Chapter 4, some final remarks are made, with some suggestions for future research. Parts of this dissertation was presented at an invited lecture at *AIAA-JPC*.[45]

2.0 JOINT VELOCITY SCALAR FILTERED MASS DENSITY FUNCTION FOR VARIABLE DENSITY FLOWS

In the work presented in this chapter, the previously developed VS-FMDF methodology is employed for LES of Sandia flame D. Following its mathematical definition, the exact VS-FMDF transport equation is presented. The unclosed terms in this equation are modeled using an equivalent system of stochastic differential equations. For this, a hybrid Eulerian/Largrangian numerical solution procedure is used. In the Eulerian part, the filtered transport equations are solved by a finite-difference method. In the Lagrangian part, the solution of the modeled VS-FMDF transport equation is obtained by a Monte Carlo method. The unclosed statistics in the Eulerian part are obtained from the Monte Carlo solver. The comparative capabilities of the VS-FMDF is assessed by comparing the predicted results with the experimental data. Also, with the utilization of progressively larger number of grid points, the effects of resolution on various statistics of the flow variables, as predicted by VS-FMDF are investigated.

2.1 FORMULATION

2.1.1 Basic equations

In a turbulent flow undergoing chemical reaction involving N_s species, the primary transport variables are the density $\rho(\mathbf{x}, t)$, the velocity vector $u_i(\mathbf{x}, t)$ ($i = 1, 2, 3$), the pressure $p(\mathbf{x}, t)$, the enthalpy $h(\mathbf{x}, t)$ and the species' mass fractions $Y_\alpha(\mathbf{x}, t)$ ($\alpha = 1, 2, \ldots, N_s$). The equations which govern the transport of these variables in space (x_i) ($i = 1, 2, 3$) and time (t) are the

continuity, momentum, enthalpy (energy) and species' mass fraction equations, along with an equation of state

$$\frac{\partial \rho}{\partial t} + \frac{\partial \rho u_j}{\partial x_j} = 0, \tag{2.1a}$$

$$\frac{\partial \rho u_i}{\partial t} + \frac{\partial \rho u_j u_i}{\partial x_j} = -\frac{\partial p}{\partial x_i} + \frac{\partial \tau_{ji}}{\partial x_j}, \tag{2.1b}$$

$$\frac{\partial \rho \phi_\alpha}{\partial t} + \frac{\partial \rho u_j \phi_\alpha}{\partial x_j} = -\frac{\partial J_j^\alpha}{\partial x_j} + \rho S_\alpha, \quad \alpha = 1, 2, \ldots, \sigma = N_s + 1, \tag{2.1c}$$

$$p = \rho R^0 T \sum_{\alpha=1}^{N_s} Y_\alpha / M_\alpha = \rho R T, \tag{2.1d}$$

where R^0 and R are the universal and mixture gas constants and M_α denotes the molecular weight of species α. The chemical reaction source terms $S_\alpha \equiv \hat{S}_\alpha (\phi(\mathbf{x}, t))$ are functions of compositional scalars ($\phi \equiv [\phi_1, \phi_2, \ldots, \phi_{N_s+1}]$). Equation (2.1c) represents the transport of species' mass fraction and enthalpy in a common form with

$$\phi_\alpha \equiv Y_\alpha, \quad \alpha = 1, 2, ..., N_s, \quad \phi_\sigma \equiv h = \sum_{\alpha=1}^{N_s} h_\alpha \phi_\alpha, \quad h_\alpha = h_\alpha^0 + \int_{T_0}^{T} c_{p\alpha}(T')dT'. \tag{2.2}$$

Here T and T_0 denote the temperature field and the reference temperature, respectively. In this equation, h_α^0 and $c_{p\alpha}$ denote the enthalpy of formation at T_0 and the specific heat at constant pressure for species α. For a Newtonian fluid, with Fick's law of diffusion, the viscous stress tensor τ_{ij} and the scalar flux J_j^α are represented by

$$\tau_{ij} = \mu \left(\frac{\partial u_i}{\partial x_j} + \frac{\partial u_j}{\partial x_i} - \frac{2}{3} \frac{\partial u_k}{\partial x_k} \delta_{ij} \right), \quad J_j^\alpha = -\rho \Gamma \frac{\partial \phi_\alpha}{\partial x_j} \tag{2.3}$$

where μ is the fluid dynamic viscosity and Γ denotes mass molecular diffusivity coefficients for all the scalars. We assume $\mu = \rho \Gamma$; *i.e.* unity Schmidt (Sc) and Prandtl (Pr) numbers. The viscosity and molecular diffusivity coefficients can, in general, be temperature dependent. In reactive flows, molecular processes are much more complicated than portrayed by Eq. (2.3). Since the molecular diffusion is typically less important than that of SGS, this simple model is adopted with justifications and caveats given in Refs.[46–48]

4

2.1.2 Filtered equations

Large eddy simulation involves the spatial filtering operation[29–32,49]

$$\langle Q(\mathbf{x},t)\rangle_\ell = \int_{-\infty}^{+\infty} Q(\mathbf{x}',t)G(\mathbf{x}',\mathbf{x})d\mathbf{x}', \tag{2.4}$$

where $G(\mathbf{x}',\mathbf{x})$ denotes a filter function, and $\langle Q(\mathbf{x},t)\rangle_\ell$ is the filtered value of the transport variable $Q(\mathbf{x},t)$. In variable-density flows it is convenient to use the Favre-filtered quantity $\langle Q(\mathbf{x},t)\rangle_L = \langle \rho Q\rangle_\ell / \langle \rho\rangle_\ell$. We consider a filter function that is spatially and temporally invariant and localized, thus: $G(\mathbf{x}',\mathbf{x}) \equiv G(\mathbf{x}' - \mathbf{x})$ with the properties $G(\mathbf{x}) \geq 0$, $\int_{-\infty}^{+\infty} G(\mathbf{x})d\mathbf{x} = 1$. Applying the filtering operation to Eqs. (2.1) and using the conventional LES approximation for the diffusion terms, we obtain

$$\frac{\partial\langle\rho\rangle_\ell}{\partial t} + \frac{\partial \langle\rho\rangle_\ell \langle u_j\rangle_L}{\partial x_j} = 0, \tag{2.5a}$$

$$\frac{\partial \langle\rho\rangle_\ell \langle u_i\rangle_L}{\partial t} + \frac{\partial \langle\rho\rangle_\ell \langle u_j\rangle_L \langle u_i\rangle_L}{\partial x_j} = -\frac{\partial \langle p\rangle_\ell}{\partial x_i} + \frac{\partial}{\partial x_j}\left(\mu\left(\frac{\partial \langle u_i\rangle_L}{\partial x_j} + \frac{\partial \langle u_j\rangle_L}{\partial x_i}\right)\right)$$
$$- \frac{2}{3}\frac{\partial}{\partial x_i}\left(\mu\frac{\partial \langle u_j\rangle_L}{\partial x_j}\right) - \frac{\partial \langle\rho\rangle_\ell \tau_L(u_i,u_j)}{\partial x_j}, \tag{2.5b}$$

$$\frac{\partial \langle\rho\rangle_\ell \langle\phi_\alpha\rangle_L}{\partial t} + \frac{\partial \langle\rho\rangle_\ell \langle u_j\rangle_L \langle\phi_\alpha\rangle_L}{\partial x_j} = \frac{\partial}{\partial x_j}\left(\langle\rho\rangle_\ell \Gamma\frac{\partial \langle\phi_\alpha\rangle_L}{\partial x_j}\right) - \frac{\partial \langle\rho\rangle_\ell \tau_L(u_j,\phi_\alpha)}{\partial x_j} + [\langle\rho\rangle_\ell \langle S_\alpha\rangle_L], \tag{2.5c}$$

In equation (2.5), the second-order Favre SGS correlations are defined by

$$\tau_L(a,b) = \langle ab\rangle_L - \langle a\rangle_L \langle b\rangle_L. \tag{2.6}$$

2.2 EXACT VS-FMDF TRANSPORT EQUATION

The "velocity-scalar filtered mass density function" (VS-FMDF), denoted by P_L, is formally defined as[2]

$$P_L\left(\boldsymbol{v}, \boldsymbol{\psi}, \mathbf{x}; t\right) = \int_{-\infty}^{+\infty} \rho(\mathbf{x}', t)\zeta\left(\boldsymbol{v}, \boldsymbol{\psi}; \boldsymbol{u}(\mathbf{x}', t), \boldsymbol{\phi}(\mathbf{x}', t)\right) G(\mathbf{x}' - \mathbf{x})d\mathbf{x}', \qquad (2.7)$$

where

$$\zeta\left(\boldsymbol{v}, \boldsymbol{\psi}; \boldsymbol{u}(\mathbf{x}, t), \boldsymbol{\phi}(\mathbf{x}, t)\right) = \prod_{i=1}^{3} \delta\left(v_i - u_i(\mathbf{x}, t)\right) \times \prod_{\alpha=1}^{\sigma} \delta\left(\psi_\alpha - \phi_\alpha(\mathbf{x}, t)\right). \qquad (2.8)$$

In this equation, δ denotes the Dirac delta function, and $\boldsymbol{v}, \boldsymbol{\psi}$ are the velocity vector and the scalar array in the sample space. The term ζ is the "fine-grained" density.[47,50] Equation (2.7) defines the VS-FMDF as the spatially filtered value of the fine-grained density. With the condition of a positive filter kernel,[51] P_L has all of the properties of a mass density function (MDF).[47] Considering the time derivative of the fine-grained density function Eq. (2.8) and using Eqs. (2.1b)-(2.1c), and Eqs. (2.3), (2.7), results in

$$
\begin{aligned}
\frac{\partial P_L}{\partial t} + \frac{\partial v_j P_L}{\partial x_j} &= \frac{\partial}{\partial v_i}\left(\left\langle \frac{1}{\rho(\boldsymbol{\phi})}\frac{\partial p}{\partial x_i} \,\Big|\, \boldsymbol{v}, \boldsymbol{\psi} \right\rangle_\ell P_L\right) - \frac{\partial}{\partial v_i}\left(\left\langle \frac{1}{\rho(\boldsymbol{\phi})}\frac{\partial \tau_{ji}}{\partial x_j} \,\Big|\, \boldsymbol{v}, \boldsymbol{\psi} \right\rangle_\ell P_L\right) \\
&+ \frac{\partial}{\partial \psi_\alpha}\left(\left\langle \frac{1}{\rho(\boldsymbol{\phi})}\frac{\partial J_i^\alpha}{\partial x_i} \,\Big|\, \boldsymbol{v}, \boldsymbol{\psi} \right\rangle_\ell P_L\right) - \frac{\partial}{\partial \psi_\alpha}\left(S_\alpha(\boldsymbol{\psi})P_L\right).
\end{aligned}
$$

This is an exact transport equation and indicates that the effects of convection, the second term on left-hand side, and chemical reaction, the last term on the right-hand side (RHS), appear in closed forms. The unclosed terms denote convective effects in the velocity-scalar sample space. The unclosed terms are exhibited by the conditional filtered[28] values as shown by the first three terms on the RHS.

2.3 MODELED VS-FMDF TRANSPORT EQUATION

For closure of the VS-FMDF transport equation, we consider the general diffusion process,[52] given by the system of stochastic differential equations (SDEs). In this context developed in Refs.[4,11,27,53,54] we utilize the simplified Langevin model (SLM) and the linear mean square estimation (LMSE) model.[50]

$$
dX_i^+ = U_i^+ dt + \sqrt{\frac{2\mu}{\langle \rho \rangle_\ell}} dW_i, \tag{2.9a}
$$

$$
dU_i^+ = \left[-\frac{1}{\langle \rho \rangle_\ell} \frac{\partial \langle p \rangle_\ell}{\partial x_i} + \frac{2}{\langle \rho \rangle_\ell} \frac{\partial}{\partial x_j} \left(\mu \frac{\partial \langle u_i \rangle_L}{\partial x_j} \right) + \frac{1}{\langle \rho \rangle_\ell} \frac{\partial}{\partial x_j} \left(\mu \frac{\partial \langle u_j \rangle_L}{\partial x_i} \right) - \frac{2}{3} \frac{1}{\langle \rho \rangle_\ell} \frac{\partial}{\partial x_i} \left(\mu \frac{\partial \langle u_j \rangle_L}{\partial x_j} \right) \right] dt
$$
$$
+ \ G_{ij} \left(U_j^+ - \langle u_j \rangle_L \right) dt + \sqrt{C_0 \epsilon}\, dW_i' + \sqrt{\frac{2\mu}{\langle \rho \rangle_\ell}} \frac{\partial \langle u_i \rangle_L}{\partial x_j} dW_j, \tag{2.9b}
$$

$$
d\phi_\alpha^+ = -C_\phi \omega \left(\phi_\alpha^+ - \langle \phi_\alpha \rangle_L \right) dt + S_\alpha(\boldsymbol{\phi}^+) dt, \tag{2.9c}
$$

where

$$
G_{ij} = -\omega \left(\frac{1}{2} + \frac{3}{4} C_0 \right) \delta_{ij}, \qquad \omega = \frac{\epsilon}{k},
$$
$$
\epsilon = C_\epsilon \frac{k^{3/2}}{\Delta_L}, \qquad k = \frac{1}{2} \tau_L \left(u_i, u_i \right). \tag{2.10}
$$

Here $X_i^+, U_i^+, \phi_\alpha^+$ are probabilistic representations of position, velocity vector, and scalar variables, respectively. W terms denote the Wiener-Lévy processes.[55,56] In equation (2.10), ω is the SGS mixing frequency, ϵ is the dissipation rate, k is the SGS kinetic energy, and Δ_L is the LES filter size. The model parameters are the same as those suggested by Sheikhi *et al.*[28]: $C_0 = 2.1$, $C_\phi = 1.0$ and $C_\epsilon = 1.0$. The Fokker-Planck equation corresponding to Eq. (2.9) is:

$$\frac{\partial F_L}{\partial t} + \frac{\partial v_i F_L}{\partial x_i} = \frac{1}{\langle \rho \rangle_\ell} \frac{\partial \langle p \rangle_\ell}{\partial x_i} \frac{\partial F_L}{\partial v_i} - \frac{2}{\langle \rho \rangle_\ell} \frac{\partial}{\partial x_j} \left(\mu \frac{\partial \langle u_i \rangle_L}{\partial x_j} \right) \frac{\partial F_L}{\partial v_i} - \frac{1}{\langle \rho \rangle_\ell} \frac{\partial}{\partial x_j} \left(\mu \frac{\partial \langle u_j \rangle_L}{\partial x_i} \right) \frac{\partial F_L}{\partial v_i}$$

$$+ \frac{2}{3} \frac{1}{\langle \rho \rangle_\ell} \frac{\partial}{\partial x_i} \left(\mu \frac{\partial \langle u_j \rangle_L}{\partial x_j} \right) \frac{\partial F_L}{\partial v_i} - \frac{\partial \left(G_{ij} \left(v_j - \langle u_j \rangle_L \right) F_L \right)}{\partial v_i} + \frac{\partial}{\partial x_i} \left(\mu \frac{\partial (F_L / \langle \rho \rangle_\ell)}{\partial x_i} \right)$$

$$+ \frac{\partial}{\partial x_i} \left(\frac{2\mu}{\langle \rho \rangle_\ell} \frac{\partial \langle u_j \rangle_L}{\partial x_i} \frac{\partial F_L}{\partial v_j} \right) + \frac{\mu}{\langle \rho \rangle_\ell} \frac{\partial \langle u_k \rangle_L}{\partial x_j} \frac{\partial \langle u_i \rangle_L}{\partial x_j} \frac{\partial^2 F_L}{\partial v_k \partial v_i} + \frac{1}{2} C_0 \epsilon \frac{\partial^2 F_L}{\partial v_i \partial v_i}$$

$$+ C_\phi \omega \frac{\partial \left(\left(\psi_\alpha - \langle \phi_\alpha \rangle_L \right) F_L \right)}{\partial \psi_\alpha} - \frac{\partial \left(S_\alpha \left(\boldsymbol{\psi} \right) F_L \right)}{\partial \psi_\alpha}.$$

$$(2.11)$$

2.4   NUMERICAL PROCEDURE

Numerical solution of the modeled VS-FMDF transport equation is obtained by a hybrid finite-difference (FD)/Monte Carlo (MC) procedure. The computational domain is discretized on equally spaced finite-difference grid points and the FMDF is represented by an ensemble of statistically identical MC particles which carry information pertaining to the velocity and the scalar values. This information is updated via temporal integration of the SDEs. Statistical information is obtained by considering an ensemble of N_E computational particles residing within an ensemble domain of characteristic length Δ_E centered around each of the FD grid points. To reduce the computational cost, a procedure involving the use of non-uniform weights is also considered. This procedure allows a smaller number of particles in regions where a low degree of variability is expected. Conversely, in regions of high variability, a large number of particles is allowed. The sum of weights within the ensemble domain is related to filtered fluid density.[57]

The FD solver is fourth-order accurate in space and second-order accurate in time.[58] All of the FD operations are conducted on fixed grid points. The transfer of information from the FD points to the MC particles is accomplished via a linear interpolation. The inverse transfer

8

is accomplished via ensemble averaging. The FD transport equations include unclosed second order moments which are obtained from the MC. Further details on the hybrid FD-MC can be found in Ref.[57].

2.5   FLOW CONFIGURATION AND SIMULATION PARAMETERS

Sandia Flame D consists of a main jet with a mixture of 25% methane and 75% air by volume. The nozzle is placed in a coflow of air and the flame is stabilized by a substantial pilot. The Reynolds number for the main jet is $Re = 22400$ based on the nozzle diameter $D = 7.2mm$ and the bulk jet velocity $49.6m/sec$.

Simulations are conducted on a three-dimensional Cartesian mesh with uniform spacings in each of the three directions. The computational domain spans a region of $20D \times 16D \times 16D$ in streamwise (x), and the two lateral (y, z) directions, respectively. The number of grid points for different test cases in the x, y and z directions are presented in Table (1). The filter size is set equal to $\Delta_{\mathcal{G}} = 2(\Delta x \Delta y \Delta z)^{(1/3)}$ where Δx, Δy and Δz denote the grid spacings in the corresponding directions. The size of the ensemble domain for evaluations of the filtered values is equal to the half of the filter size.

For efficient parallel simulations, the domain is partitioned into equally sized partitions and each partition is assigned to a different processor at the onset of the simulations. This provides an effective parallelization and is relatively easy to implement. Each CPU is assigned relatively equal number of grid points and (approximately) equal number of particles. Simulations are conducted in conjunction with MPI and the PETSC[59–61] library.

The flow variables at the inflow are set the same as those in the experiments, including the inlet profiles of the velocity and the mixture fraction. The inlet condition for the velocity is presented in Fig. (1). The flow is excited by superimposing oscillating axisymmetric perturbations at the inflow. The procedure is similar to that in Ref.[62], but the amplitude of forcing is set in such a way to match the experimentally measured turbulent intensity of the streamwise velocity at the inlet. Standard characteristic boundary conditions[63] are implemented in all of the FD simulations.

The MC particles are supplied in the inlet region and are free to move within the domain due to combined actions of convection and diffusion. There are at least 40 MC particles at each cell. Per results of extensive previous studies[28] this is sufficient to yield an excellent statistical accuracy with minimal dispersion errors. The simulation results are monitored to ensure the particles fully encompass and extend well beyond regions of non-zero vorticity and reaction.

The methane-air reaction mechanism, as occurs in this flame, is taken into account via the "flamelet" model. This model considers a laminar, one-dimensional counterflow (opposed jet) flame configuration[64]. The detailed kinetics mechanism of the Gas Research Institute (GRI2.11)[65] is employed to describe combustion. The flamelet table at strain rate of $a = 100$ $1/s$ is used to relate the thermo-chemical variables to the mixture fraction. This value is consistent with that used in previous S-FMDF[37] and PDF[66] predictions of this flame.

The overall predictive capability of VS-FMDF is demonstrated by comparing the flow statistics with the Sandia-Darmstadt[34–36]. These statistics are obtained by long-time averaging of the filtered field during 6 flow through times. The notations $\overline{Q}$ and $RMS(Q)$ denote the time-averaged mean and root mean square values of the variable Q, respectively.

2.6   RESULTS

For the purpose of flow visualization, the contour plots of FD and MC computations for $\langle RT \rangle_L$ are shown in Fig. (2). The central jet lies in the middle along the axial coordinate, surrounded by a pilot where the temperature is the highest and encircled by the air coflow. The region close to inlet is dominated by the molecular diffusion and the jet exhibits a laminar-like behavior. Further downstream, the growth of perturbations is manifested by the formation of large scale coherent vortices. The upstream feedback from the vortices created initially triggers further self-sustaining vortex rollup, and subsequent pairing and coalescence of neighboring vortices.[67,68]

Table 1: Grid parameters and the corresponding filter size

Grid	Resolution (x,y,z)	Cells $\times 10^6$
G1	$101 \times 81 \times 81$	0.662
G2	$150 \times 123 \times 123$	2.260
G3	$200 \times 161 \times 161$	5.180
G4	$270 \times 215 \times 215$	12.48

In order to assess the grid dependency of the VS-FMDF simulations, we consider four grid configurations ($G1$ through $G4$) with a progressively increasing resolution from about 0.6 to 12.2 million grid points (Table 1). To compare with the experimental data, we consider the Reynolds-averaged moments of the thermo-chemical variables. In the figures in this chapter, the overline denotes the Reynolds-averaged operator. The root mean square (RMS) includes the contributions from both the resolved and the residual fields. The capability of the method in predicting the hydrodynamics field is demonstrated by examining some of the (reported) flow statistics. The radial ($r = \sqrt{z^2 + y^2}$) distribution of the mean axial velocity and its corresponding RMS values are shown to compare well with experimental data in Fig. (3). The VS-FMDF predicts the peak value of mean axial velocity profile and the spread of the jet reasonably well. The RMS values, however, is underpredicted. The radial distribution of the mixture fraction is also shown to compare well with data in Fig. (4). The mean values agree closely with the experimental data. The RMS values, however, is underpredicted. From the grid dependency standpoint, the mean fields of velocity and mixture fraction both converge to the results corresponding to the $G4$ grid. The convergence for the RMS field is slower, but the results for $G4$ compare best with experimental data.

The radial distribution of the mean temperature values and its corresponding RMS are presented in Fig. (5). Similar to hydrodynamic quantities, the mean profiles show a relatively good agreements with measured data while the RMS values are underpredicted. The

statistics of the mass fractions (denoted by Y) of several of the species at different stream-wise locations are compared with data in Figs. (6)-(10). The mean profiles of the species show a close agreements with measurements. The RMS values show close agreements with measured data at the inner layer, but not as good at the outer layer. These disagreements can be attributed, in part, to the shortcoming of the flamelet model in relating the thermo-chemical variables to the mixture fraction. From the grid dependency standpoint, the mean fields of temperature and species mass fractions both converge to the results corresponding to the $G4$ grid.

Finally in Figs. (11)-(13), the PDFs of the resolved mixture fraction as predicted by the VS-FMDF are compared with those measured experimentally at several locations throughout the domain. In general, both the peak and the spreads of the PDFs are predicted well by the VS-FMDF. From the grid dependency standpoint, the PDF's converge to the results corresponding to the $G4$ grid; in which the best agreement with experimental data is observed.
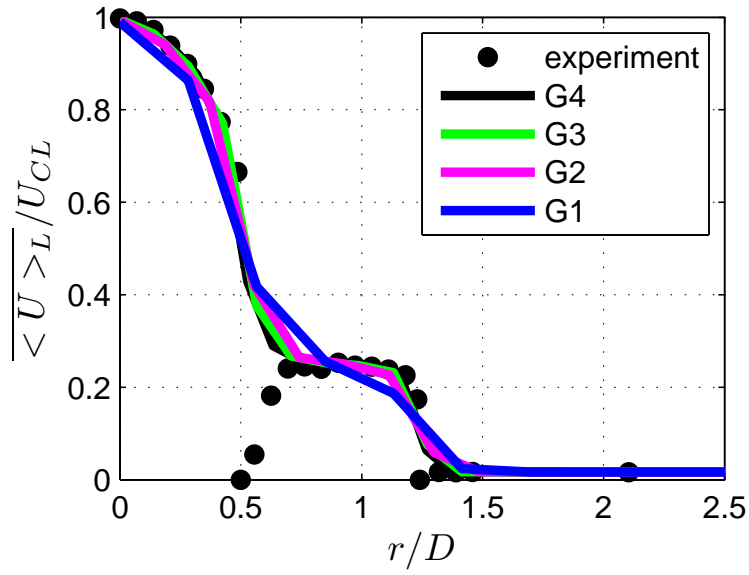
(a)
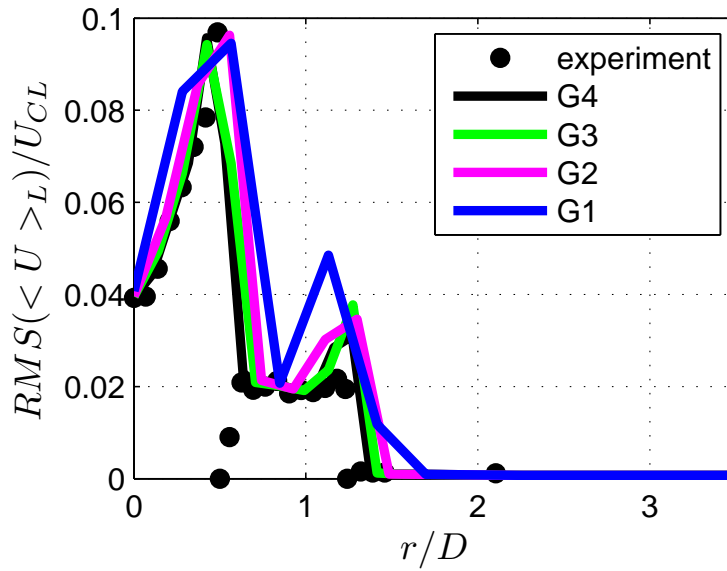
(b)

Figure 1: Radial distribution of the mean and RMS values of the filtered axial velocity. U_{cl} denotes the mean axial velocity at the centerline at the inlet, the symbols denote the experimental data. The line denotes the mean values and the thick solid line denotes the RMS values. (a) Mean axial velocity at $x/D = 0.138$, (b) RMS of the axial velocity at $x/D = 0.138$.
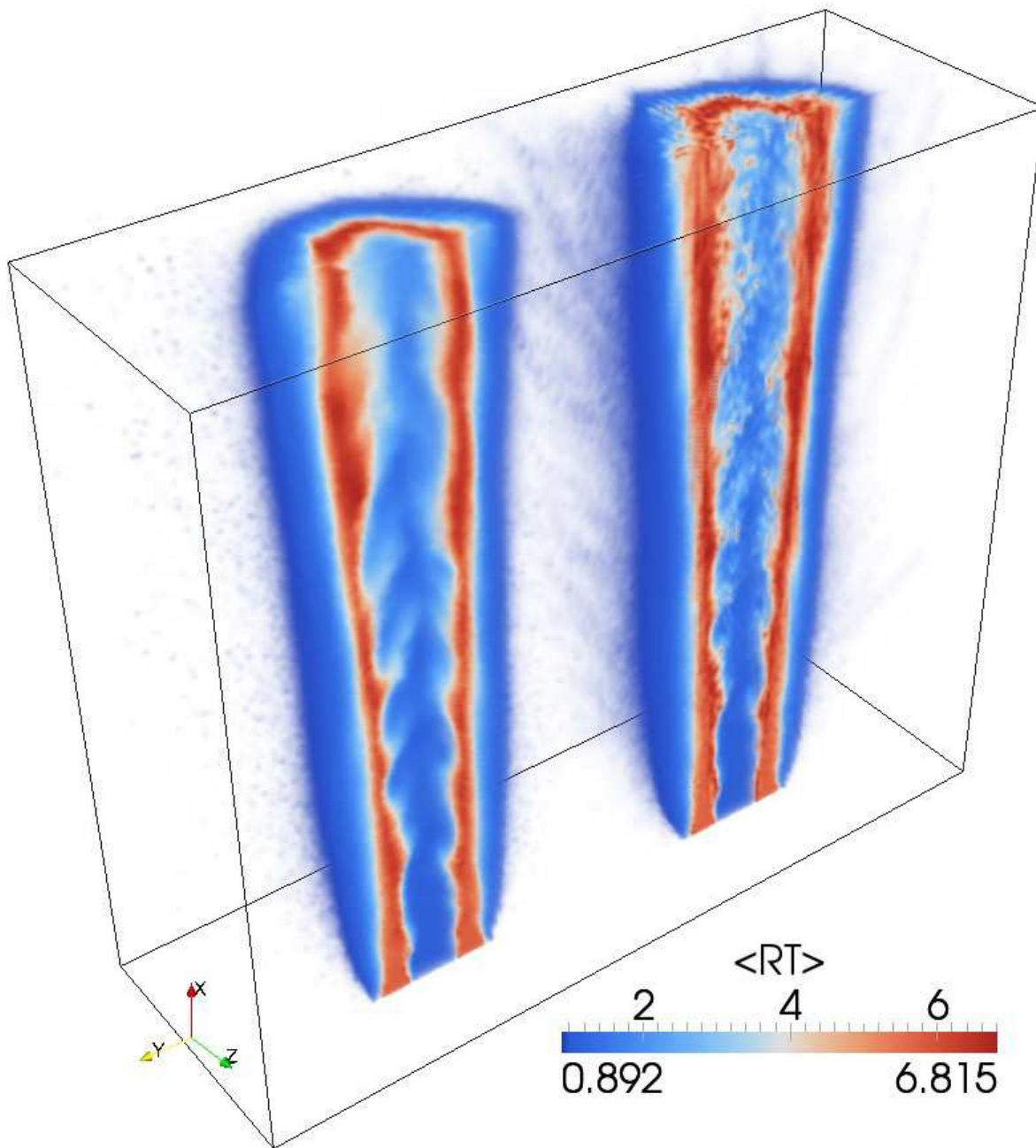
Figure 2: The instantaneous filtered RT fields obtained via MC (left) and FD (right).
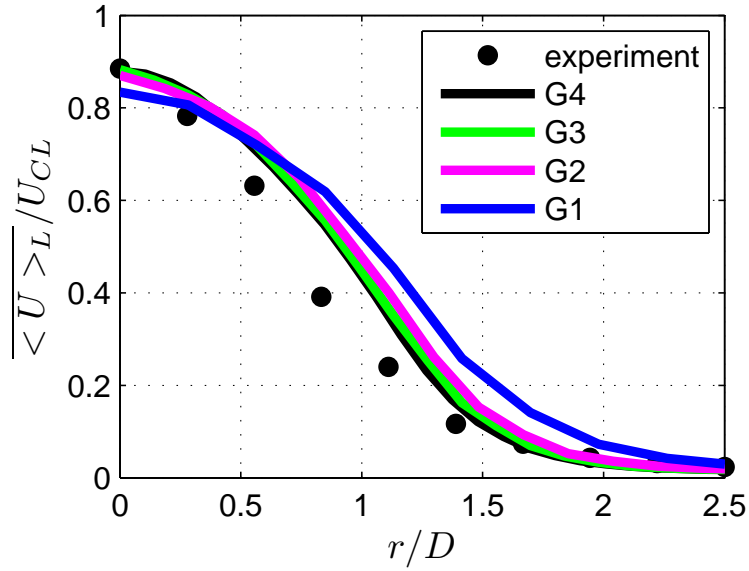
(a)
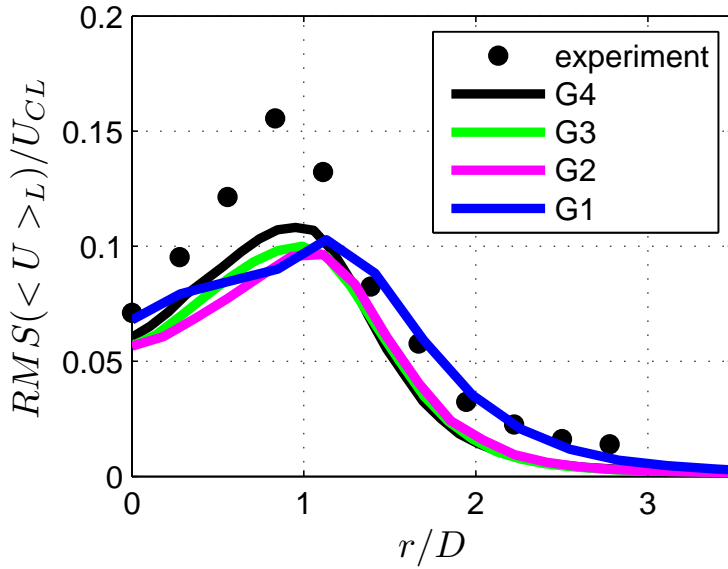
(b)

Figure 3: Radial distribution of the mean and RMS values of the filtered axial velocity. U_{cl} denotes the mean axial velocity at the centerline at the inlet, the symbols denote the experimental data. The line denotes the mean values and the thick solid line denotes the RMS values. (a) Mean axial velocity at $x/D = 15$, (b) RMS of the axial velocity at $x/D = 15$.
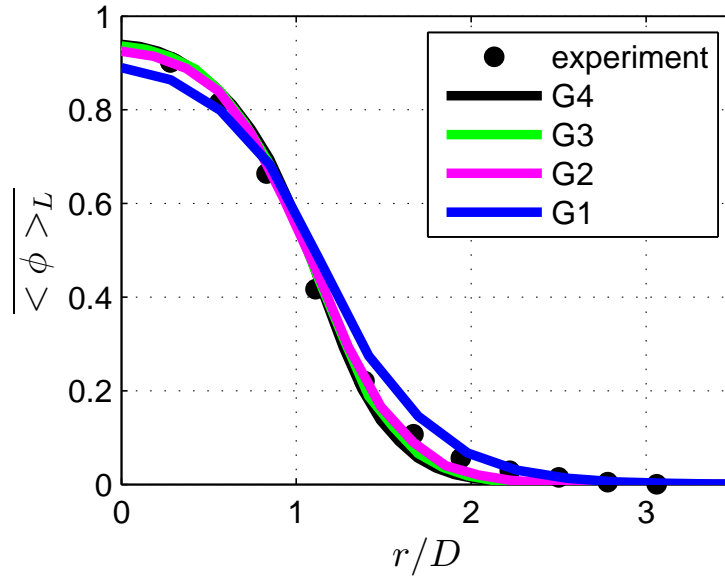
(a)
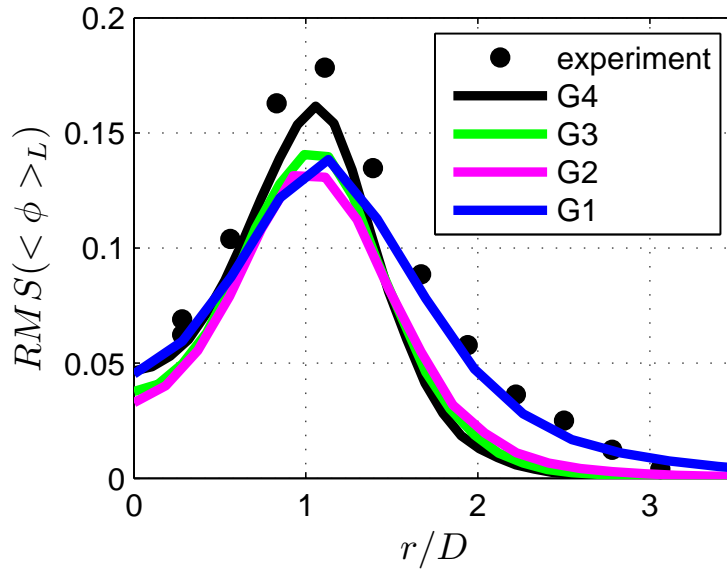
(b)

Figure 4: Radial distribution of the mean and RMS values of the filtered mixture fraction. The symbols denote the experimental data. The line denotes the mean values and the thick solid line denotes the RMS values. (a) Mean mixture fraction at $x/D = 15$, (b) RMS of the mixture fraction at $x/D = 15$.
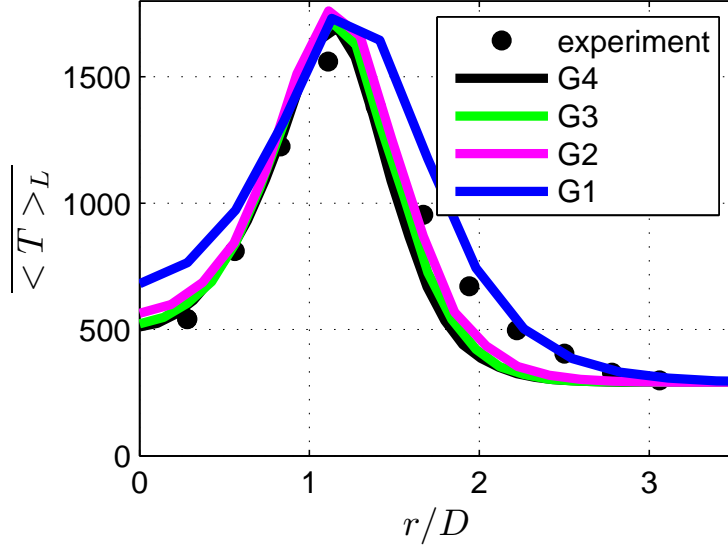
(a)
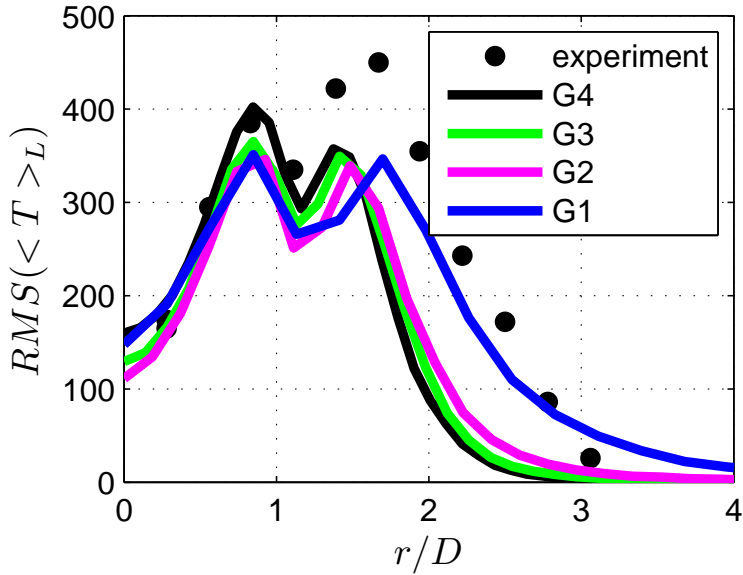
(b)

Figure 5: Radial distribution of the mean and RMS values of the filtered temperature values. The symbols denote the experimental data. The line denotes the mean values and the thick solid line denote the RMS values. (a) Mean temperature (K) at $x/D = 15$, (b) RMS of the temperature (K) at $x/D = 15$.
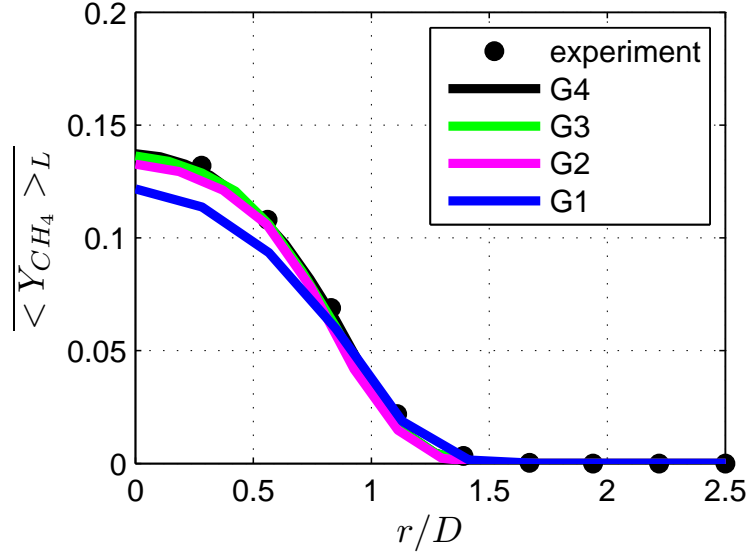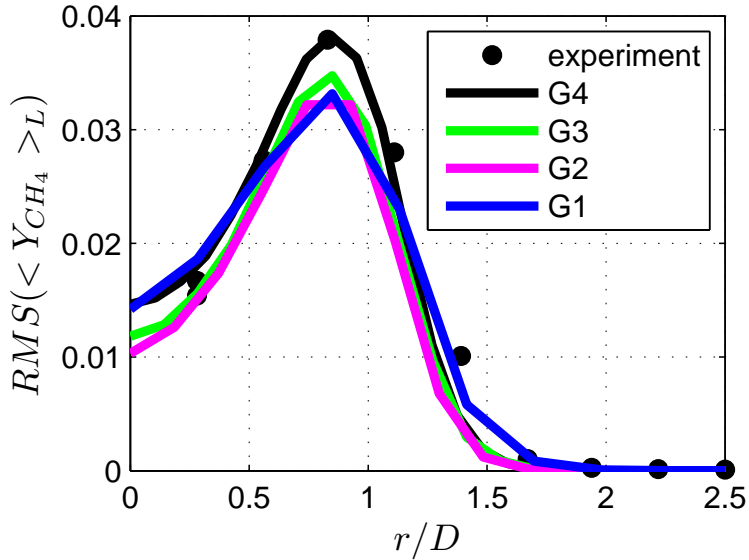
Figure 6: Radial distribution of the mean and RMS values of filtered CH_4 mass fractions. The symbols denote the experimental data. The line denotes the mean values and the thick solid line denotes the RMS values. (a) Mean CH_4 mass fraction at $x/D = 15$, (b) RMS of CH_4 mass fraction at $x/D = 15$.
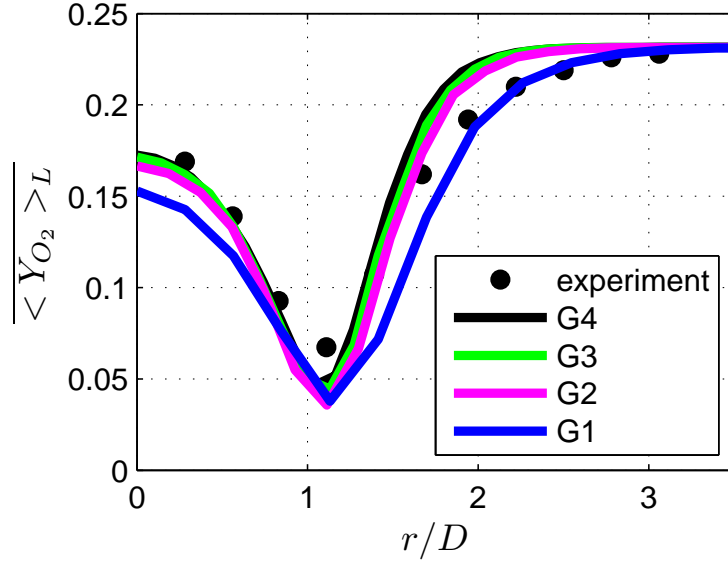
(a)
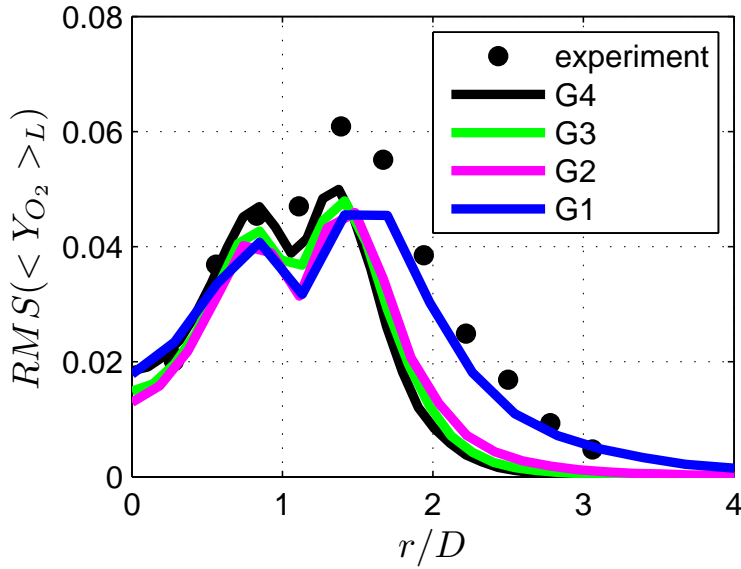
(b)

Figure 7: Radial distribution of the mean and RMS values of the filtered O_2 mass fractions. The symbols denote the experimental data. The line denotes the mean values and the thick solid line denotes the RMS values. (a) Mean O_2 mass fraction at $x/D = 15$, (b) RMS of O_2 mass fraction at $x/D = 15$.
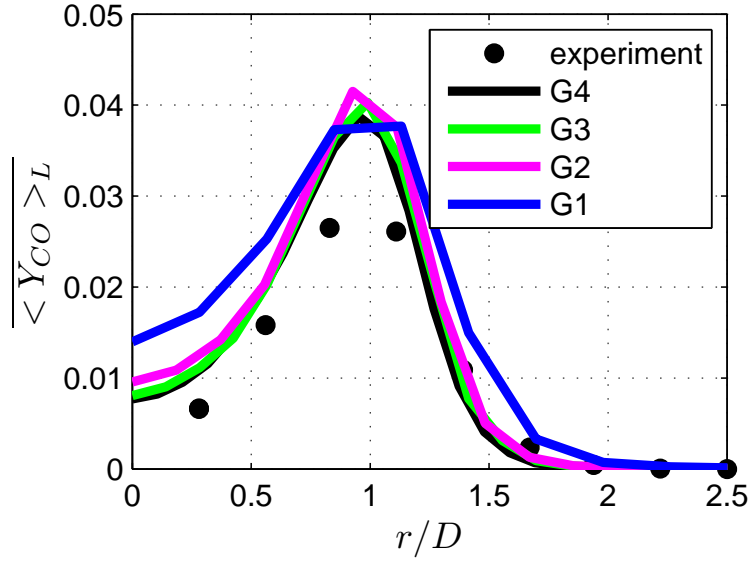
(a)
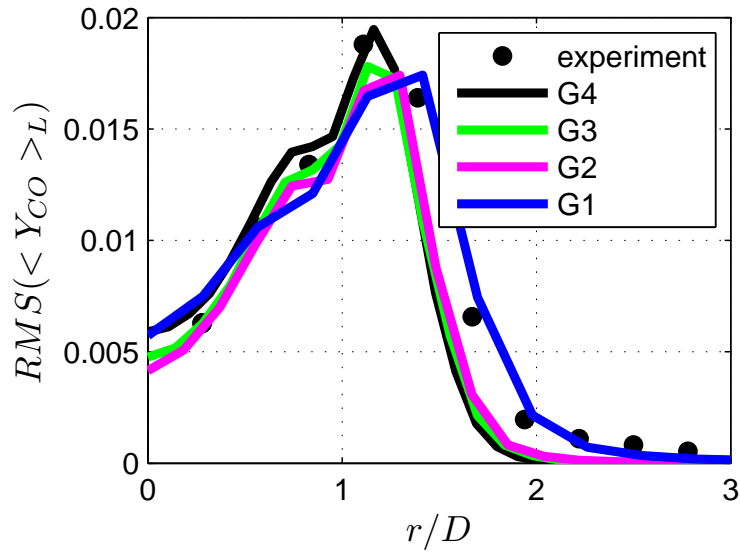
(b)

Figure 8: Radial distribution of the mean and RMS values of the filtered CO mass fractions. The symbols denote experimental data. The line denotes the mean values and the thick solid line denotes the RMS values. (a) Mean CO mass fraction at $x/D = 15$, (b) RMS of CO mass fraction at $x/D = 15$.
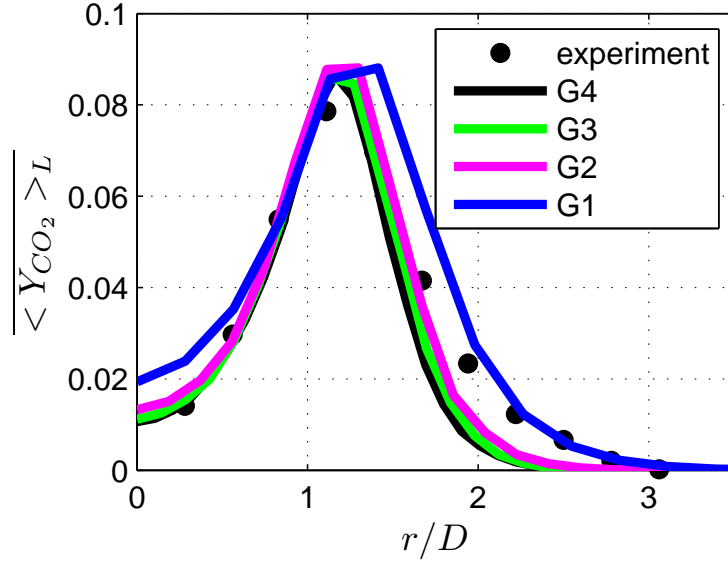
(a)
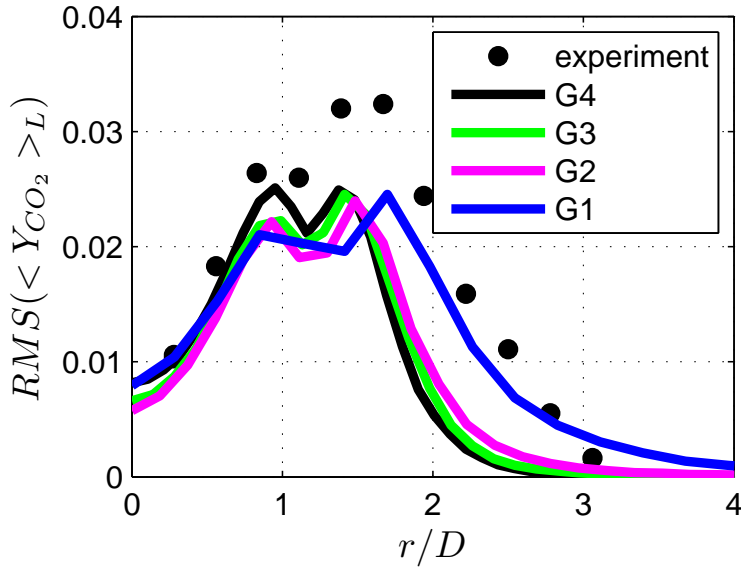
(b)

Figure 9: Radial distribution of the mean and RMS values of the filtered CO_2 mass fractions. The symbols denote the experimental data. The line denotes the mean values and the thick solid line denotes the RMS values. (a) Mean CO_2 mass fraction at $x/D = 15$, (b) RMS of CO_2 mass fraction at $x/D = 15$.
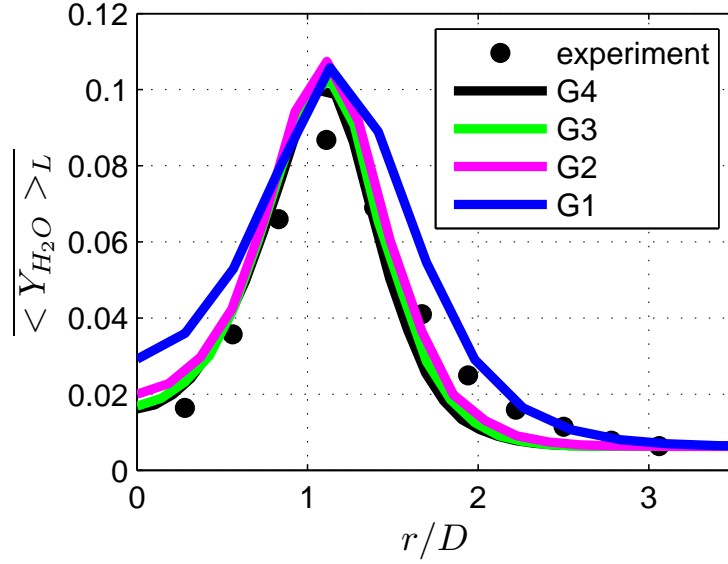
(a)
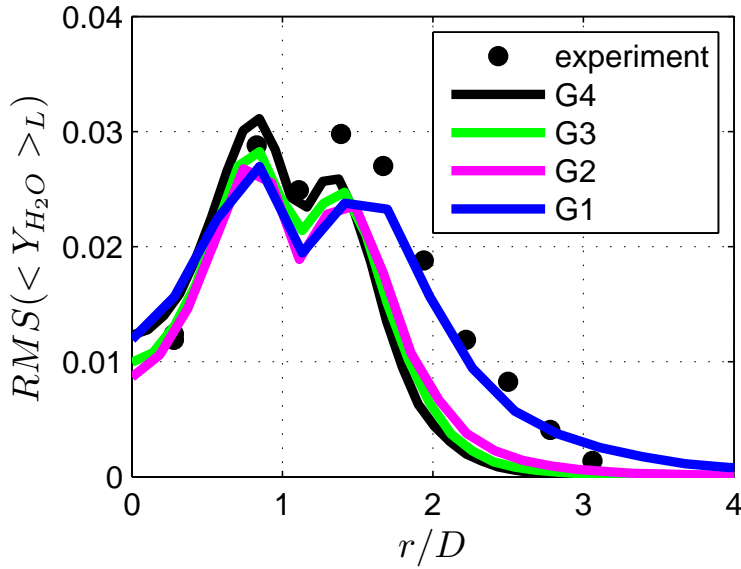
(b)

Figure 10: Radial distribution of the mean and RMS values of the filtered H_2O mass fractions. The symbols denote the experimental data. The line denotes the mean values and the thick solid line denotes the RMS values. (a) Mean H_2O mass fraction at $x/D = 15$, (b) RMS values of H_2O mass fraction at $x/D = 15$.
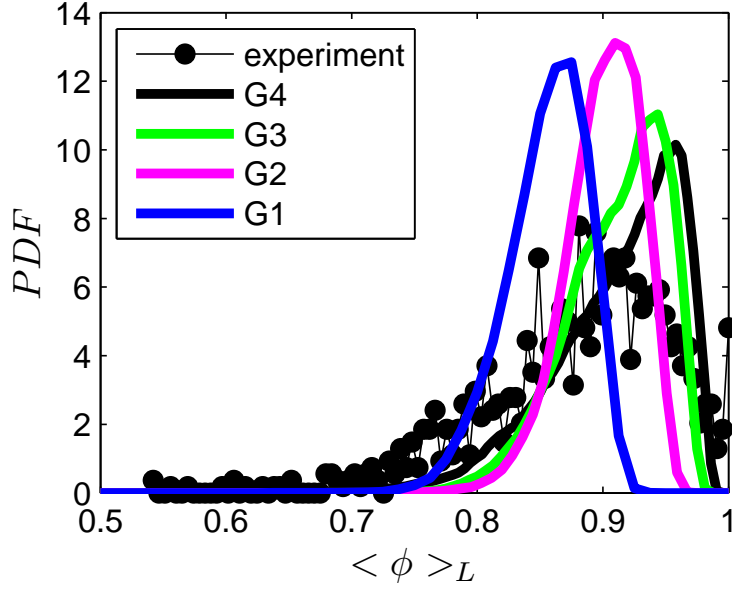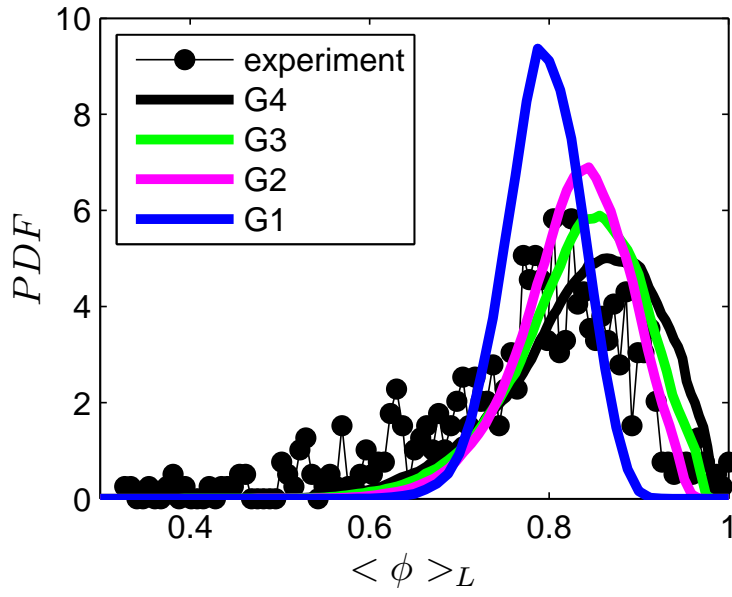
Figure 11: PDF of the resolved filtered mixture fraction at $x/D = 15$ and different radial locations. The symbols and the thick lines denote the experimental data and LES predictions, respectively. (a) Radial location $r = 2\ mm$ and (b) radial location $r = 4\ mm$.
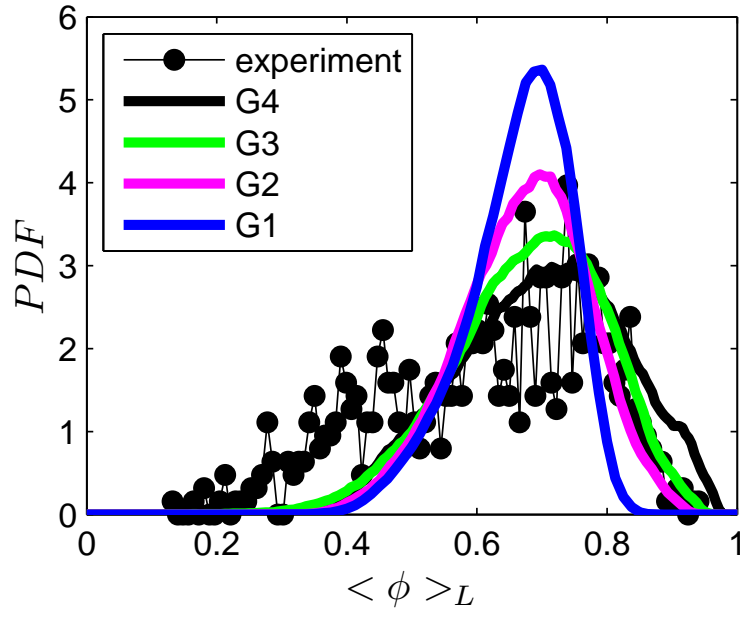
(a)
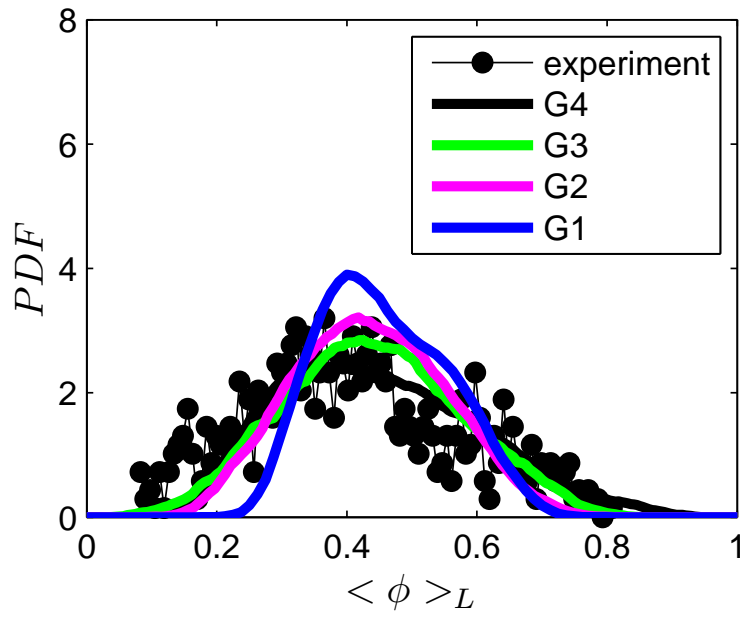
(b)

Figure 12: PDF of the resolved filtered mixture fraction at $x/D = 15$ and different radial locations. The symbols and the thick lines denote the experimental data and LES predictions, respectively. (a) Radial location $r = 6\ mm$ and (b) radial location $r = 8\ mm$.
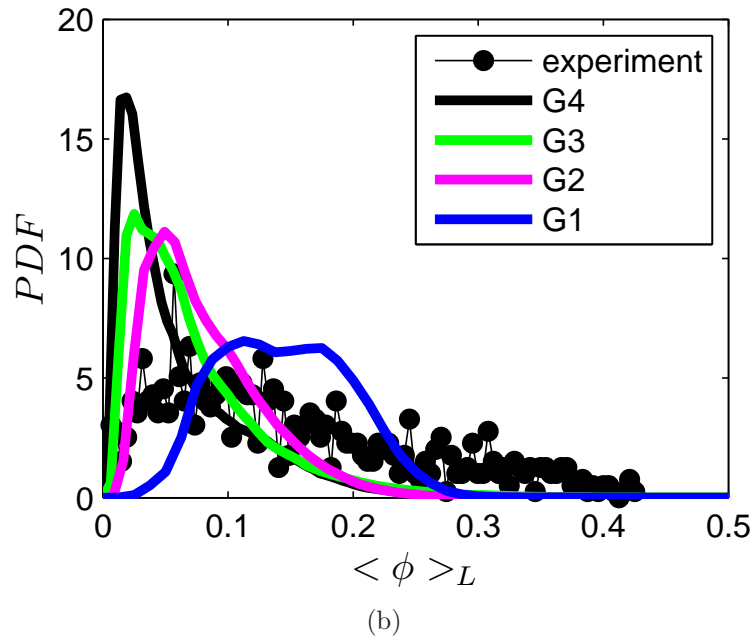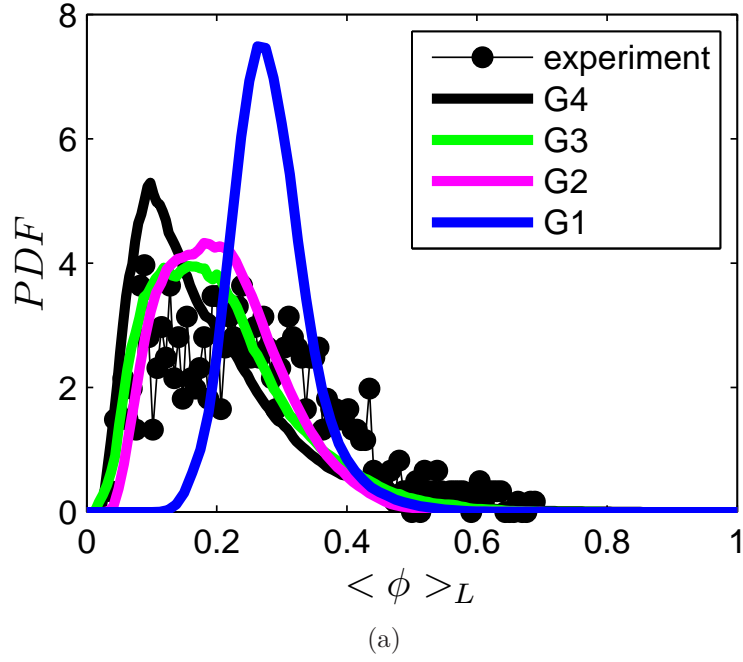
Figure 13: PDF of the resolved filtered mixture fraction at $x/D = 15$ and different radial locations. The symbols and the thick lines denote the experimental data and LES predictions, respectively. (a) Radial location $r = 10\ mm$ and (b) radial location $r = 12\ mm$.

2.7 SUMMARY

Since its original development about a decade ago, the S-FMDF[4,5] has experiences widespread applications for LES of a variety of reacting flows.[6–25] The methodology has found its way in industry[20] and is now covered as a powerful predictive tool in most modern text- and hand-books.[49,64,69–72] This popularity is partially due to the demonstrated capability of the method to simulate realistic hydrocarbon flame. The extended methodology, the VS-FMDF, is significantly more powerful as it also accounts for the effects of SGS convection in an exact manner. This superiority has been demonstrated by comparative assessment of the method in several "basic" flow configurations.[28]

The objective of the work in this chapter is to asses the prospects of the VS-FMDF for LES of realistic hydrocarbon flames. For that, we consider the piloted, non-premixed, turbulent, methane jet flame (Sandia Flame D). For this near-equilibrium flame, the thermo-chemical variables are determined by the related to the mixture fraction. A modeled transport equation for the mass weighted joint FDF of the velocity and the mixture fraction[28] is considered. This equation is solved by a hybrid finite-difference / Monte Carlo method. The predictive capability of the overall scheme is assessed by comparison of the ensemble (long time Reynolds-averaged) values of the thermo-chemical variables with laboratory data. Also, the grid dependency of the predicted results is assessed via consideration of progressively larger number of grid points. In the case with the finest resolution, there are over 10 million grid points. The results of this resolution assessment indicate that the first order moments converges quickly; but the rate of convergence for the second order moments and the PDFs of the resolved field is slower. All of the mean quantities are, generally, in good comparison with experimental data. For the RMS values, the predicted values agree closely with the experimental data in the inner layer, but not as good in the outer layer. This discrepancy is attributed, in part, to the use of the flamelet model in relating thermo-chemical variables to the mixture fraction.

The obvious extension of this work is to consider flames which experience non-equilibrium effects (such as Sandia Flames E and F). Such simulations require consideration of finite-rate chemistry. Currently it is not computationally feasible to implement detailed kinetics

in VS-FMDF; nor is it possible in S-FMDF. Implementation of reduced kinetics schemes is within reach provided that sufficient computational resources are available. It is predicted that VS-FMDF will be the primary method of FDF prediction in a decade or so from now.

3.0 JOINT ENERGY PRESSURE VELOCITY SCALAR FILTERED MASS DENSITY FUNCTION FOR HIGH SPEED FLOWS

In the work described in this chapter, the VS-FMDF methodology is extended for LES of high speed turbulent flows, by considering the joint "energy-pressure-velocity-scalar filtered mass density function" (EPVS-FMDF). Following its mathematical definition, an exact transport equation is derived for the EPVS-FMDF. This equation is modeled in a probabilistic manner. By consideration of a "systems of stochastic differential equations" (SDEs). The procedure for numerical solution of the EPVS-FMDF is based on a hybrid Eulerian/Largrangian procedure. The Eulerian part involves finite-difference solution of the filtered transport equations. The Lagrangian part involves Monte Carlo solution of the modeled EPVS-FMDF transport. The unclosed moments in the Eulerian part are obtained from the Monte Carlo solver. The consistency and the accuracy of this procedure are established by the simulation of a three-dimensional, temporally evolving mixing layer involving the transport of a passive scalar. These simulations are assessed by comparing the EPVS-FMDF results with those of direct numerical simulation (DNS).

3.1 FORMULATION

3.1.1 Basic equations

In a multiple species non reacting high speed turbulent flow, the primary transport variables are the density $\rho(\mathbf{x}, t)$, the velocity vector $u_i(\mathbf{x}, t)$ $(i = 1, 2, 3)$, the pressure $p(\mathbf{x}, t)$, the internal energy $e(\mathbf{x}, t)$ and the species mass fractions ϕ_α $(\alpha = 1..N_s)$. The equations which govern

the transport of these variables in space (x_i) $(i = 1, 2, 3)$ and time (t) are the continuity, momentum, energy, pressure and scalar equations along with an equation of state:

$$\frac{\partial \rho}{\partial t} + \frac{\partial \rho u_j}{\partial x_j} = 0, \tag{3.1a}$$

$$\frac{\partial \rho u_i}{\partial t} + \frac{\partial \rho u_j u_i}{\partial x_j} = -\frac{\partial p}{\partial x_i} + \frac{\partial \tau_{ji}}{\partial x_j}, \tag{3.1b}$$

$$\frac{\partial \rho e}{\partial t} + \frac{\partial \rho u_j e}{\partial x_j} = -\frac{\partial q_j}{\partial x_j} + \sigma_{ij} \frac{\partial u_i}{\partial x_j}, \tag{3.1c}$$

$$\frac{\partial p}{\partial t} + \frac{\partial p u_j}{\partial x_j} = -(\gamma - 1) \frac{\partial q_j}{\partial x_j} + (\gamma - 1) \sigma_{ij} \frac{\partial u_i}{\partial x_j}, \tag{3.1d}$$

$$\frac{\partial \rho \phi_\alpha}{\partial t} + \frac{\partial \rho u_j \phi_\alpha}{\partial x_j} = -\frac{\partial J_j^\alpha}{\partial x_j} \tag{3.1e}$$

$$p = \rho \frac{R^0}{W} T, \tag{3.1f}$$

where R^0 are the universal gas constants and W is the mean molecular weight of the mixture given by $\frac{1}{W} = \sum\limits_{\alpha=1}^{N_s} \frac{\phi_\alpha}{W_\alpha}$. Here T denote the temperature field, e is the internal energy and $\gamma = \frac{c_p}{c_v}$ is the specific heat ratio. For a Newtonian fluid, the viscous stress tensor τ_{ij}, the energy flux q_j, the species α diffusive mass flux vector J_j^α and σ_{ij} tensor are represented by

$$\sigma_{ij} = \tau_{ij} - p\delta_{ij}, \tag{3.2a}$$

$$\tau_{ij} = \mu(T) \left(\frac{\partial u_i}{\partial x_j} + \frac{\partial u_j}{\partial x_i} - \frac{2}{3} \frac{\partial u_k}{\partial x_k} \delta_{ij} \right), \tag{3.2b}$$

$$q_j = -\lambda(T) \frac{\partial T}{\partial x_j}, \tag{3.2c}$$

$$J_j^\alpha = -\rho \Gamma(T) \frac{\partial \phi_\alpha}{\partial x_j}, \tag{3.2d}$$

where μ is the fluid dynamic viscosity, λ denotes the thermal diffusivity and Γ is the mass diffusion coefficient. In this formulation, we assume using calorically perfect gas in which the

29

specific heat at constant pressure c_p and specific heat at constant volume c_v are constants. Also, $p = (\gamma - 1)\rho e$ holds for a calorically perfect gas.

3.1.2 Filtered equations

Large eddy simulation involves the spatial filtering operation[29–32,49]

$$\langle Q(\mathbf{x}, t)\rangle_\ell = \int_{-\infty}^{+\infty} Q(\mathbf{x}', t) G_{\Delta_{l_1}}(\mathbf{x}', \mathbf{x}) d\mathbf{x}', \tag{3.3}$$

where $G_{\Delta_{l_1}}(\mathbf{x}', \mathbf{x})$ denotes a filter function, and $\langle Q(\mathbf{x}, t)\rangle_\ell$ is the filtered value of the transport variable $Q(\mathbf{x}, t)$. In this definition, the subscript l_1 for the filter function indicates that $\langle Q(\mathbf{x}, t)\rangle_\ell$ is the first level filter value of variable $Q(\mathbf{x}, t)$.[73] In variable-density flows it is convenient to use the Favre-filtered quantity $\langle Q(\mathbf{x}, t)\rangle_L = \langle \rho Q \rangle_\ell / \langle \rho \rangle_\ell$. We consider a filter function that is spatially and temporally invariant and localized, thus: $G_{\Delta_{l_1}}(\mathbf{x}', \mathbf{x}) \equiv G_{\Delta_{l_1}}(\mathbf{x}' - \mathbf{x})$ with the properties $G_{\Delta_{l_1}}(\mathbf{x}) \geq 0$, $\int_{-\infty}^{+\infty} G_{\Delta_{l_1}}(\mathbf{x}) d\mathbf{x} = 1$. Also, the second level spatial filtering operation is defined as:

$$\langle\langle Q(\mathbf{x}, t)\rangle_\ell\rangle_{\ell_2} = \int_{-\infty}^{+\infty} \langle Q(\mathbf{x}', t)\rangle_\ell \, G_{\Delta_{l_2}}(\mathbf{x}', \mathbf{x}) d\mathbf{x}', \tag{3.4}$$

where $G_{\Delta_{l_2}}(\mathbf{x}', \mathbf{x})$ denotes a secondary filter function. In variable-density flows it is convenient to use the Favre-filtered quantity, similarly to the first level filtering operation, $\langle\langle Q(\mathbf{x}, t)\rangle_L\rangle_{L_2} = \langle\langle \rho Q \rangle_\ell\rangle_{\ell_2} / \langle\langle \rho \rangle_\ell\rangle_{\ell_2}$.

30

Applying the first level filtering operation to Eqs. (3.1) and using the conventional LES approximation for the diffusion terms, we obtain

$$\frac{\partial \langle \rho \rangle_\ell}{\partial t} + \frac{\partial \langle \rho \rangle_\ell \langle u_j \rangle_L}{\partial x_j} = 0, \tag{3.5a}$$

$$\frac{\partial \langle \rho \rangle_\ell \langle u_i \rangle_L}{\partial t} + \frac{\partial \langle \rho \rangle_\ell \langle u_j \rangle_L \langle u_i \rangle_L}{\partial x_j} = -\frac{\partial \langle p \rangle_\ell}{\partial x_i} + \frac{\partial \breve{\tau}_{ij}}{\partial x_j} - \frac{\partial \langle \rho \rangle_\ell \tau_L(u_i, u_j)}{\partial x_j}, \tag{3.5b}$$

$$\frac{\partial \langle \rho \rangle_\ell \langle e \rangle_L}{\partial t} + \frac{\partial \langle \rho \rangle_\ell \langle u_j \rangle_L \langle e \rangle_L}{\partial x_j} = -\frac{\partial \breve{q}_j}{\partial x_j} - \frac{\partial \langle \rho \rangle_\ell \tau_L(e, u_j)}{\partial x_j}$$

$$+ \quad \epsilon + \breve{\tau}_{ij} \frac{\partial \langle u_i \rangle_L}{\partial x_j}$$

$$- \quad \Pi_d - \langle p \rangle_\ell \frac{\partial \langle u_i \rangle_L}{\partial x_i}, \tag{3.5c}$$

$$\frac{\partial \langle p \rangle_\ell}{\partial t} + \langle u_j \rangle_L \frac{\partial \langle p \rangle_\ell}{\partial x_j} = -(\gamma - 1) \frac{\partial \breve{q}_j}{\partial x_j} - \frac{\partial \tau(p, u_j)}{\partial x_j}$$

$$+ \quad (\gamma - 1) \epsilon + (\gamma - 1) \breve{\tau}_{ij} \frac{\partial \langle u_i \rangle_L}{\partial x_j}$$

$$- \quad (\gamma - 1) \Pi_d - \gamma \langle p \rangle_\ell \frac{\partial \langle u_i \rangle_L}{\partial x_i}, \tag{3.5d}$$

$$\frac{\partial \langle \rho \rangle_\ell \langle \phi_\alpha \rangle_L}{\partial t} + \frac{\partial \langle \rho \rangle_\ell \langle u_j \rangle_L \langle \phi_\alpha \rangle_L}{\partial x_j} = -\frac{\partial \breve{J}_j^\alpha}{\partial x_j} - \frac{\partial \langle \rho \rangle_\ell \tau_L(\phi_\alpha, u_j)}{\partial x_j}. \tag{3.5e}$$

In Eq. (3.5), the filtered viscous stress tensor $\breve{\tau}_{ij}$, the filtered energy flux $\breve{q}_j$ and the filtered diffusive mass flux vector $\breve{J}_j^\alpha$ are defined as

$$\breve{\tau}_{ij} = \mu\left(\langle T\rangle_L\right)\left(\frac{\partial\langle u_i\rangle_L}{\partial x_j} + \frac{\partial\langle u_j\rangle_L}{\partial x_i} - \frac{2}{3}\frac{\partial\langle u_k\rangle_L}{\partial x_k}\delta_{ij}\right), \tag{3.6a}$$

$$\breve{q}_j = -\lambda\left(\langle T\rangle_L\right)\frac{\partial\langle T\rangle_L}{\partial x_j}, \tag{3.6b}$$

$$\breve{J}_j^\alpha = -\langle\rho\rangle_\ell\,\Gamma\left(\langle T\rangle_L\right)\frac{\partial\langle\phi_\alpha\rangle_L}{\partial x_j}, \tag{3.6c}$$

$$\Pi_d = \left\langle p\frac{\partial u_i}{\partial x_i}\right\rangle_\ell - \langle p\rangle_\ell\frac{\partial\langle u_i\rangle_L}{\partial x_i}, \tag{3.6d}$$

$$\epsilon = \left\langle \tau_{ij}\frac{\partial u_i}{\partial x_j}\right\rangle_\ell - \breve{\tau}_{ij}\frac{\partial\langle u_i\rangle_L}{\partial x_j}. \tag{3.6e}$$

The second-order and third-order regular SGS correlations and Favre SGS correlations are defined by

$$\tau_\ell(a,b) = \langle ab\rangle_\ell - \langle a\rangle_\ell\langle b\rangle_\ell, \tag{3.7a}$$

$$\tau_\ell(a,b,c) = \langle abc\rangle_\ell - \langle a\rangle_\ell\tau_\ell(b,c) - \langle b\rangle_\ell\tau_\ell(a,c) - \langle c\rangle_\ell\tau_\ell(a,c) - \langle a\rangle_\ell\langle b\rangle_\ell\langle c\rangle_\ell, \tag{3.7b}$$

$$\tau_L(a,b) = \langle ab\rangle_L - \langle a\rangle_L\langle b\rangle_L, \tag{3.7c}$$

$$\tau_L(a,b,c) = \langle abc\rangle_L - \langle a\rangle_L\tau_L(b,c) - \langle b\rangle_L\tau_L(a,c) - \langle c\rangle_L\tau_L(a,c) - \langle a\rangle_L\langle b\rangle_L\langle c\rangle_L. \tag{3.7d}$$

In case of not specifying the subscript, the subgrid term will be defined explicitly. In Eq. (3.5d), the subgrid term without the subscript is defined as:

$$\tau\left(p, u_j\right) = \langle pu_j\rangle_\ell - \langle p\rangle_\ell\langle u_j\rangle_L. \tag{3.8}$$

The second order velocity correlations are governed by

$$\frac{\partial \langle \rho \rangle_\ell \, \tau_L \, (u_i, u_j)}{\partial t} + \frac{\partial \langle \rho \rangle_\ell \, \langle u_k \rangle_L \, \tau_L \, (u_i, u_j)}{\partial x_k} \;\; = \;\; \langle \rho \rangle_\ell \, P_{ij} - \frac{\partial T_{ijk}}{\partial x_k} - \epsilon_{ij} + \Pi_{ij}. \qquad (3.9)$$

Equation (3.9) provides an "exact" form of the transport equations for the second order velocity correlations. In this equation, the production term P_{ij}, the transport term T_{ijk}, the dissipation term ϵ_{ij} and the pressure-rate-of-strain tensor Π_{ij} are defined as:

$$P_{ij} \;\; = \;\; -\tau_L \, (u_i, u_k) \frac{\partial \langle u_j \rangle_L}{\partial x_k} - \tau_L \, (u_j, u_k) \frac{\partial \langle u_i \rangle_L}{\partial x_k}, \qquad (3.10a)$$

$$
\begin{aligned}
T_{ijk} \;\; = \;\; & \langle \rho \rangle_\ell \, \tau_L \, (u_i, u_j, u_k) + \tau \, (p, u_i) \, \delta_{jk} + \tau \, (p, u_j) \, \delta_{ik} \\
& - \left(\tau \, (u_i, \tau_{jk}) + \tau \, (u_j, \tau_{ik}) \right),
\end{aligned}
\qquad (3.10b)
$$

$$\epsilon_{ij} \;\; = \;\; \left(\left\langle \tau_{ik} \frac{\partial u_j}{\partial x_k} \right\rangle_\ell - \breve{\tau}_{ik} \frac{\partial \langle u_j \rangle_L}{\partial x_k} \right) + \left(\left\langle \tau_{jk} \frac{\partial u_i}{\partial x_k} \right\rangle_\ell - \breve{\tau}_{jk} \frac{\partial \langle u_i \rangle_L}{\partial x_k} \right), \qquad (3.10c)$$

$$\Pi_{ij} \;\; = \;\; \left(\left\langle p \frac{\partial u_i}{\partial x_j} \right\rangle_\ell - \langle p \rangle_\ell \frac{\partial \langle u_i \rangle_L}{\partial x_j} \right) + \left(\left\langle p \frac{\partial u_j}{\partial x_i} \right\rangle_\ell - \langle p \rangle_\ell \frac{\partial \langle u_j \rangle_L}{\partial x_i} \right). \qquad (3.10d)$$

In Eq. (3.10b), the subgrid terms without the subscript are defined as:

$$\tau \, (p, u_i) \;\; = \;\; \langle p u_i \rangle_\ell - \langle p \rangle_\ell \, \langle u_i \rangle_L, \qquad (3.11a)$$

$$\tau \, (p, u_j) \;\; = \;\; \langle p u_j \rangle_\ell - \langle p \rangle_\ell \, \langle u_j \rangle_L, \qquad (3.11b)$$

$$\tau \, (u_i, \tau_{jk}) \;\; = \;\; \langle u_i \tau_{jk} \rangle_\ell - \langle u_i \rangle_L \, \breve{\tau}_{jk}, \qquad (3.11c)$$

$$\tau \, (u_j, \tau_{ik}) \;\; = \;\; \langle u_j \tau_{ik} \rangle_\ell - \langle u_j \rangle_L \, \breve{\tau}_{ik}. \qquad (3.11d)$$

From Eqs. (3.10c) and (3.6e), the dissipation is defined as: $\epsilon = \epsilon_{ii}/2$. Also from Eqs. (3.10d) and (3.6d), the pressure dilatation term is defined as: $\Pi_d = \Pi_{ii}/2$.

The second order scalar correlations are governed by

$$\frac{\partial \langle \rho \rangle_\ell \, \tau_L \, (\phi_\alpha, \phi_\beta)}{\partial t} + \frac{\partial \langle \rho \rangle_\ell \, \langle u_k \rangle_L \, \tau_L \, (\phi_\alpha, \phi_\beta)}{\partial x_k} = \langle \rho \rangle_\ell \, P^{\alpha\beta} - \frac{\partial T_k^{\alpha\beta}}{\partial x_k} - \epsilon^{\alpha\beta}. \qquad (3.12)$$

Equation (3.12) provides an "exact" form of the transport for the second order scalar correlations. In this equation, the production term $P^{\alpha\beta}$, the transport term $T_k^{\alpha\beta}$, and the dissipation term $\epsilon^{\alpha\beta}$ are defined as:

$$P^{\alpha\beta} = -\tau_L \, (\phi_\alpha, u_k) \frac{\partial \langle \phi_\beta \rangle_L}{\partial x_k} - \tau_L \, (\phi_\beta, u_k) \frac{\partial \langle \phi_\alpha \rangle_L}{\partial x_k}, \qquad (3.13a)$$

$$T_k^{\alpha\beta} = \langle \rho \rangle_\ell \, \tau_L \, (\phi_\alpha, \phi_\beta, u_k) - \langle \rho \rangle_\ell \, \Gamma \frac{\partial \tau_L \, (\phi_\alpha, \phi_\beta)}{\partial x_k}, \qquad (3.13b)$$

$$\epsilon^{\alpha\beta} = 2 \langle \rho \rangle_\ell \, \Gamma \tau_L \left(\frac{\partial \phi_\alpha}{\partial x_j}, \frac{\partial \phi_\beta}{\partial x_j} \right). \qquad (3.13c)$$

The second order velocity-scalar correlations are governed by

$$\frac{\partial \langle \rho \rangle_\ell \, \tau_L \left(u_i, \phi_\alpha \right)}{\partial t} + \frac{\partial \langle \rho \rangle_\ell \, \langle u_k \rangle_L \, \tau_L \left(u_i, \phi_\alpha \right)}{\partial x_k} \;\; = \;\; \langle \rho \rangle_\ell \, P_i^\alpha - \frac{\partial T_{ik}^\alpha}{\partial x_k} - \epsilon_i^\alpha + \Pi_i^\alpha. \quad (3.14)$$

Equation (3.14) provides an "exact" form of the transport for the second order velocity scalar correlations. In this equation, the production term P_i^α, the transport term T_{ik}^α, the dissipation term ϵ_i^α and the pressure-rate-of-scalar-strain Π_i^α are defined as:

$$P_i^\alpha \;\; = \;\; -\tau_L \left(u_i, u_k \right) \frac{\partial \langle \phi_\alpha \rangle_L}{\partial x_k} - \tau_L \left(\phi_\alpha, u_k \right) \frac{\partial \langle u_i \rangle_L}{\partial x_k}, \qquad\qquad (3.15a)$$

$$T_{ik}^\alpha \;\; = \;\; \langle \rho \rangle_\ell \, \tau_L \left(u_i, \phi_\alpha, u_k \right) + \tau \left(p, \phi_\alpha \right) \delta_{ik} - \left(\tau \left(\phi_\alpha, \tau_{ik} \right) - \tau \left(u_i, J_k^\alpha \right) \right), \qquad (3.15b)$$

$$\epsilon_i^\alpha \;\; = \;\; \left(\left\langle \tau_{ik} \frac{\partial \phi_\alpha}{\partial x_k} \right\rangle_\ell - \breve{\tau}_{ik} \frac{\partial \langle \phi_\alpha \rangle_L}{\partial x_k} \right) - \left(\left\langle J_k^\alpha \frac{\partial u_i}{\partial x_k} \right\rangle_\ell - \breve{J}_k^\alpha \frac{\partial \langle u_i \rangle_L}{\partial x_k} \right), \qquad (3.15c)$$

$$\Pi_i^\alpha \;\; = \;\; \left\langle p \frac{\partial \phi_\alpha}{\partial x_i} \right\rangle_\ell - \langle p \rangle_\ell \frac{\partial \langle \phi_\alpha \rangle_L}{\partial x_i}. \qquad\qquad (3.15d)$$

In Eq. (3.15b), the subgrid terms without the subscript are defined as:

$$\tau \left(p, \phi_\alpha \right) \;\; = \;\; \langle p \phi_\alpha \rangle_\ell - \langle p \rangle_\ell \, \langle \phi_\alpha \rangle_L, \qquad\qquad (3.16a)$$

$$\tau \left(u_i, J_k^\alpha \right) \;\; = \;\; \langle u_i J_k^\alpha \rangle_\ell - \langle u_i \rangle_L \, \breve{J}_k^\alpha, \qquad\qquad (3.16b)$$

$$\tau \left(\phi_\alpha, \tau_{ik} \right) \;\; = \;\; \langle \phi_\alpha \tau_{ik} \rangle_\ell - \langle \phi_\alpha \rangle_L \, \breve{\tau}_{ik}. \qquad\qquad (3.16c)$$

The second order velocity-energy correlations are governed by

$$\frac{\partial \langle \rho \rangle_\ell \tau_L (u_i, e)}{\partial t} + \frac{\partial \langle \rho \rangle_\ell \langle u_k \rangle_L \tau_L (u_i, e)}{\partial x_k} = \langle \rho \rangle_\ell P_i^e - \frac{\partial T_{ik}^e}{\partial x_k} - \epsilon_i^e + \Pi_i^e$$

$$+ \left(\left\langle u_i \tau_{kj} \frac{\partial u_k}{\partial x_j} \right\rangle_\ell - \langle u_i \rangle_L \left\langle \tau_{kj} \frac{\partial u_k}{\partial x_j} \right\rangle_\ell \right)$$

$$- \left(\left\langle u_i p \frac{\partial u_j}{\partial x_j} \right\rangle_\ell - \langle u_i \rangle_L \left\langle p \frac{\partial u_j}{\partial x_j} \right\rangle_\ell \right). \quad (3.17)$$

Equation (3.17) provides an "exact" form of the transport for the second order velocity-energy correlations. In this equation, the production term P_i^e, the transport term T_{ik}^e, the dissipation term ϵ_i^e and the pressure-rate-of-scalar-strain Π_i^e are defined as:

$$P_i^e = -\tau_L (u_i, u_k) \frac{\partial \langle e \rangle_L}{\partial x_k} - \tau_L (e, u_k) \frac{\partial \langle u_i \rangle_L}{\partial x_k}, \quad (3.18a)$$

$$T_{ik}^e = \langle \rho \rangle_\ell \tau_L (u_i, e, u_k) + \tau (p, e) \delta_{ik} - (\tau (e, \tau_{ik}) - \tau (u_i, q_k)), \quad (3.18b)$$

$$\epsilon_i^e = \left(\left\langle \tau_{ik} \frac{\partial e}{\partial x_k} \right\rangle_\ell - \breve{\tau}_{ik} \frac{\partial \langle e \rangle_L}{\partial x_k} \right) - \left(\left\langle q_k \frac{\partial u_i}{\partial x_k} \right\rangle_\ell - \breve{q}_k \frac{\partial \langle u_i \rangle_L}{\partial x_k} \right), \quad (3.18c)$$

$$\Pi_i^e = \left\langle p \frac{\partial e}{\partial x_i} \right\rangle_\ell - \langle p \rangle_\ell \frac{\partial \langle e \rangle_L}{\partial x_i}. \quad (3.18d)$$

In Eq. (3.18b), the subgrid terms without the subscript are defined as:

$$\tau (p, e) = \langle pe \rangle_\ell - \langle p \rangle_\ell \langle e \rangle_L, \quad (3.19a)$$

$$\tau (u_i, q_k) = \langle u_i q_k \rangle_\ell - \langle u_i \rangle_L \breve{q}_k, \quad (3.19b)$$

$$\tau (e, \tau_{ik}) = \langle e \tau_{ik} \rangle_\ell - \langle e \rangle_L \breve{\tau}_{ik}. \quad (3.19c)$$

The second order energy correlations are governed by

$$\frac{\partial \langle \rho \rangle_\ell \frac{\tau_L(e,e)}{2}}{\partial t} + \frac{\partial \langle \rho \rangle_\ell \langle u_k \rangle_L \frac{\tau_L(e,e)}{2}}{\partial x_k} = \langle \rho \rangle_\ell P^{ee} - \frac{1}{2} \frac{\partial T_k^{ee}}{\partial x_k} - \epsilon^{ee}$$

$$+ \left(\left\langle e\tau_{ij} \frac{\partial u_i}{\partial x_j} \right\rangle_\ell - \langle e \rangle_L \left\langle \tau_{ij} \frac{\partial u_i}{\partial x_j} \right\rangle_\ell \right)$$

$$- \left(\left\langle ep \frac{\partial u_j}{\partial x_j} \right\rangle_\ell - \langle e \rangle_L \left\langle p \frac{\partial u_j}{\partial x_j} \right\rangle_\ell \right). \qquad (3.20)$$

Equation (3.20) provides an "exact" form of the transport for the second order energy correlations. In this equation, the production term P^{ee}, the transport term T_k^{ee} and the dissipation term ϵ^{ee} are defined as:

$$P^{ee} = -\tau_L(e, u_k) \frac{\partial \langle u_i \rangle_L}{\partial x_k}, \qquad (3.21a)$$

$$T_k^{ee} = \langle \rho \rangle_\ell \tau_L(e, e, u_k) + 2\tau(e, q_k), \qquad (3.21b)$$

$$\epsilon^{ee} = -\left(\left\langle q_k \frac{\partial e}{\partial x_k} \right\rangle_\ell - \breve{q}_k \frac{\partial \langle e \rangle_L}{\partial x_k} \right). \qquad (3.21c)$$

In Eq. (3.21b), the subgrid term without the subscript is defined as:

$$\tau(e, q_k) = \langle eq_k \rangle_\ell - \langle e \rangle_L \breve{q}_k. \qquad (3.22)$$

37

The second order pressure correlations are governed by

$$\frac{\partial \frac{\tau_\ell(p,p)}{2}}{\partial t} + \langle u_k \rangle_L \frac{\partial \frac{\tau_\ell(p,p)}{2}}{\partial x_k} = P^{pp} - \frac{1}{2} \frac{\partial T_k^{pp}}{\partial x_k} - (\gamma - 1)\, \epsilon^{pp} - \gamma \langle p \rangle_\ell \Pi_d$$

$$- \gamma \tau_\ell(p,p) \frac{\partial \langle u_j \rangle_L}{\partial x_j}$$

$$- \frac{2\gamma - 1}{2} \tau\left(p, p, \frac{\partial u_i}{\partial x_i}\right)$$

$$+ (\gamma - 1)\left(\left\langle \tau_{ij} p \frac{\partial u_i}{\partial x_j} \right\rangle_\ell - \langle p \rangle_\ell \left\langle \tau_{ij} \frac{\partial u_i}{\partial x_j} \right\rangle_\ell \right). \qquad (3.23)$$

Equation (3.23) provides an "exact" form of the transport equations for the second order pressure correlations. In this equation, the production term P^{pp}, the transport term T_k^{pp} and the dissipation term ϵ^{pp} are defined as:

$$P^{pp} = -\tau(p, u_k) \frac{\partial \langle p \rangle_\ell}{\partial x_k}, \qquad (3.24a)$$

$$T_k^{pp} = \tau(p, p, u_k) + 2(\gamma - 1)\tau(p, q_k), \qquad (3.24b)$$

$$\epsilon^{pp} = -\left(\left\langle q_k \frac{\partial p}{\partial x_k} \right\rangle_\ell - \breve{q}_k \frac{\partial \langle p \rangle_\ell}{\partial x_k}\right). \qquad (3.24c)$$

In Eq. (3.24b), the subgrid terms without the subscripts are defined as:

$$\tau(p, p, u_k) = \langle p^2 u_k \rangle_\ell - 2 \langle p \rangle_\ell \tau(p, u_k) - \langle u_k \rangle_L \tau_\ell(p, p) - \langle p \rangle_\ell^2 \langle u_k \rangle_L, \qquad (3.25a)$$

$$\tau(p, u_k) = \langle p u_k \rangle_\ell - \langle p \rangle_\ell \langle u_k \rangle_L, \qquad (3.25b)$$

$$\tau(p, q_k) = \langle p q_k \rangle_\ell - \langle p \rangle_L \breve{q}_k. \qquad (3.25c)$$

3.2 EXACT EPVS-FMDF TRANSPORT EQUATION

The "energy-pressure-velocity-scalar filtered mass density function" (EPVS-FMDF), denoted by P_L, is formally defined as[2]

$$P_L\left(\boldsymbol{v}, \boldsymbol{\psi}, \boldsymbol{\theta}, \boldsymbol{\eta}, \mathbf{x}; t\right) = \int_{-\infty}^{+\infty} \rho(\mathbf{x}', t)\zeta\left(\boldsymbol{v}, \boldsymbol{\psi}, \boldsymbol{\theta}, \boldsymbol{\eta}; \boldsymbol{u}(\mathbf{x}', t), \boldsymbol{\phi}(\mathbf{x}', t), \boldsymbol{e}(\mathbf{x}', t), \boldsymbol{p}(\mathbf{x}', t)\right) G(\mathbf{x}'-\mathbf{x})d\mathbf{x}',$$

(3.26)

where

$$\zeta\left(\boldsymbol{v}, \boldsymbol{\psi}, \boldsymbol{\theta}, \boldsymbol{\eta}; \boldsymbol{u}(\mathbf{x}, t), \boldsymbol{\phi}(\mathbf{x}, t), \boldsymbol{e}(\mathbf{x}, t), \boldsymbol{p}(\mathbf{x}, t)\right) =$$

$$\left(\prod_{i=1}^{3} \delta\left(v_i - u_i(\mathbf{x}, t)\right)\right) \times \left(\prod_{\alpha=1}^{\sigma=N_s} \delta\left(\psi_\alpha - \phi_\alpha(\mathbf{x}, t)\right)\right) \times \delta\left(\boldsymbol{\theta} - \boldsymbol{e}(\mathbf{x}, t)\right) \times \delta\left(\boldsymbol{\eta} - \boldsymbol{p}(\mathbf{x}, t)\right).$$

(3.27)

In this equation, δ denotes the Dirac delta function, and $\boldsymbol{v}$, $\boldsymbol{\psi}$, $\boldsymbol{\theta}$ and $\boldsymbol{\eta}$ are the velocity vector, the scalar array, the sensible internal energy and pressure in the sample space. The term ζ is the "fine-grained" density.[47,50] Equation (3.26) defines the EPVS-FMDF as the spatially filtered value of the fine-grained density. With the condition of a positive filter kernel,[51] P_L has all of the properties of a mass density function (MDF).[47] For further developments it is useful to define the "conditional filtered value" of the variable $Q(\mathbf{x}, t)$ as

$$\left\langle Q(\mathbf{x}, t) \,\middle|\, \boldsymbol{u}(\mathbf{x}, t) = \boldsymbol{v}, \boldsymbol{\phi}(\mathbf{x}, t) = \boldsymbol{\psi}, \boldsymbol{e}(\mathbf{x}, t) = \boldsymbol{\theta}, \boldsymbol{p}(\mathbf{x}, t) = \boldsymbol{\eta} \right\rangle_\ell \equiv \left\langle Q \,\middle|\, \boldsymbol{v}, \boldsymbol{\psi}, \boldsymbol{\theta}, \boldsymbol{\eta} \right\rangle_\ell =$$

$$\frac{\int_{-\infty}^{+\infty} \rho(\mathbf{x}', t)\zeta\left(\boldsymbol{v}, \boldsymbol{\psi}, \boldsymbol{\theta}, \boldsymbol{\eta}; \boldsymbol{u}(\mathbf{x}', t), \boldsymbol{\phi}(\mathbf{x}', t), \boldsymbol{e}(\mathbf{x}', t), \boldsymbol{p}(\mathbf{x}', t)\right) G(\mathbf{x}' - \mathbf{x})d\mathbf{x}'}{P_L\left(\boldsymbol{v}, \boldsymbol{\psi}, \boldsymbol{\theta}, \boldsymbol{\eta}, \mathbf{x}; t\right)}.$$

(3.28)

Equation (3.28) implies the following:

1. for $Q(\mathbf{x}, t) = c$

$$\left\langle Q(\mathbf{x}, t) \,\middle|\, \boldsymbol{v}, \boldsymbol{\psi}, \boldsymbol{\theta}, \boldsymbol{\eta} \right\rangle_\ell = c,$$

(3.29)

2. for $Q(\mathbf{x}, t) \equiv \hat{Q}(\boldsymbol{u}(\mathbf{x}, t), \boldsymbol{\phi}(\mathbf{x}, t), \boldsymbol{e}(\mathbf{x}, t), \boldsymbol{p}(\mathbf{x}, t))$

$$\left\langle Q(\mathbf{x}, t) \,\Big|\, \boldsymbol{v}, \boldsymbol{\psi}, \boldsymbol{\theta}, \boldsymbol{\eta} \right\rangle_\ell = \hat{Q}(\boldsymbol{v}, \boldsymbol{\psi}, \boldsymbol{\theta}, \boldsymbol{\eta}), \tag{3.30}$$

3. Integral properties:

$$\langle \rho(\mathbf{x}, t) Q(\mathbf{x}, t) \rangle_\ell = \int_{-\infty}^{+\infty} \int_{-\infty}^{+\infty} \left\langle Q(\mathbf{x}, t) \,\Big|\, \boldsymbol{v}, \boldsymbol{\psi}, \boldsymbol{\theta}, \boldsymbol{\eta} \right\rangle_\ell P_L(\boldsymbol{v}, \boldsymbol{\psi}, \boldsymbol{\theta}, \boldsymbol{\eta}, \mathbf{x}; t) d\boldsymbol{v} d\boldsymbol{\psi} d\boldsymbol{\theta} d\boldsymbol{\eta},$$
$$\tag{3.31}$$

From Eqs. (3.29), (3.30, (3.31) it follows that the filtered value of any function of the velocity and/or scalar variables is obtained by its integration over the sample spaces:

$$\langle \rho(\mathbf{x}, t) \rangle_\ell \, \langle Q(\mathbf{x}, t) \rangle_L = \int_{-\infty}^{+\infty} \int_{-\infty}^{+\infty} \hat{Q}(\boldsymbol{v}, \boldsymbol{\psi}, \boldsymbol{\theta}, \boldsymbol{\eta}) P_L(\boldsymbol{v}, \boldsymbol{\psi}, \boldsymbol{\theta}, \boldsymbol{\eta}, \mathbf{x}; t) d\boldsymbol{v} d\boldsymbol{\psi} d\boldsymbol{\theta} d\boldsymbol{\eta}. \tag{3.32}$$

To develop the EPVS-FMDF transport equation, we consider the time derivative of the fine-grained density function Eq. (3.27)

$$\frac{\partial \zeta}{\partial t} = -\left(\frac{\partial u_k}{\partial t} \frac{\partial \zeta}{\partial \boldsymbol{v}_k} + \frac{\partial \phi_\alpha}{\partial t} \frac{\partial \zeta}{\partial \boldsymbol{\psi}_\alpha} + \frac{\partial e}{\partial t} \frac{\partial \zeta}{\partial \boldsymbol{\theta}} + \frac{\partial p}{\partial t} \frac{\partial \zeta}{\partial \boldsymbol{\eta}} \right). \tag{3.33}$$

Substituting Eqs. (3.1b)-(3.1c)-(3.1e), into Eq. (3.33) we obtain

$$
\begin{aligned}
\frac{\partial \rho \zeta}{\partial t} + \frac{\partial \rho u_j \zeta}{\partial x_j} &= \left(\frac{\partial p}{\partial x_j} - \frac{\partial \tau_{kj}}{\partial x_k} \right) \frac{\partial \zeta}{\partial \boldsymbol{v}_j} + \left(\frac{\partial J_j^\alpha}{\partial x_j} \right) \frac{\partial \zeta}{\partial \boldsymbol{\psi}_\alpha} \\
&+ \left(\gamma \rho p \frac{\partial u_j}{\partial x_j} + (\gamma - 1) \rho \frac{\partial q_i}{\partial x_i} - (\gamma - 1) \rho \tau_{ij} \frac{\partial u_i}{\partial x_j} \right) \frac{\partial \zeta}{\partial \boldsymbol{\eta}} \\
&+ \left(\frac{\partial q_i}{\partial x_i} - \tau_{ij} \frac{\partial u_i}{\partial x_j} + p \frac{\partial u_j}{\partial x_j} \right) \frac{\partial \zeta}{\partial \boldsymbol{\theta}}.
\end{aligned}
\tag{3.34}
$$

Integration of this equation according to Eq. (3.26), while employing Eq. (3.28) results in

$$
\begin{aligned}
\frac{\partial P_L}{\partial t} + \frac{\partial \boldsymbol{v}_j P_L}{\partial x_j} &= \frac{\partial}{\partial \boldsymbol{v}_i} \left(\left\langle \frac{1}{\rho} \frac{\partial p}{\partial x_i} \,\middle|\, \boldsymbol{v}, \boldsymbol{\psi}, \boldsymbol{\theta}, \boldsymbol{\eta} \right\rangle_\ell P_L \right) \\
&\quad - \frac{\partial}{\partial \boldsymbol{v}_i} \left(\left\langle \frac{1}{\rho} \frac{\partial \tau_{ij}}{\partial x_j} \,\middle|\, \boldsymbol{v}, \boldsymbol{\psi}, \boldsymbol{\theta}, \boldsymbol{\eta} \right\rangle_\ell P_L \right) \\
&\quad + \frac{\partial}{\partial \psi_\alpha} \left(\left\langle \frac{1}{\rho} \frac{\partial J_j^\alpha}{\partial x_j} \,\middle|\, \boldsymbol{v}, \boldsymbol{\psi}, \boldsymbol{\theta}, \boldsymbol{\eta} \right\rangle_\ell P_L \right) \\
&\quad + \frac{\partial}{\partial \boldsymbol{\theta}} \left(\left\langle \frac{1}{\rho} \frac{\partial q_i}{\partial x_i} \,\middle|\, \boldsymbol{v}, \boldsymbol{\psi}, \boldsymbol{\theta}, \boldsymbol{\eta} \right\rangle_\ell P_L \right) \\
&\quad - \frac{\partial}{\partial \boldsymbol{\theta}} \left(\left\langle \frac{1}{\rho} \tau_{ij} \frac{\partial u_i}{\partial x_j} \,\middle|\, \boldsymbol{v}, \boldsymbol{\psi}, \boldsymbol{\theta}, \boldsymbol{\eta} \right\rangle_\ell P_L \right) \\
&\quad + \frac{\partial}{\partial \boldsymbol{\theta}} \left(\left\langle \frac{1}{\rho} p \frac{\partial u_j}{\partial x_j} \,\middle|\, \boldsymbol{v}, \boldsymbol{\psi}, \boldsymbol{\theta}, \boldsymbol{\eta} \right\rangle_\ell P_L \right) \\
&\quad + (\gamma - 1) \frac{\partial}{\partial \boldsymbol{\eta}} \left(\left\langle \frac{\partial q_i}{\partial x_i} \,\middle|\, \boldsymbol{v}, \boldsymbol{\psi}, \boldsymbol{\theta}, \boldsymbol{\eta} \right\rangle_\ell P_L \right) \\
&\quad - (\gamma - 1) \frac{\partial}{\partial \boldsymbol{\eta}} \left(\left\langle \tau_{ij} \frac{\partial u_i}{\partial x_j} \,\middle|\, \boldsymbol{v}, \boldsymbol{\psi}, \boldsymbol{\theta}, \boldsymbol{\eta} \right\rangle_\ell P_L \right) \\
&\quad + \gamma \frac{\partial}{\partial \boldsymbol{\eta}} \left(\left\langle p \frac{\partial u_j}{\partial x_j} \,\middle|\, \boldsymbol{v}, \boldsymbol{\psi}, \boldsymbol{\theta}, \boldsymbol{\eta} \right\rangle_\ell P_L \right).
\end{aligned}
\tag{3.35}
$$

This is an exact EPVS-FMDF transport equation in which the effect of convection appears in a closed form. The conditional terms at the right hand side are unclosed.

Using the decompositions:

$$\left\langle \frac{1}{\rho}\frac{\partial p}{\partial x_i} \,\middle|\, \boldsymbol{v}, \boldsymbol{\psi}, \boldsymbol{\theta}, \boldsymbol{\eta} \right\rangle_\ell P_L \;=\; \frac{1}{\langle\rho\rangle_\ell}\frac{\partial \langle p\rangle_\ell}{\partial x_i}P_L + \left[\left\langle \frac{1}{\rho}\frac{\partial p}{\partial x_i} \,\middle|\, \boldsymbol{v}, \boldsymbol{\psi}, \boldsymbol{\theta}, \boldsymbol{\eta} \right\rangle_\ell - \frac{1}{\langle\rho\rangle_\ell}\frac{\partial \langle p\rangle_\ell}{\partial x_i}\right]P_L$$

$$\left\langle \frac{1}{\rho}\frac{\partial \tau_{ij}}{\partial x_j} \,\middle|\, \boldsymbol{v}, \boldsymbol{\psi}, \boldsymbol{\theta}, \boldsymbol{\eta} \right\rangle_\ell P_L \;=\; \frac{1}{\langle\rho\rangle_\ell}\frac{\partial \breve{\tau}_{ij}}{\partial x_j}P_L + \left[\left\langle \frac{1}{\rho}\frac{\partial \tau_{ij}}{\partial x_j} \,\middle|\, \boldsymbol{v}, \boldsymbol{\psi}, \boldsymbol{\theta}, \boldsymbol{\eta} \right\rangle_\ell - \frac{1}{\langle\rho\rangle_\ell}\frac{\partial \breve{\tau}_{ij}}{\partial x_j}\right]P_L$$

$$\left\langle \frac{1}{\rho}\frac{\partial J_j^\alpha}{\partial x_j} \,\middle|\, \boldsymbol{v}, \boldsymbol{\psi}, \boldsymbol{\theta}, \boldsymbol{\eta} \right\rangle_\ell P_L \;=\; \frac{1}{\langle\rho\rangle_\ell}\frac{\partial \breve{J}_j^\alpha}{\partial x_j}P_L + \left[\left\langle \frac{1}{\rho}\frac{\partial J_j^\alpha}{\partial x_j} \,\middle|\, \boldsymbol{v}, \boldsymbol{\psi}, \boldsymbol{\theta}, \boldsymbol{\eta} \right\rangle_\ell - \frac{1}{\langle\rho\rangle_\ell}\frac{\partial \breve{J}_j^\alpha}{\partial x_j}\right]P_L$$

$$\left\langle \frac{1}{\rho}\frac{\partial q_i}{\partial x_i} \,\middle|\, \boldsymbol{v}, \boldsymbol{\psi}, \boldsymbol{\theta}, \boldsymbol{\eta} \right\rangle_\ell P_L \;=\; \frac{1}{\langle\rho\rangle_\ell}\frac{\partial \breve{q}_i}{\partial x_i}P_L + \left[\left\langle \frac{1}{\rho}\frac{\partial q_i}{\partial x_i} \,\middle|\, \boldsymbol{v}, \boldsymbol{\psi}, \boldsymbol{\theta}, \boldsymbol{\eta} \right\rangle_\ell - \frac{1}{\langle\rho\rangle_\ell}\frac{\partial \breve{q}_i}{\partial x_i}\right]P_L$$

$$\left\langle \frac{1}{\rho}\tau_{ij}\frac{\partial u_i}{\partial x_j} \,\middle|\, \boldsymbol{v}, \boldsymbol{\psi}, \boldsymbol{\theta}, \boldsymbol{\eta} \right\rangle_\ell P_L \;=\; \frac{1}{\langle\rho\rangle_\ell}\breve{\tau}_{ij}\frac{\partial \langle u_i\rangle_L}{\partial x_j}P_L + \left[\left\langle \frac{1}{\rho}\tau_{ij}\frac{\partial u_i}{\partial x_j} \,\middle|\, \boldsymbol{v}, \boldsymbol{\psi}, \boldsymbol{\theta}, \boldsymbol{\eta} \right\rangle_\ell - \frac{1}{\langle\rho\rangle_\ell}\breve{\tau}_{ij}\frac{\partial \langle u_i\rangle_L}{\partial x_j}\right]P_L$$

$$\left\langle \frac{1}{\rho}p\frac{\partial u_j}{\partial x_j} \,\middle|\, \boldsymbol{v}, \boldsymbol{\psi}, \boldsymbol{\theta}, \boldsymbol{\eta} \right\rangle_\ell P_L \;=\; \frac{1}{\langle\rho\rangle_\ell}\langle p\rangle_\ell\frac{\partial \langle u_j\rangle_L}{\partial x_j}P_L + \left[\left\langle \frac{1}{\rho}p\frac{\partial u_j}{\partial x_j} \,\middle|\, \boldsymbol{v}, \boldsymbol{\psi}, \boldsymbol{\theta}, \boldsymbol{\eta} \right\rangle_\ell - \frac{1}{\langle\rho\rangle_\ell}\langle p\rangle_\ell\frac{\partial \langle u_j\rangle_L}{\partial x_j}\right]P_L$$

$$\left\langle \frac{\partial q_i}{\partial x_i} \,\middle|\, \boldsymbol{v}, \boldsymbol{\psi}, \boldsymbol{\theta}, \boldsymbol{\eta} \right\rangle_\ell P_L \;=\; \frac{\partial \breve{q}_i}{\partial x_i}P_L + \left[\left\langle \frac{\partial q_i}{\partial x_i} \,\middle|\, \boldsymbol{v}, \boldsymbol{\psi}, \boldsymbol{\theta}, \boldsymbol{\eta} \right\rangle_\ell - \frac{\partial \breve{q}_i}{\partial x_i}\right]P_L$$

$$\left\langle \tau_{ij}\frac{\partial u_i}{\partial x_j} \,\middle|\, \boldsymbol{v}, \boldsymbol{\psi}, \boldsymbol{\theta}, \boldsymbol{\eta} \right\rangle_\ell P_L \;=\; \breve{\tau}_{ij}\frac{\partial \langle u_i\rangle_L}{\partial x_j}P_L + \left[\left\langle \tau_{ij}\frac{\partial u_i}{\partial x_j} \,\middle|\, \boldsymbol{v}, \boldsymbol{\psi}, \boldsymbol{\theta}, \boldsymbol{\eta} \right\rangle_\ell - \breve{\tau}_{ij}\frac{\partial \langle u_i\rangle_L}{\partial x_j}\right]P_L$$

$$\left\langle p\frac{\partial u_j}{\partial x_j} \,\middle|\, \boldsymbol{v}, \boldsymbol{\psi}, \boldsymbol{\theta}, \boldsymbol{\eta} \right\rangle_\ell P_L \;=\; \langle p\rangle_\ell\frac{\partial \langle u_j\rangle_L}{\partial x_j}P_L + \left[\left\langle p\frac{\partial u_j}{\partial x_j} \,\middle|\, \boldsymbol{v}, \boldsymbol{\psi}, \boldsymbol{\theta}, \boldsymbol{\eta} \right\rangle_\ell - \langle p\rangle_\ell\frac{\partial \langle u_j\rangle_L}{\partial x_j}\right]P_L,$$

42

the exact EPVS-FMDF transport equation becomes:

$$
\begin{aligned}
\frac{\partial P_L}{\partial t} + \frac{\partial \boldsymbol{v}_j P_L}{\partial x_j} \;=\;& \frac{1}{\langle\rho\rangle_\ell}\frac{\partial \langle p\rangle_\ell}{\partial x_i}\frac{\partial P_L}{\partial \boldsymbol{v}_i} - \frac{1}{\langle\rho\rangle_\ell}\frac{\partial \breve{\tau}_{ij}}{\partial x_j}\frac{\partial P_L}{\partial \boldsymbol{v}_i} + \frac{1}{\langle\rho\rangle_\ell}\frac{\partial \breve{J}_j^\alpha}{\partial x_j}\frac{\partial P_L}{\partial \boldsymbol{\psi}_\alpha} + \frac{1}{\langle\rho\rangle_\ell}\frac{\partial \breve{q}_i}{\partial x_i}\frac{\partial P_L}{\partial \boldsymbol{\theta}} \\[2mm]
&- \frac{\breve{\tau}_{ij}}{\langle\rho\rangle_\ell}\frac{\partial \langle u_j\rangle_L}{\partial x_i}\frac{\partial P_L}{\partial \boldsymbol{\theta}} + \frac{\langle p\rangle_\ell}{\langle\rho\rangle_\ell}\frac{\partial \langle u_j\rangle_L}{\partial x_j}\frac{\partial P_L}{\partial \boldsymbol{\theta}} + (\gamma - 1)\frac{\partial \breve{q}_i}{\partial x_i}\frac{\partial P_L}{\partial \boldsymbol{\eta}} \\[2mm]
&- (\gamma - 1)\,\breve{\tau}_{ij}\frac{\partial \langle u_i\rangle_L}{\partial x_j}\frac{\partial P_L}{\partial \boldsymbol{\eta}} + \gamma\,\langle p\rangle_\ell\frac{\partial \langle u_j\rangle_\ell}{\partial x_j}\frac{\partial P_L}{\partial \boldsymbol{\eta}} \\[2mm]
&+ \frac{\partial}{\partial \boldsymbol{v}_i}\left[\left(\left\langle\frac{1}{\rho}\frac{\partial p}{\partial x_i}\,\Big|\,\boldsymbol{v},\boldsymbol{\psi},\boldsymbol{\theta},\boldsymbol{\eta}\right\rangle_\ell - \frac{1}{\langle\rho\rangle_\ell}\frac{\partial \langle p\rangle_\ell}{\partial x_i}\right)P_L\right] \\[2mm]
&- \frac{\partial}{\partial \boldsymbol{v}_i}\left[\left(\left\langle\frac{1}{\rho}\frac{\partial \tau_{ij}}{\partial x_j}\,\Big|\,\boldsymbol{v},\boldsymbol{\psi},\boldsymbol{\theta},\boldsymbol{\eta}\right\rangle_\ell - \frac{1}{\langle\rho\rangle_\ell}\frac{\partial \breve{\tau}_{ij}}{\partial x_j}\right)P_L\right] \\[2mm]
&+ \frac{\partial}{\partial \boldsymbol{\psi}_\alpha}\left[\left(\left\langle\frac{1}{\rho}\frac{\partial J_j^\alpha}{\partial x_j}\,\Big|\,\boldsymbol{v},\boldsymbol{\psi},\boldsymbol{\theta},\boldsymbol{\eta}\right\rangle_\ell - \frac{1}{\langle\rho\rangle_\ell}\frac{\partial \breve{J}_j^\alpha}{\partial x_j}\right)P_L\right] \\[2mm]
&+ \frac{\partial}{\partial \boldsymbol{\theta}}\left[\left(\left\langle\frac{1}{\rho}\frac{\partial q_i}{\partial x_i}\,\Big|\,\boldsymbol{v},\boldsymbol{\psi},\boldsymbol{\theta},\boldsymbol{\eta}\right\rangle_\ell - \frac{1}{\langle\rho\rangle_\ell}\frac{\partial \breve{q}_i}{\partial x_i}\right)P_L\right] \\[2mm]
&- \frac{\partial}{\partial \boldsymbol{\theta}}\left[\left(\left\langle\frac{1}{\rho}\tau_{ij}\frac{\partial u_i}{\partial x_j}\,\Big|\,\boldsymbol{v},\boldsymbol{\psi},\boldsymbol{\theta},\boldsymbol{\eta}\right\rangle_\ell - \frac{1}{\langle\rho\rangle_\ell}\breve{\tau}_{ij}\frac{\partial \langle u_i\rangle_L}{\partial x_j}\right)P_L\right] \\[2mm]
&+ \frac{\partial}{\partial \boldsymbol{\theta}}\left[\left(\left\langle\frac{1}{\rho}p\frac{\partial u_j}{\partial x_j}\,\Big|\,\boldsymbol{v},\boldsymbol{\psi},\boldsymbol{\theta},\boldsymbol{\eta}\right\rangle_\ell - \frac{1}{\langle\rho\rangle_\ell}\langle p\rangle_\ell\frac{\partial \langle u_j\rangle_L}{\partial x_j}\right)P_L\right] \\[2mm]
&+ (\gamma - 1)\frac{\partial}{\partial \boldsymbol{\eta}}\left[\left(\left\langle\frac{\partial q_i}{\partial x_i}\,\Big|\,\boldsymbol{v},\boldsymbol{\psi},\boldsymbol{\theta},\boldsymbol{\eta}\right\rangle_\ell - \frac{\partial \breve{q}_i}{\partial x_i}\right)P_L\right] \\[2mm]
&- (\gamma - 1)\frac{\partial}{\partial \boldsymbol{\eta}}\left[\left(\left\langle\tau_{ij}\frac{\partial u_i}{\partial x_j}\,\Big|\,\boldsymbol{v},\boldsymbol{\psi},\boldsymbol{\theta},\boldsymbol{\eta}\right\rangle_\ell - \breve{\tau}_{ij}\frac{\partial \langle u_i\rangle_L}{\partial x_j}\right)P_L\right] \\[2mm]
&+ \gamma\frac{\partial}{\partial \boldsymbol{\eta}}\left[\left(\left\langle p\frac{\partial u_j}{\partial x_j}\,\Big|\,\boldsymbol{v},\boldsymbol{\psi},\boldsymbol{\theta},\boldsymbol{\eta}\right\rangle_\ell - \langle p\rangle_\ell\frac{\partial \langle u_j\rangle_L}{\partial x_j}\right)P_L\right].
\end{aligned}
$$

$$(3.36)$$

3.3 MODELED EPVS-FMDF TRANSPORT EQUATION

For closure of the EPVS-FMDF transport equation, we consider the general diffusion process,[52] given by the system of stochastic differential equations (SDEs):

$$
\begin{aligned}
dX_i^+(t) &= D_i^X dt + B_{ij}^X dW_j^X(t) + F_{ij}^{XU} dW_j^U(t) + F_{ij}^{X\phi} dW_j^\phi(t) \\
&\quad + F_{ij}^{XE} dW_j^E(t) + F_{ij}^{XP} dW_j^P(t),
\end{aligned}
\tag{3.37a}
$$

$$
\begin{aligned}
dU_i^+(t) &= D_i^U dt + B_{ij}^U dW_j^U(t) + F_{ij}^{UX} dW_j^X(t) + F_{ij}^{U\phi} dW_j^\phi(t) \\
&\quad + F_{ij}^{UE} dW_j^E(t) + F_{ij}^{UP} dW_j^P(t),
\end{aligned}
\tag{3.37b}
$$

$$
\begin{aligned}
d\phi_\alpha^+(t) &= D_\alpha^\phi dt + B_{\alpha j}^\phi dW_j^\phi(t) + F_{\alpha j}^{\phi X} dW_j^X(t) + F_{\alpha j}^{\phi U} dW_j^U(t) \\
&\quad + F_{\alpha j}^{\phi E} dW_j^E(t) + F_{\alpha j}^{\phi P} dW_j^P(t),
\end{aligned}
\tag{3.37c}
$$

$$
\begin{aligned}
dE^+(t) &= D^E dt + B_j^E dW_j^E(t) + F_j^{EX} dW_j^X(t) + F_j^{EU} dW_j^U(t) \\
&\quad + F_j^{E\phi} dW_j^\phi(t) + F_j^{EP} dW_j^P(t),
\end{aligned}
\tag{3.37d}
$$

$$
\begin{aligned}
dP^+(t) &= D^P dt + B_j^P dW_j^P(t) + F_j^{PX} dW_j^X(t) + F_j^{PU} dW_j^U(t) \\
&\quad + F_j^{P\phi} dW_j^\phi(t) + F_j^{PE} dW_j^E(t).
\end{aligned}
\tag{3.37e}
$$

where X_i^+, U_i^+, ϕ_α^+, E^+, P^+ are probabilistic representations of position, velocity vector, scalars, pressure and energy variables. The coefficients in Eq. (3.37) can be also a function of position, velocity vector, scalar, pressure and energy variables as well. The $D(\mathbf{X}^+, \mathbf{U}^+, \boldsymbol{\phi}^+, \mathbf{E}^+, \mathbf{P}^+; t)$ terms denote drift coefficient, the $B(\mathbf{X}^+, \mathbf{U}^+, \boldsymbol{\phi}^+, \mathbf{E}^+, \mathbf{P}^+; t)$ terms denote diffusion, the $F(\mathbf{X}^+, \mathbf{U}^+, \boldsymbol{\phi}^+, \mathbf{E}^+, \mathbf{P}^+; t)$ terms denote diffusion couplings, and the W terms denote the Wiener-Lévy processes.[55,56]

Following Refs. [4,11,27,53,54] we utilize the simplified Langevin model (SLM) and linear mean-square estimation (LMSE).[74] In order to model the internal energy and the pressure, following Refs. [75,76] we utilize the first law of thermodynamics and equation of state (for an ideal gas with constant specific heats):

$$
dX_i^+ = U_i^+ dt + \sqrt{\frac{2\mu}{\langle\rho\rangle_\ell}} dW_i, \tag{3.38a}
$$

$$
\begin{aligned}
dU_i^+ = {} & -\frac{1}{\langle\rho\rangle_\ell}\frac{\partial\langle p\rangle_\ell}{\partial x_i}dt + \frac{2}{\langle\rho\rangle_\ell}\frac{\partial}{\partial x_j}\left(\mu\frac{\partial\langle u_i\rangle_L}{\partial x_j}\right)dt \\
& + \frac{1}{\langle\rho\rangle_\ell}\frac{\partial}{\partial x_j}\left(\mu\frac{\partial\langle u_j\rangle_L}{\partial x_i}\right)dt - \frac{2}{3}\frac{1}{\langle\rho\rangle_\ell}\frac{\partial}{\partial x_i}\left(\mu\frac{\partial\langle u_j\rangle_L}{\partial x_j}\right)dt \\
& + G_{ij}\left(U_j^+ - \langle u_j\rangle_L\right)dt + \sqrt{C_0\frac{\epsilon}{\langle\rho\rangle_\ell}}dW_i' + \sqrt{\frac{2\mu}{\langle\rho\rangle_\ell}}\frac{\partial\langle u_i\rangle_L}{\partial x_j}dW_j, \tag{3.38b}
\end{aligned}
$$

$$
d\phi_\alpha^+ = -C_\phi\omega\left(\phi_\alpha^+ - \langle\phi_\alpha\rangle_L\right)dt, \tag{3.38c}
$$

$$
\begin{aligned}
dE^+ = {} & \left(-\frac{C_e\omega}{\gamma}\left(E^+ - \langle e\rangle_L\right) + \frac{1}{\gamma}\left(\frac{\epsilon}{\rho^+} + \frac{\breve{\tau}_{ij}}{\rho^+}\frac{\partial\langle u_i\rangle_\ell}{\partial x_j}\right) + \frac{\gamma-1}{\gamma}E^+\left(A - \frac{B^2}{\gamma}\right)\right)dt \\
& + \frac{\gamma-1}{\gamma}E^+ B dW_p, \tag{3.38d}
\end{aligned}
$$

$$
dP^+ = P^+\left(Adt + BdW_p\right) \tag{3.38e}
$$

where

$$
G_{ij} = \frac{\Pi_d}{2k\langle\rho\rangle_\ell} - \omega\left(\frac{1}{2} + \frac{3}{4}C_0\right)\delta_{ij},
$$

$$
k = \frac{1}{2}\tau_L\left(u_i, u_i\right),
$$

$$
\epsilon = \langle\rho\rangle_\ell C_\epsilon\frac{k^{3/2}}{\Delta_L},
$$

$$
\omega = \frac{1}{\langle\rho\rangle_\ell}\frac{\epsilon}{k},
$$

$$
\Pi_d = C_\Pi\left(\left\langle\langle p\rangle_\ell\frac{\partial\langle u_i\rangle_L}{\partial x_i}\right\rangle_{\ell_2} - \langle\langle p\rangle_\ell\rangle_{\ell_1}\frac{\partial\langle\langle u_i\rangle_L\rangle_{L_2}}{\partial x_i}\right),
$$

$$
\begin{aligned}
A = {} & -\frac{C_e\omega}{E^+}\left(E^+ - \langle e\rangle_L\right) + \frac{1}{E^+}\left(\frac{\epsilon}{\rho^+} + \frac{1}{\rho^+}\breve{\tau}_{ij}\frac{\partial\langle u_i\rangle_L}{\partial x_j}\right) - \gamma\frac{\Pi_d}{\tau_\ell\left(p,p\right)}\left(P^+ - \langle p\rangle_\ell\right) - \gamma\frac{\partial\langle u_i\rangle_L}{\partial x_i} \\
& - \frac{\gamma}{\gamma-1}\frac{1}{\rho^+ E^+}\left(\frac{\partial\breve{q}_i}{\partial x_i} + \frac{\partial}{\partial x_i}\left(\mu\frac{\partial\langle e\rangle_L}{\partial x_i}\right)\right),
\end{aligned}
$$

$$
B = 0. \tag{3.39}
$$

Here ω is the SGS mixing frequency, ϵ is the dissipation rate, k is the SGS kinetic energy, and Δ_L is the LES filter size. The parameters C_0, C_ϕ, C_e, C_ϵ and C_Π are model constants and need to be specified.[28,77] In this equations, A and B are the drift and diffusion coefficients for the energy and the pressure stochastic equations, respectively. The dissipation term ϵ and the pressure dilatation term Π_d are modeled.[27,77] The Fokker-Planck equation,[78] $F_L(\boldsymbol{v}, \boldsymbol{\psi}, \boldsymbol{\theta}, \boldsymbol{\eta}, \mathbf{x}; t)$, the joint PDF of U^+, ϕ^+, $\mathbf{E}^+$, $\mathbf{P}^+$ and $\mathbf{X}^+$ is:

$$
\begin{aligned}
\frac{\partial F_L}{\partial t} + \frac{\partial v_i F_L}{\partial x_i} &= \frac{1}{\langle \rho \rangle_\ell} \frac{\partial \langle p \rangle_\ell}{\partial x_i} \frac{\partial F_L}{\partial v_i} - \frac{2}{\langle \rho \rangle_\ell} \frac{\partial}{\partial x_j} \left(\mu \frac{\partial \langle u_i \rangle_L}{\partial x_j} \right) \frac{\partial F_L}{\partial v_i} - \frac{1}{\langle \rho \rangle_\ell} \frac{\partial}{\partial x_j} \left(\mu \frac{\partial \langle u_j \rangle_L}{\partial x_i} \right) \frac{\partial F_L}{\partial v_i} \\
&+ \frac{2}{3} \frac{1}{\langle \rho \rangle_\ell} \frac{\partial}{\partial x_i} \left(\mu \frac{\partial \langle u_j \rangle_L}{\partial x_j} \right) \frac{\partial F_L}{\partial v_i} - \frac{\partial \left(G_{ij} \left(v_j - \langle u_j \rangle_L \right) F_L \right)}{\partial v_i} + \frac{\partial}{\partial x_i} \left(\mu \frac{\partial (F_L / \langle \rho \rangle_\ell)}{\partial x_i} \right) \\
&+ \frac{\partial}{\partial x_i} \left(\frac{2\mu}{\langle \rho \rangle_\ell} \frac{\partial \langle u_j \rangle_L}{\partial x_i} \frac{\partial F_L}{\partial v_j} \right) + \frac{\mu}{\langle \rho \rangle_\ell} \frac{\partial \langle u_k \rangle_L}{\partial x_j} \frac{\partial \langle u_i \rangle_L}{\partial x_j} \frac{\partial^2 F_L}{\partial v_k \partial v_i} + \frac{1}{2} C_0 \frac{\epsilon}{\langle \rho \rangle_\ell} \frac{\partial^2 F_L}{\partial v_i \partial v_i} \\
&+ C_\phi \omega \frac{\partial \left(\left(\psi_\alpha - \langle \phi_\alpha \rangle_L \right) F_L \right)}{\partial \psi_\alpha} \\
&+ \frac{C_e \omega}{\gamma} \frac{\partial \left(\left(\theta - \langle e \rangle_L \right) F_L \right)}{\partial \theta} \\
&- \frac{\gamma - 1}{\gamma} \left(\epsilon + \breve{\tau}_{ij} \frac{\partial \langle u_i \rangle_L}{\partial x_j} \right) \frac{\partial}{\partial \theta} \left(\frac{\theta}{\eta} F_L \right) \\
&- \frac{\gamma - 1}{\gamma} \frac{\partial \left(\theta A F_L \right)}{\partial \theta} + \frac{\gamma - 1}{\gamma^2} \frac{\partial \left(\theta B^2 F_L \right)}{\partial \theta} - \frac{\partial \left(\eta A F_L \right)}{\partial \eta} \\
&+ \frac{1}{2} \frac{(\gamma - 1)^2}{\gamma^2} \frac{\partial^2 \left(\theta^2 B^2 F_L \right)}{\partial \theta \partial \theta} + \frac{\gamma - 1}{\gamma} \frac{\partial^2 \left(\theta \eta B^2 F_L \right)}{\partial \theta \partial \eta} + \frac{1}{2} \frac{\partial^2 \left(\eta^2 B^2 F_L \right)}{\partial \eta \partial \eta}.
\end{aligned}
$$

$$(3.40)$$

The transcript equations for the first order moments are obtained by integration of Eq. (3.40) according to Eq. (3.31):

$$\frac{\partial \langle \rho \rangle_\ell}{\partial t} + \frac{\partial \langle \rho \rangle_\ell \langle u_j \rangle_L}{\partial x_j} = 0, \tag{3.41a}$$

$$\frac{\partial \langle \rho \rangle_\ell \langle u_i \rangle_L}{\partial t} + \frac{\partial \langle \rho \rangle_\ell \langle u_j \rangle_L \langle u_i \rangle_L}{\partial x_j} = -\frac{\partial \langle p \rangle_\ell}{\partial x_i} + \frac{\partial \breve{\tau}_{ij}}{\partial x_j} - \frac{\partial \langle \rho \rangle_\ell \tau_L(u_i, u_j)}{\partial x_j}, \tag{3.41b}$$

$$\frac{\partial \langle \rho \rangle_\ell \langle e \rangle_L}{\partial t} + \frac{\partial \langle \rho \rangle_\ell \langle u_j \rangle_L \langle e \rangle_L}{\partial x_j} = -\frac{\partial \breve{q}_j}{\partial x_j} - \frac{\partial \langle \rho \rangle_\ell \tau_L(e, u_j)}{\partial x_j}$$

$$+ \epsilon + \breve{\tau}_{ij} \frac{\partial \langle u_i \rangle_L}{\partial x_j} - \Pi_d - \langle p \rangle_\ell \frac{\partial \langle u_i \rangle_L}{\partial x_i}, \tag{3.41c}$$

$$\frac{\partial \langle \rho \rangle_\ell \langle \phi_\alpha \rangle_L}{\partial t} + \frac{\partial \langle \rho \rangle_\ell \langle u_j \rangle_L \langle \phi_\alpha \rangle_L}{\partial x_j} = -\frac{\partial}{\partial x_j} \left(-\mu \frac{\partial \langle \phi_\alpha \rangle_L}{\partial x_j} \right) - \frac{\partial \langle \rho \rangle_\ell \tau_L(\phi_\alpha, u_j)}{\partial x_j}. \tag{3.41d}$$

Assuming $\mu = \rho \Gamma$; *i.e.* unity Schmidt (Sc) numbers, the set of Eqs. (3.41) are identical to Eq. (3.5).

The transport equations for the second order correlations are obtained by integration of Eq. (3.40) according to Eq. (3.31). The second order modeled correlations for velocity and scalar variables are governed by:

$$
\frac{\partial \langle \rho \rangle_\ell \tau_L (u_i, u_j)}{\partial t} + \frac{\partial \langle \rho \rangle_\ell \langle u_k \rangle_L \tau_L (u_i, u_j)}{\partial x_k} = \langle \rho \rangle_\ell P_{ij} - \frac{\partial \langle \rho \rangle_\ell \tau_L (u_k, u_i, u_j)}{\partial x_k}
$$

$$
+ \quad G_{jk} \langle \rho \rangle_\ell \tau_L (u_k, u_i) + G_{ik} \langle \rho \rangle_\ell \tau_L (u_k, u_j)
$$

$$
+ \quad \frac{\partial}{\partial x_k} \left(\mu \frac{\partial \tau_L (u_i, u_j)}{\partial x_k} \right) + C_0 \epsilon \delta_{ij}, \tag{3.42}
$$

$$
\frac{\partial \langle \rho \rangle_\ell \tau_L (\phi_\alpha, \phi_\beta)}{\partial t} + \frac{\partial \langle \rho \rangle_\ell \langle u_k \rangle_L \tau_L (\phi_\alpha, \phi_\beta)}{\partial x_k} = \langle \rho \rangle_\ell P^{\alpha\beta} - \frac{\partial \langle \rho \rangle_\ell \tau_L (u_k, \phi_\alpha, \phi_\beta)}{\partial x_k}
$$

$$
+ \quad 2\mu \frac{\partial \langle \phi_\alpha \rangle_L}{\partial x_k} \frac{\partial \langle \phi_\beta \rangle_L}{\partial x_k}
$$

$$
+ \quad \frac{\partial}{\partial x_k} \left(\mu \frac{\partial \tau_L (\phi_\alpha, \phi\beta)}{\partial x_k} \right) - 2C_\phi \omega \langle \rho \rangle_\ell \tau_L (\phi_\alpha, \phi_\beta),
$$

$$
\tag{3.43}
$$

$$
\frac{\partial \langle \rho \rangle_\ell \tau_L (u_i, \phi_\alpha)}{\partial t} + \frac{\partial \langle \rho \rangle_\ell \langle u_k \rangle_L \tau_L (u_i, \phi_\alpha)}{\partial x_k} = \langle \rho \rangle_\ell P_i^\alpha - \frac{\partial \langle \rho \rangle_\ell \tau_L (u_k, u_i, \phi_\alpha)}{\partial x_k}
$$

$$
+ \quad \frac{\partial}{\partial x_k} \left(\mu \frac{\partial \tau_L (u_i, \phi_\alpha)}{\partial x_k} \right)
$$

$$
+ \quad G_{ik} \langle \rho \rangle_\ell \tau_L (u_k, \phi_\alpha) - C_\phi \omega \langle \rho \rangle_\ell \tau_L (u_i, \phi_\alpha).
$$

$$
\tag{3.44}
$$

By integration of Eq. (3.40) according to Eq. (3.31), the second order modeled velocity-energy correlations are governed by:

$$
\frac{\partial \langle \rho \rangle_\ell \, \tau_L \, (u_i, e)}{\partial t} + \frac{\partial \langle \rho \rangle_\ell \, \langle u_k \rangle_L \, \tau_L \, (u_i, e)}{\partial x_k} \;=\; \langle \rho \rangle_\ell \, P_i^e - \frac{\partial \langle \rho \rangle_\ell \, \tau_L \, (u_k, u_i, e)}{\partial x_k}
$$

$$
+ \;\; \frac{\partial}{\partial x_k} \left(\mu \frac{\partial \tau_L \, (u_i, e)}{\partial x_k} \right)
$$

$$
+ \;\; G_{ik} \, \langle \rho \rangle_\ell \, \tau_L \, (u_k, e) - C_e \omega \, \langle \rho \rangle_\ell \, \tau_L \, (u_i, e)
$$

$$
- \;\; (\gamma - 1) \, \langle \rho \rangle_\ell \, \tau_L \, (u_i, e) \, \frac{\partial \langle u_k \rangle_L}{\partial x_k}
$$

$$
- \;\; \frac{\langle p \rangle_\ell \, \tau \, (p, u_i) + \tau \, (p, p, u_i)}{\tau_\ell \, (p, p)} \Pi_d
$$

$$
+ \;\; (\langle e \rangle_\ell - \langle e \rangle_L) \left(\epsilon + \breve{\tau}_{ij} \frac{\partial \langle u_i \rangle_L}{\partial x_j} \right)
$$

$$
- \;\; (\langle e \rangle_\ell - \langle e \rangle_L) \left(\frac{\partial \breve{q}_i}{\partial x_i} + \frac{\partial}{\partial x_j} \left(\mu \frac{\partial \langle e \rangle_L}{\partial x_j} \right) \right).
$$

$$(3.45)$$

In Eq. (3.45), the subgrid terms without the subscripts are defined as:

$$
\tau \, (p, u_i) \;=\; \langle p u_i \rangle_\ell - \langle p \rangle_\ell \, \langle u_i \rangle_L , \tag{3.46a}
$$

$$
\tau \, (p, p, u_i) \;=\; \langle p^2 u_i \rangle_\ell - 2 \langle p \rangle_\ell \, \tau \, (p, u_i) - \langle u_i \rangle_L \, \tau_\ell \, (p, p) - \langle p \rangle_\ell^2 \, \langle u_i \rangle_L . \tag{3.46b}
$$

By integration of Eq. (3.40) according to Eq. (3.31), the second order modeled energy correlations are governed by:

$$\frac{\partial \langle \rho \rangle_\ell \frac{\tau_L(e,e)}{2}}{\partial t} + \frac{\partial \langle \rho \rangle_\ell \langle u_k \rangle_L \frac{\tau_L(e,e)}{2}}{\partial x_k} = \langle \rho \rangle_\ell P^{ee} - \frac{1}{2} \frac{\partial \langle \rho \rangle_\ell \tau_L(u_k, e, e)}{\partial x_k}$$

$$+ \frac{\partial}{\partial x_k} \left(\mu \frac{\partial \frac{\tau_L(e,e)}{2}}{\partial x_k} \right)$$

$$+ \mu \frac{\partial \langle e \rangle_L}{\partial x_k} \frac{\partial \langle e \rangle_L}{\partial x_k}$$

$$- C_e \omega \langle \rho \rangle_\ell \tau_L(e,e)$$

$$- (\gamma - 1) \langle \rho \rangle_\ell \tau_L(e,e) \frac{\partial \langle u_k \rangle_L}{\partial x_k}$$

$$- \frac{\langle p \rangle_\ell \tau(p,e) + \tau(p,p,e)}{\tau_\ell(p,p)} \Pi_d$$

$$+ (\langle e \rangle_\ell - \langle e \rangle_L) \left(\epsilon + \breve{\tau}_{ij} \frac{\partial \langle u_i \rangle_L}{\partial x_j} \right)$$

$$- (\langle e \rangle_\ell - \langle e \rangle_L) \left(\frac{\partial \breve{q}_i}{\partial x_i} + \frac{\partial}{\partial x_j} \left(\mu \frac{\partial \langle e \rangle_L}{\partial x_j} \right) \right). \quad (3.47)$$

In Eq. (3.47), the subgrid terms without the subscripts are defined as:

$$\tau(p,e) = \langle pe \rangle_\ell - \langle p \rangle_\ell \langle e \rangle_L, \quad (3.48a)$$

$$\tau(p,p,e) = \langle p^2 e \rangle_\ell - 2 \langle p \rangle_\ell \tau(p,e) - \langle e \rangle_L \tau_\ell(p,p) - \langle p \rangle_\ell^2 \langle e \rangle_L. \quad (3.48b)$$

By integration of Eq. (3.40) according to Eq. (3.31), the second order modeled pressure correlations are governed by:

$$
\frac{\partial \frac{\tau_\ell(p,p)}{2}}{\partial t} + \langle u_j \rangle_L \frac{\partial \frac{\tau_\ell(p,p)}{2}}{\partial x_j} = P^{pp} - \frac{1}{2} \frac{\partial \tau(p,p,u_k)}{\partial x_k} - \gamma \langle p \rangle_\ell \Pi_d
$$

$$
- \gamma \tau_\ell(p,p) \frac{\partial \langle u_i \rangle_L}{\partial x_i} + \frac{\partial}{\partial x_i} \left(\mu \frac{\partial \frac{\tau_L(p,p)}{2}}{\partial x_i} \right)
$$

$$
+ \mu \frac{\partial \langle p \rangle_L}{\partial x_i} \frac{\partial \langle p \rangle_L}{\partial x_i}
$$

$$
- (\gamma - 1) C_e \omega \langle \rho \rangle_\ell \tau_L(p,e)
$$

$$
- \frac{2\gamma - 1}{2} \frac{\tau_\ell(p,p,p)}{\tau_\ell(p,p)} \Pi_d
$$

$$
- \frac{1}{2} \left(\lambda \frac{\partial \langle T \rangle_L}{\partial x_j} - (2\gamma - 1) \mu c_v \frac{\partial \langle T \rangle_L}{\partial x_j} \right) \frac{\partial \langle p \rangle_\ell}{\partial x_j}
$$

$$
+ \frac{1}{2} \frac{\partial}{\partial x_j} \left[\langle p \rangle_\ell \left(\lambda \frac{\partial \langle T \rangle_L}{\partial x_j} - (2\gamma - 1) \mu c_v \frac{\partial \langle T \rangle_L}{\partial x_j} \right) + \mu \frac{\partial \langle p \rangle_L \langle p \rangle_L}{\partial x_j} \right].
$$

$$(3.49)$$

In Eq. (3.49), the subgrid terms without the subscripts are defined as:

$$
\tau(p, u_k) = \langle p u_k \rangle_\ell - \langle p \rangle_\ell \langle u_k \rangle_L, \tag{3.50a}
$$

$$
\tau(p, p, u_k) = \langle p^2 u_k \rangle_\ell - 2 \langle p \rangle_\ell \tau(p, u_k) - \langle u_k \rangle_L \tau_\ell(p,p) - \langle p \rangle_\ell^2 \langle u_k \rangle_L. \tag{3.50b}
$$

Assuming $\mu c_v = \lambda$; *i.e.* Prandtl (Pr) number equal to γ, the transport equation for the second order modeled energy correlations, Eq. (3.47), modeled energy-velocity correlations, Eq. (3.45), and pressure correlations, Eq. (3.49), will be good approximations to their exact counterparts, Eq. (3.20), Eq. (3.17) and Eq. (3.23).

51

3.4 NUMERICAL PROCEDURE

Numerical solution of the modeled EPVS-FMDF transport equation is obtained by a hybrid finite-difference/Monte Carlo procedure. The basis is similar to those in RAS,[79,80] in previous FDF simulations[4,5,27] and in VS-FMDF simulations.[28] For simulations, the FDF is represented by an ensemble of N_p statistically identical Monte Carlo (MC) particles. Each particle carries information pertaining to its position, $\mathbf{X}^{(n)}(t)$, velocity, $\boldsymbol{U}^{(n)}(t)$, scalar value, $\boldsymbol{\phi}^{(n)}(t)$, $n = 1, \ldots, N_p$, energy, $\mathbf{E}^{(n)}(t)$ and pressure, $\mathbf{P}^{(n)}(t)$. This information is updated via temporal integration of the SDEs. The simplest way of performing this integration is via Euler-Maruyama discretization.[81] For example, for Eq. (3.37a),

$$
\begin{aligned}
X_i^n(t_{k+1}) = {}& X_i^n(t_k) + \left(D_i^X(t_k)\right)^n \Delta t + \left(B_{ij}^X(t_k)\right)^n (\Delta t)^{1/2} \left(\zeta_j^X(t_k)\right)^n \\
& + \left(F_{ij}^{XU}(t_k)\right)^n (\Delta t)^{1/2} \left(\zeta_j^U(t_k)\right)^n + \left(F_{ij}^{X\phi}(t_k)\right)^n (\Delta t)^{1/2} \left(\zeta_j^\phi(t_k)\right)^n \\
& + \left(F_{ij}^{XE}(t_k)\right)^n (\Delta t)^{1/2} \left(\zeta_j^E(t_k)\right)^n + \left(F_{ij}^{XP}(t_k)\right)^n (\Delta t)^{1/2} \left(\zeta_j^P(t_k)\right)^n, \quad (3.51)
\end{aligned}
$$

where $D_i(t_k) = D_i(\mathbf{X}^{(n)}(t_k), \boldsymbol{U}^{(n)}(t_k), \boldsymbol{\phi}^{(n)}(t_k), \mathbf{E}^{(n)}(t_k), \mathbf{P}^{(n)}(t_k); t_k)$, $\ldots$, and $\zeta(t_k)$'s are independent standardized Gaussian random variables. This scheme preserves the Itô-Gikhman character of the SDEs.[82]

The computational domain is discretized on equally spaced finite-difference grid points. These points are used for three purposes: (1) to identify the regions where the statistical information from the MC simulations are obtained and (2) to perform a set of complementary LES primarily by the finite-difference methodology for assessing the consistency and convergence of the MC results. The LES procedure via the finite-difference discretization is referred to as LES-FD and will be further discussed below.

Statistical information is obtained by considering an ensemble of N_E computational particles residing within an ensemble domain of characteristic length Δ_E centered around each of the finite-difference grid points. This is illustrated schematically in Fig. (14). For reliable statistics with minimal numerical dispersion, it is desired to minimize the size of ensemble

domain and maximize the number of the MC particles.[47] In this way, the ensemble statistics would tend to the desired filtered values:

$$
\begin{aligned}
\langle a \rangle_E &\equiv \frac{1}{N_E} \sum_{n \in \Delta_E} a^{(n)} \xrightarrow[\substack{N_E \to \infty \\ \Delta_E \to 0}]{} \langle a \rangle_L, \\
\tau_E(a,b) &\equiv \left(\frac{1}{N_E} \sum_{n \in \Delta_E} a^{(n)} b^{(n)} \right) - \langle a \rangle_E \langle b \rangle_E \xrightarrow[\substack{N_E \to \infty \\ \Delta_E \to 0}]{} \tau_L(a,b),
\end{aligned}
\tag{3.52}
$$

where $a^{(n)}$ denotes the information carried by n^{th} MC particle pertaining to transport variable a. To reduce the computational cost, a procedure involving the use of non-uniform weights[5] is also considered. This procedure allows a smaller number of particles in regions where a low degree of variability is expected. Conversely, in regions of high variability, a large number of particles is allowed. It has been shown[5,47] that the sum of weights within the ensemble domain is related to filtered fluid density as

$$
\langle \rho \rangle_l \approx \frac{\Delta m}{V_E} \sum_{n \in \Delta_E} w^{(n)}, \tag{3.53}
$$

where V_E is the volume of ensemble domain and Δm is the mass of particle with unit weight. The Favre-filtered value of a transport quantity $Q(\boldsymbol{v}, \boldsymbol{\phi})$ is constructed from the weighted average as

$$
\langle Q \rangle_L \approx \frac{\sum_{n \in \Delta_E} w^{(n)} Q(\boldsymbol{v}^{(n)}, \boldsymbol{\phi}^{(n)})}{\sum_{n \in \Delta_E} w^{(n)}}. \tag{3.54}
$$

With uniform weights,[47] the particle number density decreases significantly in regions of low density such as reaction zone. The implementation of variable weight allows the increase in particle density without increasing the particle number density in these regions.

The LES-FD solver is based on the forth order finite-difference scheme.[58] This is a variant of the MacCormack scheme in which fourth-order differencing schemes are used to approximate the spatial derivatives, and second-order symmetric predictor-corrector sequence is employed for time discretization. All of the finite-difference operations are conducted on fixed grid points. The transfer of information from the grid points to the MC particles is accomplished via a linear interpolation. The transfer of information from the particles to the grid points is accomplished via ensemble averaging as described above.

The transport equations to be solved by the LES-FD solver include unclosed second order moments which are obtained from the MC solver. The LES-FD also determines the filtered velocity, scalar fields, density and energy field. That is, there is a "redundancy" in the determination of the first filtered moments as both the LES-FD and the MC procedures provides the solution of this field. This redundancy is actually very useful in monitoring the accuracy of the simulated results.[5,27,79,80]

3.5   FLOW CONFIGURATION AND SIMULATION PARAMETERS

Simulations are conducted of a three-dimensional temporally developing mixing layer involving transport of a passive scalar variable. These simulations are used to assess the consistency and the overall capabilities of the EPVS-FMDF methodology. The predictions are compared with data obtained by direct numerical simulation (DNS) of the same layer. In the representation below, x, y and z denote the streamwise, the cross-stream, and the spanwise directions, respectively. The velocity components along these directions are denoted by u, v and w in the x, y and z directions, respectively. The temporal mixing layer consists of two parallel streams traveling in opposite directions with the same speed.[83–85] Both the filtered streamwise velocity, scalar fields are initialized with a hyperbolic tangent profiles with $\langle u \rangle_L = 1$, $\langle \phi \rangle_L = 1$, on the top stream and $\langle u \rangle_L = -1$, $\langle \phi \rangle_L = 0$ on the bottom stream. The density and temperature fields are initially uniform $\langle \rho \rangle_\ell = 1$, $\langle T \rangle_L = 1$. The length L_v is specified such that $L_v = 2^{N_P} \lambda_u$, where N_P is the desired number of successive vortex pairings and λ_u is the wavelength of the most unstable mode corresponding to the mean streamwise velocity profile imposed at the initial time. The flow variables are normalized with respect to the half initial vorticity thickness, $L_r = \frac{\delta_v(t=0)}{2}$, ($\delta_v = \frac{\Delta U}{|\partial \overline{\langle u \rangle}_L / \partial y|_{max}}$, where $\overline{\langle u \rangle_L}$ is the Reynolds-averaged value of the filtered streamwise velocity and ΔU is the velocity difference across the layer). The reference velocity is $U_r = \Delta U/2$. In these simulations, the Reynolds number is $Re = \frac{U_r L_r}{\nu} = 50$ and the Mach number is $Ma = \frac{U_r}{\sqrt{\gamma R T_r}} = 0.6$.

The temporal simulations are conducted for a cubic box, $0 \leq x \leq L$, $\frac{-L}{2} \leq y \leq \frac{L}{2}$, $0 \leq z \leq L$ where $L = L_v/L_r$. The 3D field is parameterized in a procedure somewhat similar to

that by Vreman *et al.*[86] The formation of the large scale structures are expedited through eigenfunction based initial perturbations.[87,88] This includes two-dimensional[84,86,89] and three-dimensional[84,90] perturbations with a random phase shift between the $3D$ modes. This results in the formation of two successive vortex pairings and strong three-dimensionality.

Simulations are conducted on equally-spaced grid points. The temporal simulations, have grid spacings $\Delta x = \Delta y = \Delta z = \Delta$ with the number of grid points 193^3 and 65^3 for DNS and LES, respectively. To filter the DNS data, a top-hat function of the form below is used with $\Delta_L = 2\Delta$,

$$G(\mathbf{x}' - \mathbf{x}) = \prod_{i=1}^{3} \widetilde{G}(x_i' - x_i),$$

$$\widetilde{G}(x_i' - x_i) = \begin{cases} \frac{1}{\Delta_L} & |x_i' - x_i| \leq \frac{\Delta_L}{2}, \\ 0 & |x_i' - x_i| > \frac{\Delta_L}{2}, \end{cases} \tag{3.55}$$

No attempt is made to investigate the sensitivity of the results to the filter function[51] or the size of the filter.[91–93]

A hyperbolic tangent profile is utilized to assign the velocity, scalar and uniform temperature and density profiles initially. The temporal simulations are conducted with periodic boundary conditions in homogeneous directions (x and z) and zero-derivative boundary condition in cross-stream direction. All simulations are performed with variable particle weights.[5] In temporal simulations, the MC particles are initially distributed throughout the computational region in a random fashion. Due to flow periodicity in the streamwise and spanwise directions, if the particle leaves the domain at one of these boundaries, new particles are introduced at the other boundary with the same velocity, compositional, energy and pressure values. In the cross-stream directions, the free-slip boundary condition is satisfied by the mirror-reflection of the particles leaving through these boundaries. The particle weights are set according to filtered fluid density at the initial time. The number of particles per grid point is $NPG = 64$ ($N_E = 64$) and the ensemble domain size (Δ_E) is set equal to the grid spacing in each (x, y or z) direction. The effects of both of these parameters are assessed in the previous works.[4,5,27,28] All results are analyzed both "instantaneously" and "statistically." In the former, the instantaneous scatter plots of the variables of interest are

analyzed. In the latter, the "Reynolds-averaged" statistics constructed from the instantaneous data are considered. These are constructed by spatial averaging over homogeneous directions (x and z). All Reynolds-averaged results are denoted by an overbar.

No attempt is made to determine the appropriate values of the model constants; the values suggested in the literature are adopted[94] $C_0 = 2.1$, $C_\epsilon = 1$, $C_\phi = 1$, $C_e = 1$ and $C_\Pi = 0.0$. The model parameters are the same as those suggested by Sheikhi et $al.$[28] No attempt is made to optimize the values of these parameters. The values of $Sc = 1$ and $Pr = 1.4$ are set accordingly.

3.6 RESULTS

The first objective of this section is to demonstrate the consistency of the EPVS-FMDF formulation. Since the accuracy of the LES-FD procedure is well-established (at least for the first order filtered quantities), such a comparative assessment provides a good means of assessing the performance of the MC solution. Consistency assessments are obtained by presenting the scatter plots of instantaneous results obtained from LES-FD and MC. The consistency assessment for flow variables at $t = 80$ is presented in Fig. (15). As shown, the MC density

$$\langle \rho \rangle^{MC} \equiv \left(\frac{\sum_{n \in \Delta_E} w^{(n)} \left(1/\rho^{(n)} \right)}{\sum_{n \in \Delta_E} w^{(n)}} \right)^{-1} \tag{3.56}$$

is in good agreement with the filtered density obtained from LES-FD. The consistency is observed for all first order moments; the regression and the 45° lines almost coincide.

The second objective of this section is to analyze some of the characteristics of the EPVS-FMDF via comparative assessments against DNS data. Figure (16) shows the instantaneous iso-surface of the scalar field ($\langle \phi \rangle_L$) obtained by EPVS-FMDF at $t = 80$. By this time, the flow is going through pairings and exhibits strong 3D effects. This is evident by the formation of large scale spanwise rollers with the presence of secondary structures in streamwise planes.[87] For comparison, the DNS data are filtered from the original high

resolution 193^3 points to the coarse 65^3 points. The Reynolds-averaged values of the filtered first order moments at $t = 80$ are shown in Fig. (17). In the comparisons, we also consider the "resolved" and the "total" components of the Reynolds-averaged moments. The former is denoted by $R(a,b) = \frac{1}{\overline{\langle \rho \rangle_\ell}} \left(\overline{\langle \rho \rangle_\ell \langle a \rangle_L \langle b \rangle_L} - \frac{\overline{\langle \rho \rangle_\ell \langle a \rangle_L} \; \overline{\langle \rho \rangle_\ell \langle b \rangle_L}}{\overline{\langle \rho \rangle_\ell}} \right)$; and the latter is $r(a,b) = \widetilde{ab} - \widetilde{a}\widetilde{b}$; in which overbar indicates the Reynolds averaging operation and overtilde is the Favre Reynolds averaging operation; This operation is denoted by $\widetilde{a} = \frac{\overline{\rho a}}{\overline{\rho}} \approx \frac{\overline{\langle \rho a \rangle_\ell}}{\overline{\langle \rho \rangle_\ell}}$. In DNS, the "total" components are directly available, while in LES they are approximated by $r(a,b) \approx R(a,b) + \tau_L^F(a,b)$, in which $\tau_L^F(a,b) = \frac{\overline{\langle \rho \rangle_\ell \tau_L(a,b)}}{\overline{\langle \rho \rangle_\ell}}$.[95] Several components of the Reynolds-averaged values of the second order moments of the resolved, subgrid and the total field are compared with DNS data in Figs. (18)-(25). As it is shown, EPVS-FMDF yields accurate predictions of the resolved, the SGS and the total fields.

All EPVS-FMDF predictions compare well with DNS data in predicting the spread of the layer as indicated in Figs. (26) and (27). Figure (26) shows the temporal variations of the "scalar thickness,"

$$\delta_s(t) = \left| y(\langle \widetilde{\phi} \rangle_L = 0.9) \right| + \left| y(\langle \widetilde{\phi} \rangle_L = 0.1) \right|, \tag{3.57}$$

and the "momentum thickness,"[96]

$$\delta_m(t) = \frac{1}{4} \int_{-\infty}^{+\infty} \overline{\langle \rho \rangle_\ell} \left(1 - \frac{\overline{\langle \rho \rangle_\ell \langle u_1 \rangle_L}}{\overline{\langle \rho \rangle_\ell}} \right) \left(1 + \frac{\overline{\langle \rho \rangle_\ell \langle u_1 \rangle_L}}{\overline{\langle \rho \rangle_\ell}} \right) dy. \tag{3.58}$$

Figure (27) shows the temporal variations of the "total resolved kinetic energy,"[97]

$$E_f(t) = \int_{-\infty}^{+\infty} \frac{1}{2} \langle \rho \rangle_\ell \langle u_i \rangle_L \langle u_i \rangle_L \, \mathbf{dx}, \tag{3.59}$$

and the "production rate of the SGS kinetic energy,"[97]

$$P_k(t) = \int_{-\infty}^{+\infty} - \langle \rho \rangle_L \tau_L(u_i, u_j) \frac{\partial \langle u_i \rangle_L}{\partial x_j} \mathbf{dx}. \tag{3.60}$$

57

3.7   SUMMARY

The filtered density function (FDF) methodology has proven very effective for large eddy simulation (LES) of turbulent reactive flows.[26] All previous contributions in FDF are concentrated on LES of low-speed flows. The objective of the work in this chapter is to develop the joint energy-pressure-velocity-scalar filtered mass density function (EPVS-FMDF) methodology for LES of high-speed turbulent flows. The exact transport equation governing the evolution of the EPVS-FMDF is derived. It is shown that the effect of subgrid scale (SGS) convection appears in a closed form. The unclosed terms are modeled in a fashion similar to that in probability density function (PDF) methods. The capability of the EPVS-FMDF is demonstrated by conducting LES of a temporally developing mixing layer. The preliminary comparisons with DNS data are encouraging. Work is in progress on fine-tuning of the EPVS-FMDF sub-closures and applying the methodology for LES of a wider class of high-speed flows.
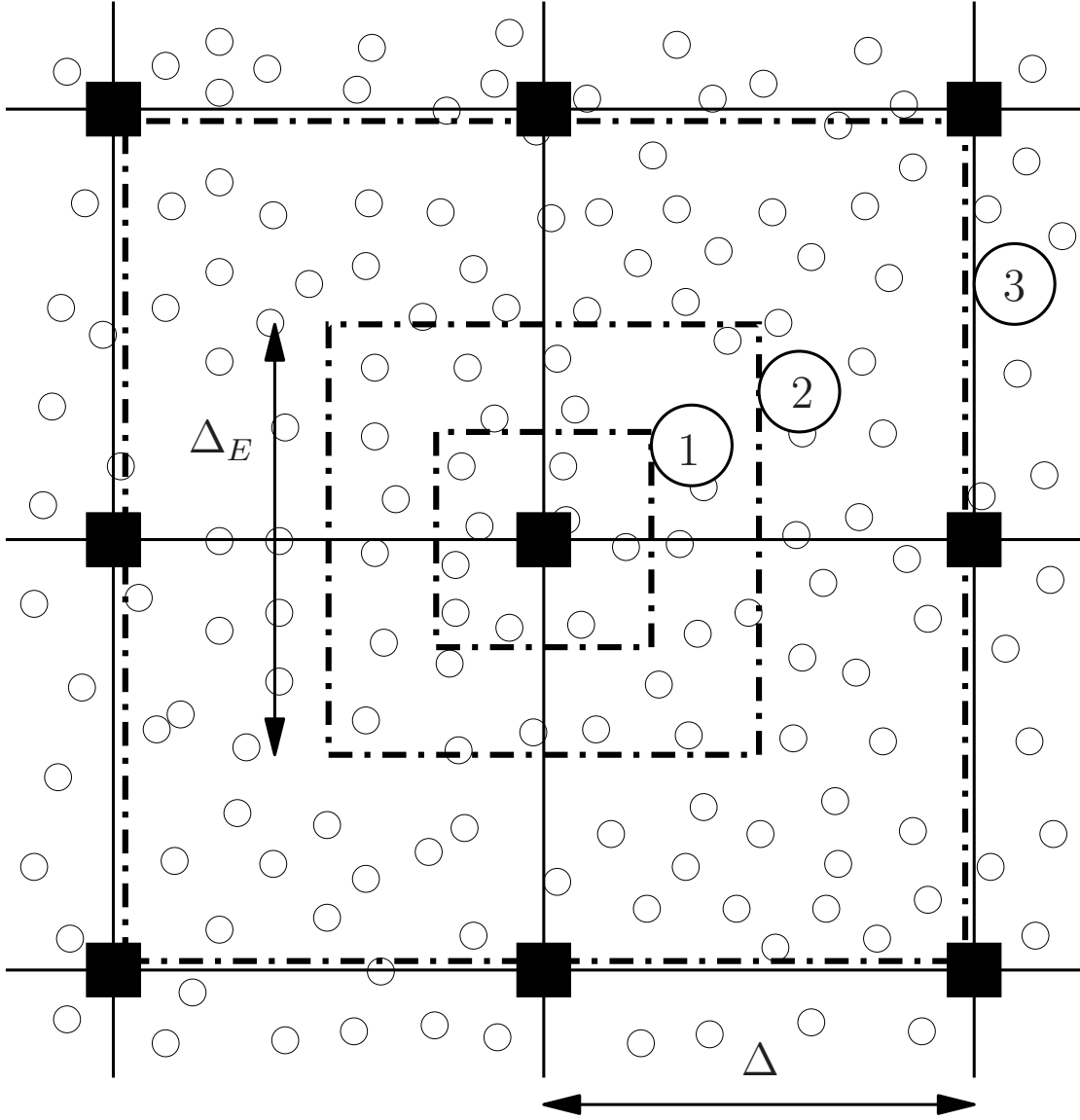
Figure 14: Ensemble averaging in MC simulations: $1(\Delta_E = \Delta/2)$, $2(\Delta_E = \Delta)$, $3(\Delta_E = 2\Delta)$. Black squares denote the FD grid points, and the circles denote the MC particles.

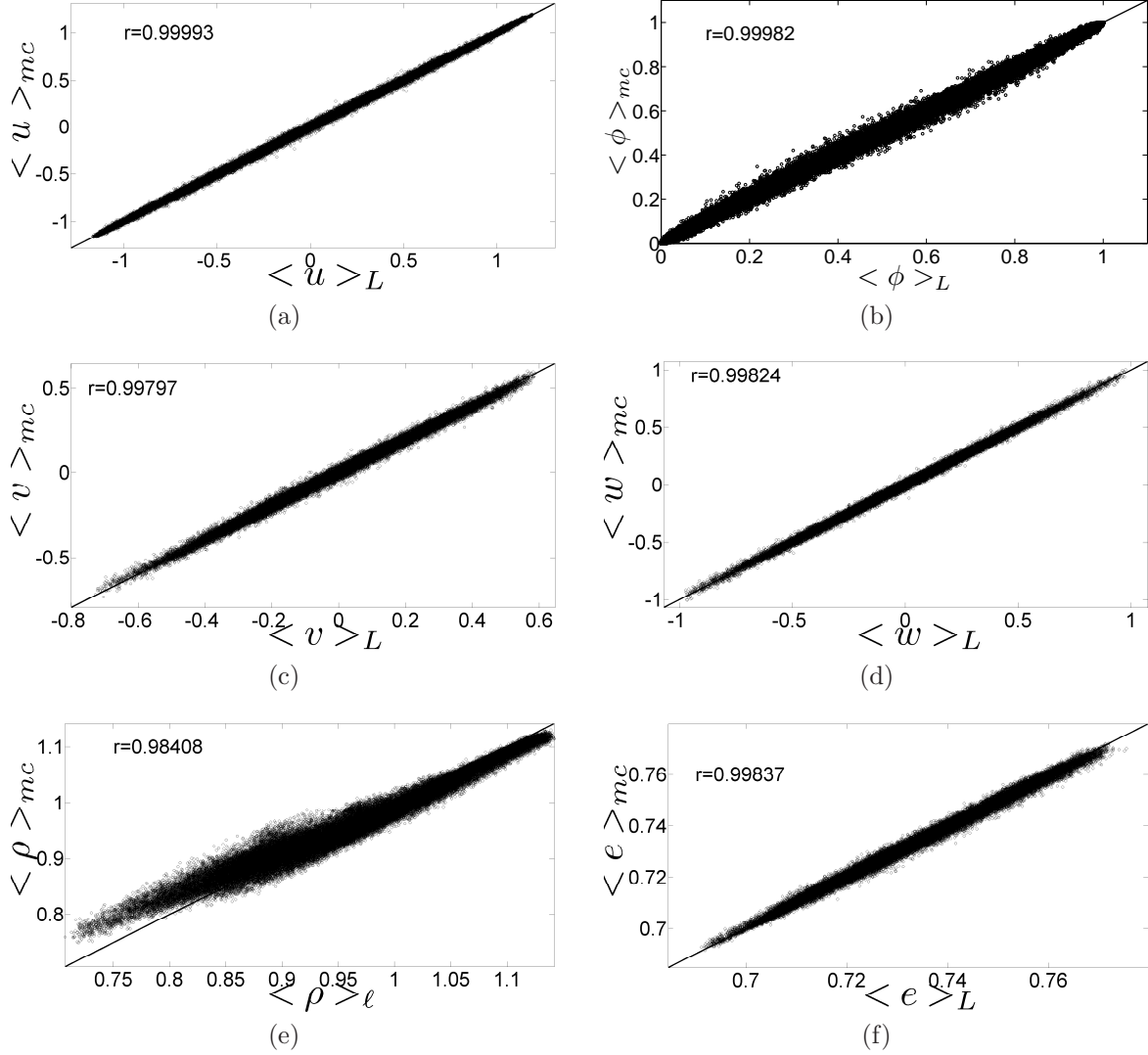Figure 15: Scatter plots of (a) $<u>_L$, (b) $<\phi>_L$, (c) $<v>_L$, (d) $<w>_L$, (e) $<\rho>_\ell$ and (f) $<e>_L$. The thick solid line denotes 45°. The parameter r denotes the correlation coefficient.
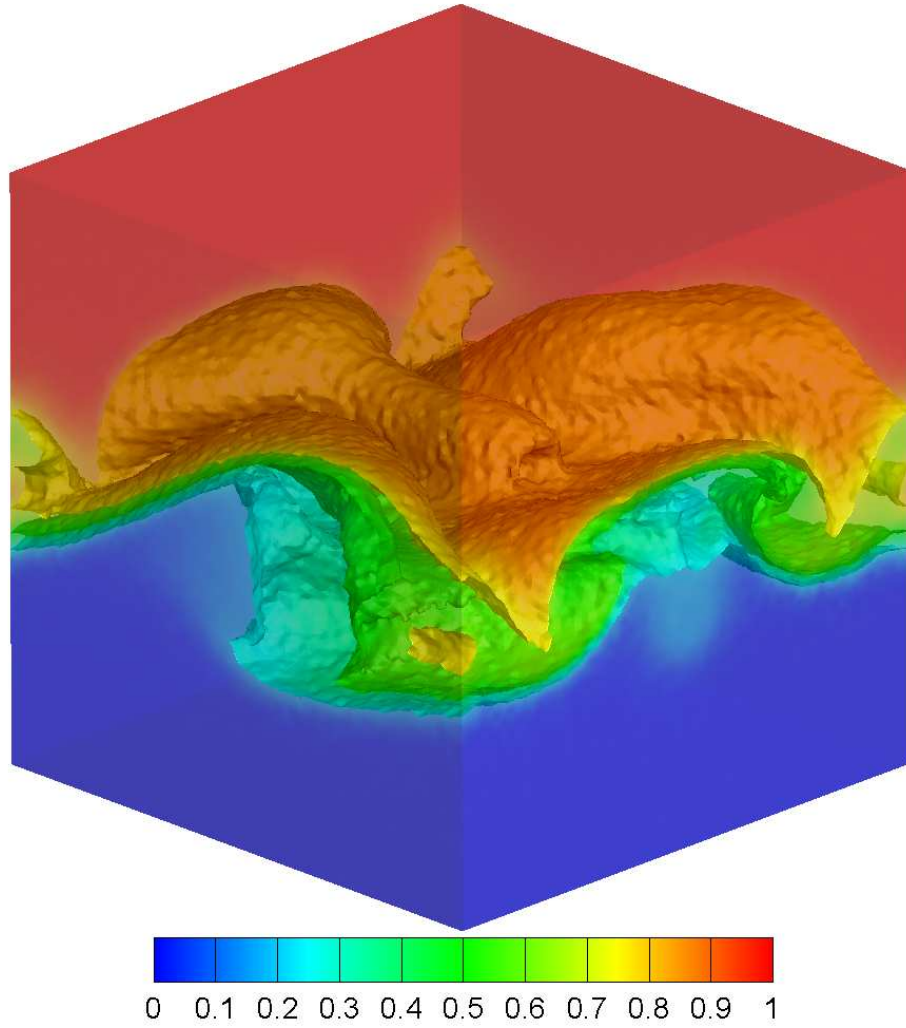
Figure 16: Contour surfaces of the instantaneous $\langle\phi\rangle_L$ field in temporal mixing layer simulations via EPVS-FMDF.
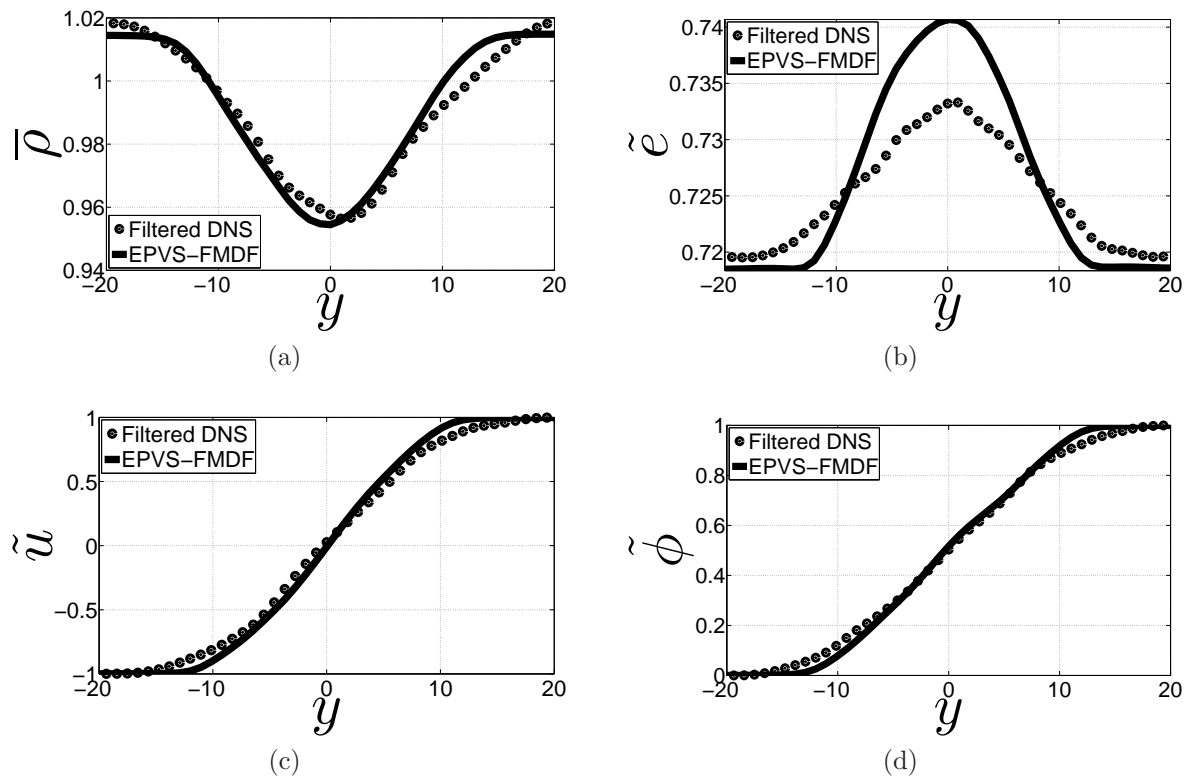
Figure 17: Cross-stream variations of (a) $\overline{\rho}$, (b) $\widetilde{e}$, (c) $\widetilde{u}$ and (d) $\widetilde{\phi}$. The thick solid line denotes EPVS-FMDF predictions. The circles denote DNS data.
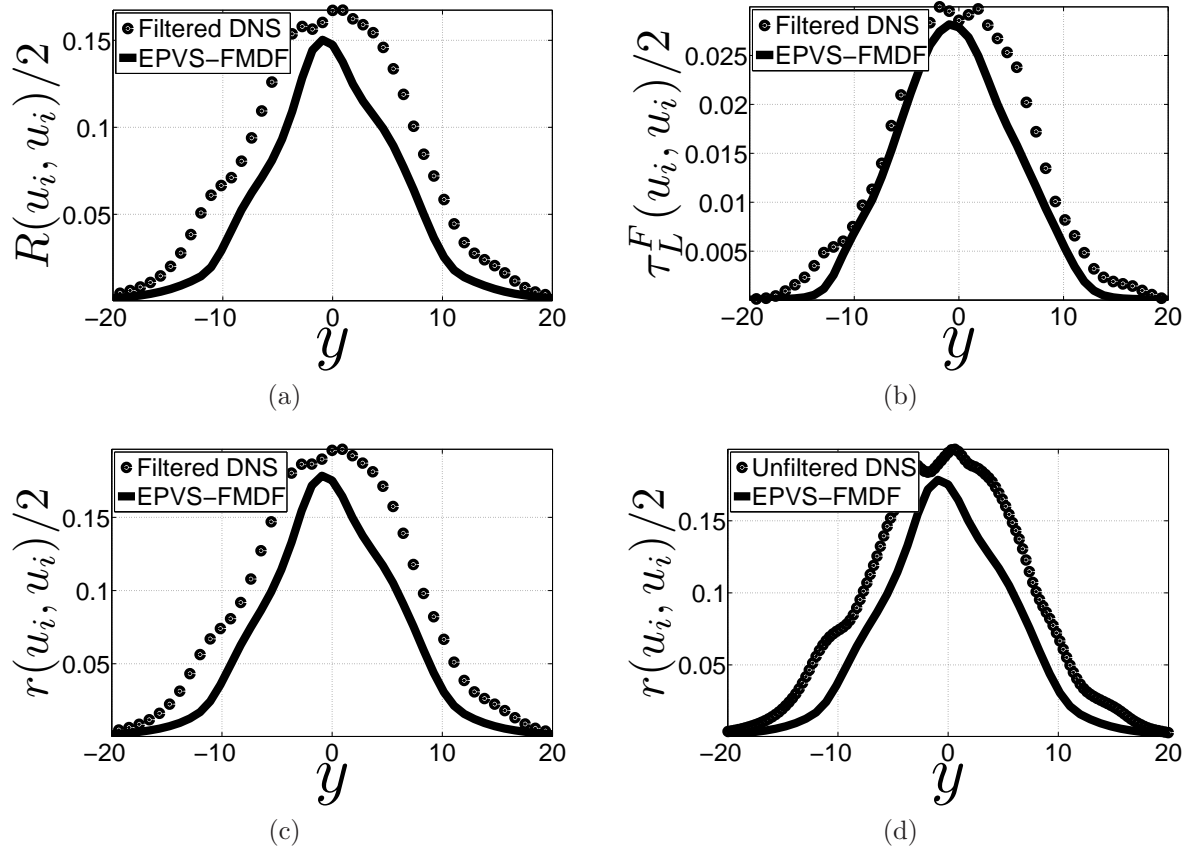
Figure 18: Cross-stream variations of (a) $R(u_i, u_i)/2$, (b) $\tau_L^F(u_i, u_i)/2$, (c) $r(u_i, u_i)/2$ from filtered DNS and (d) $r(u_i, u_i)/2$ from unfiltered DNS. The thick solid line denotes EPVS-FMDF predictions. The circles denote DNS data.
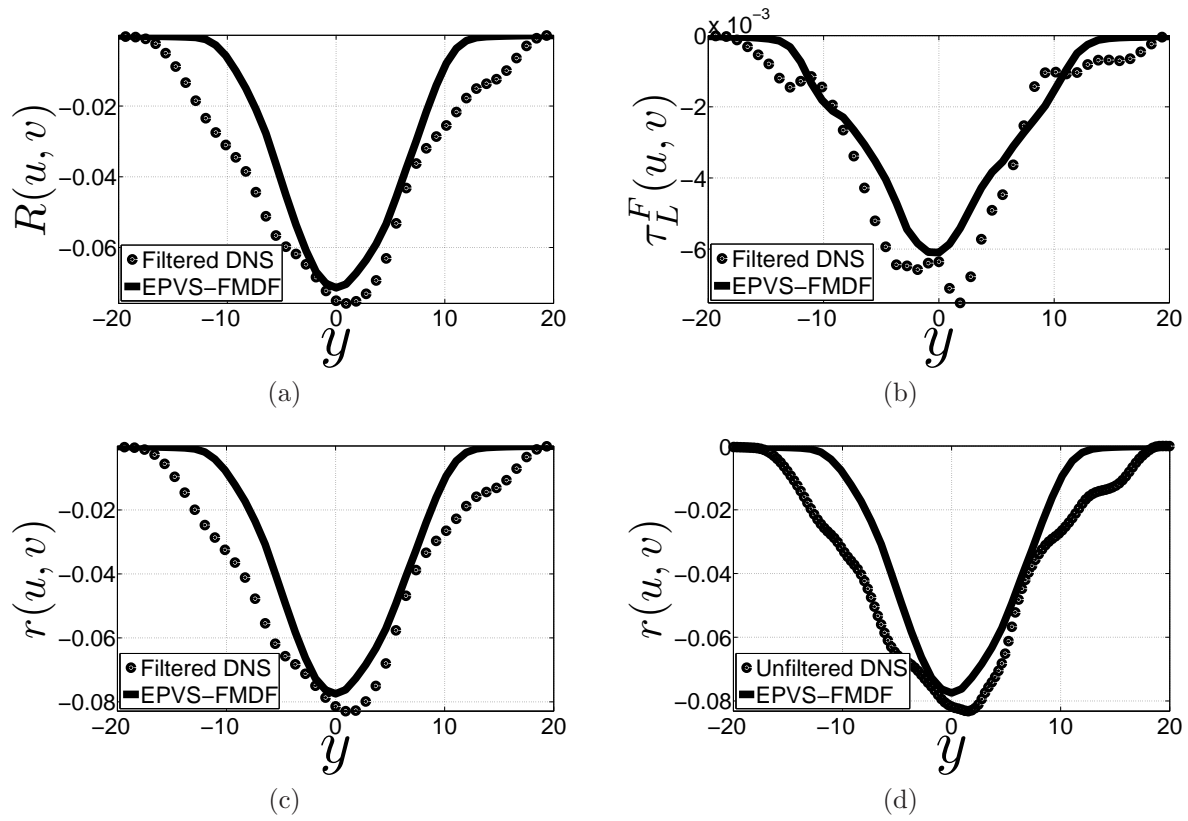
Figure 19: Cross-stream variations of (a) $R(u,v)$, (b) $\tau_L^F(u,v)$, (c) $r(u,v)$ from filtered DNS and (d) $r(u,v)$ from unfiltered DNS. The thick solid line denotes EPVS-FMDF predictions. The circles denote DNS data.
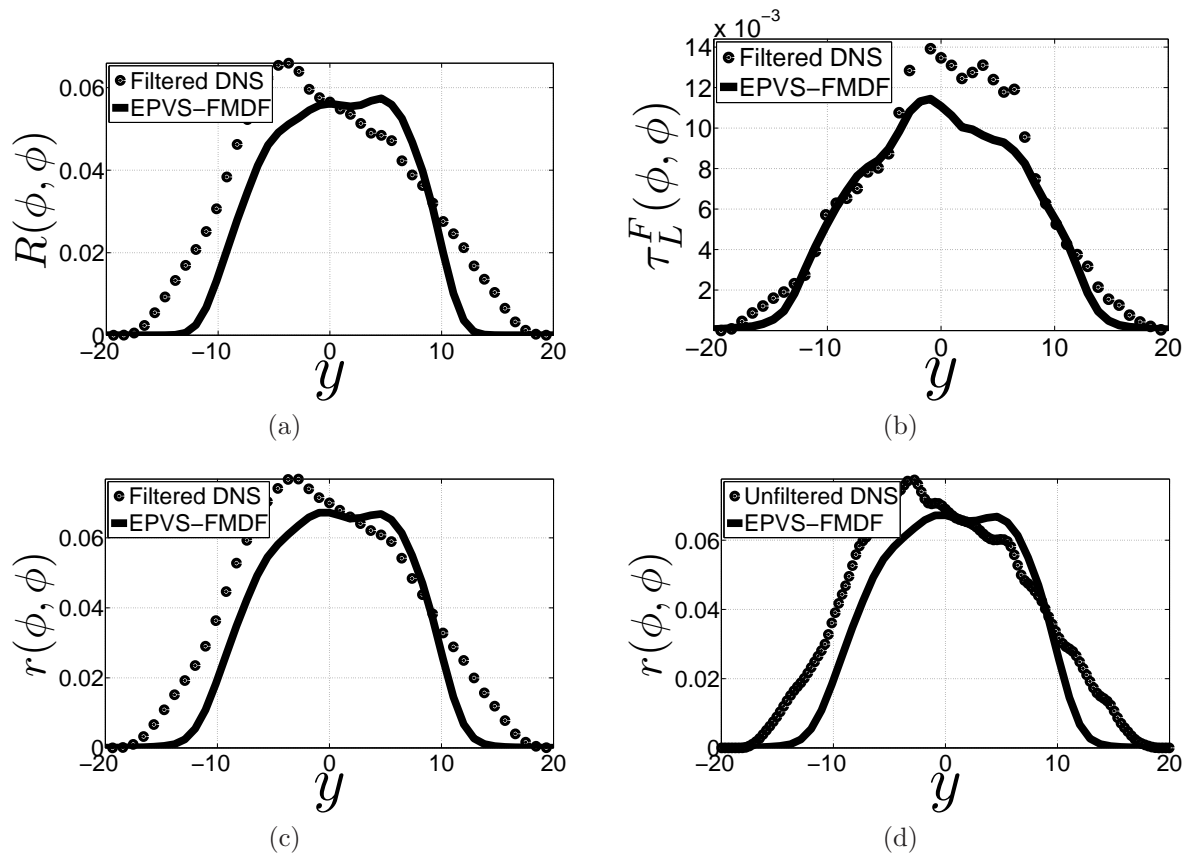
Figure 20: Cross-stream variations of (a) $R(\phi, \phi)$, (b) $\tau_L^F(\phi, \phi)$, (c) $r(\phi, \phi)$ from filtered DNS and (d) $r(\phi, \phi)$ from unfiltered DNS. The thick solid line denotes EPVS-FMDF predictions. The circles denote DNS data.

Figure 21: Cross-stream variations of (a) $R(u, \phi)$, (b) $\tau_L^F(u, \phi)$, (c) $r(u, \phi)$ from filtered DNS and (d) $r(u, \phi)$ from unfiltered DNS. The thick solid line denotes EPVS-FMDF predictions. The circles denote DNS data.
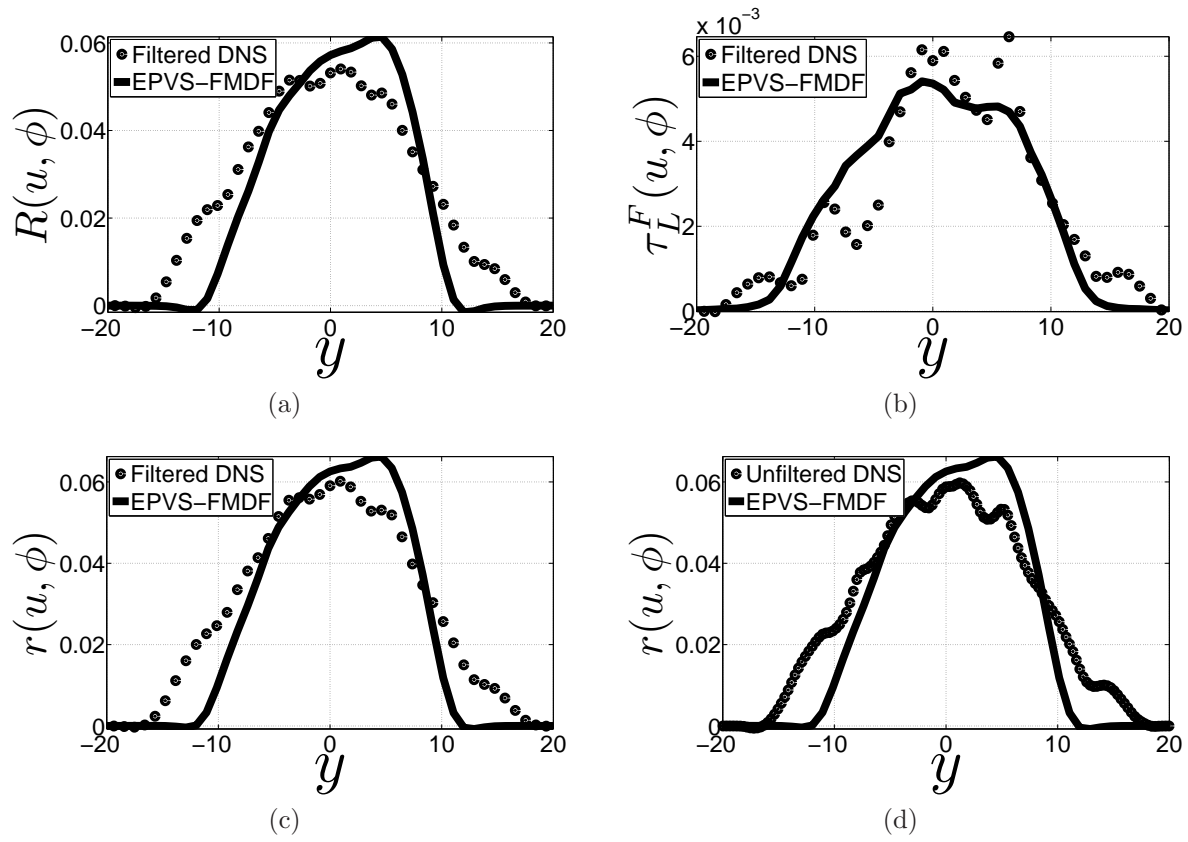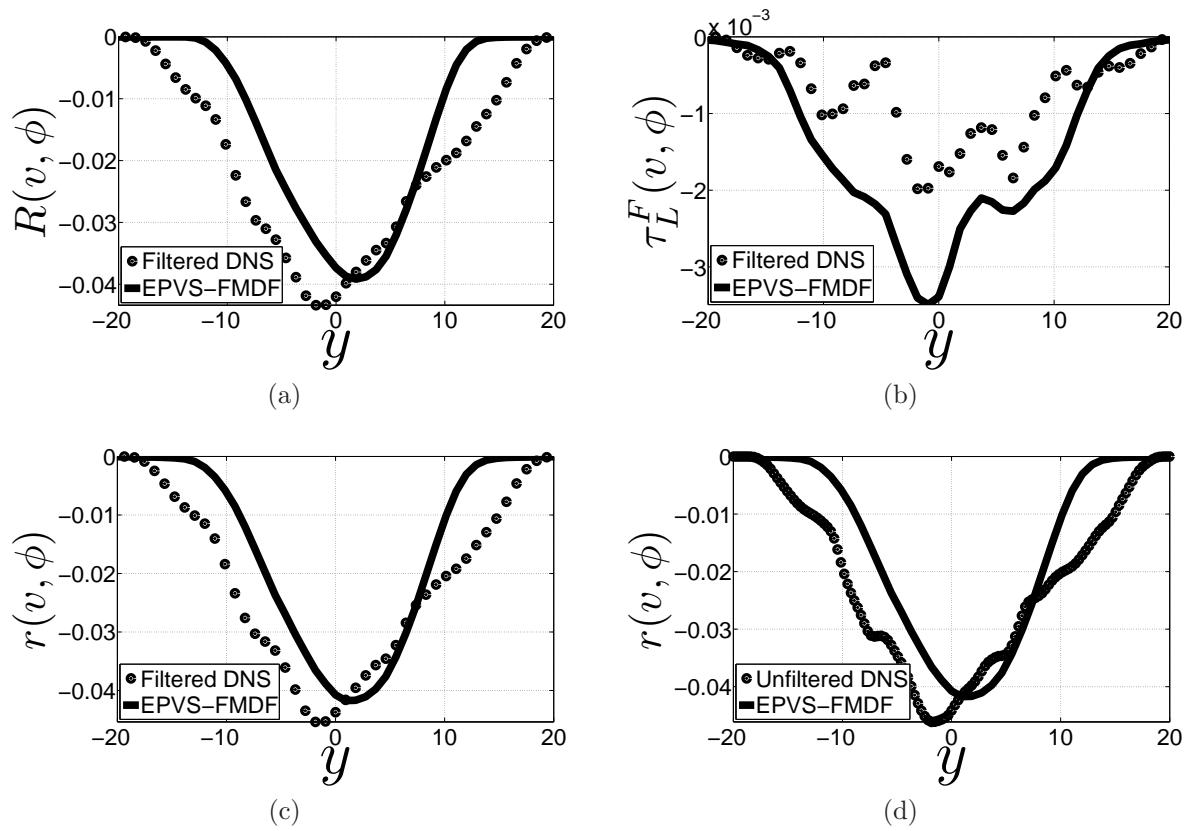
Figure 22: Cross-stream variations of (a) $R(v, \phi)$, (b) $\tau_L^F(v, \phi)$, (c) $r(v, \phi)$ from filtered DNS and (d) $r(v, \phi)$ from unfiltered DNS. The thick solid line denotes EPVS-FMDF predictions. The circles denote DNS data.
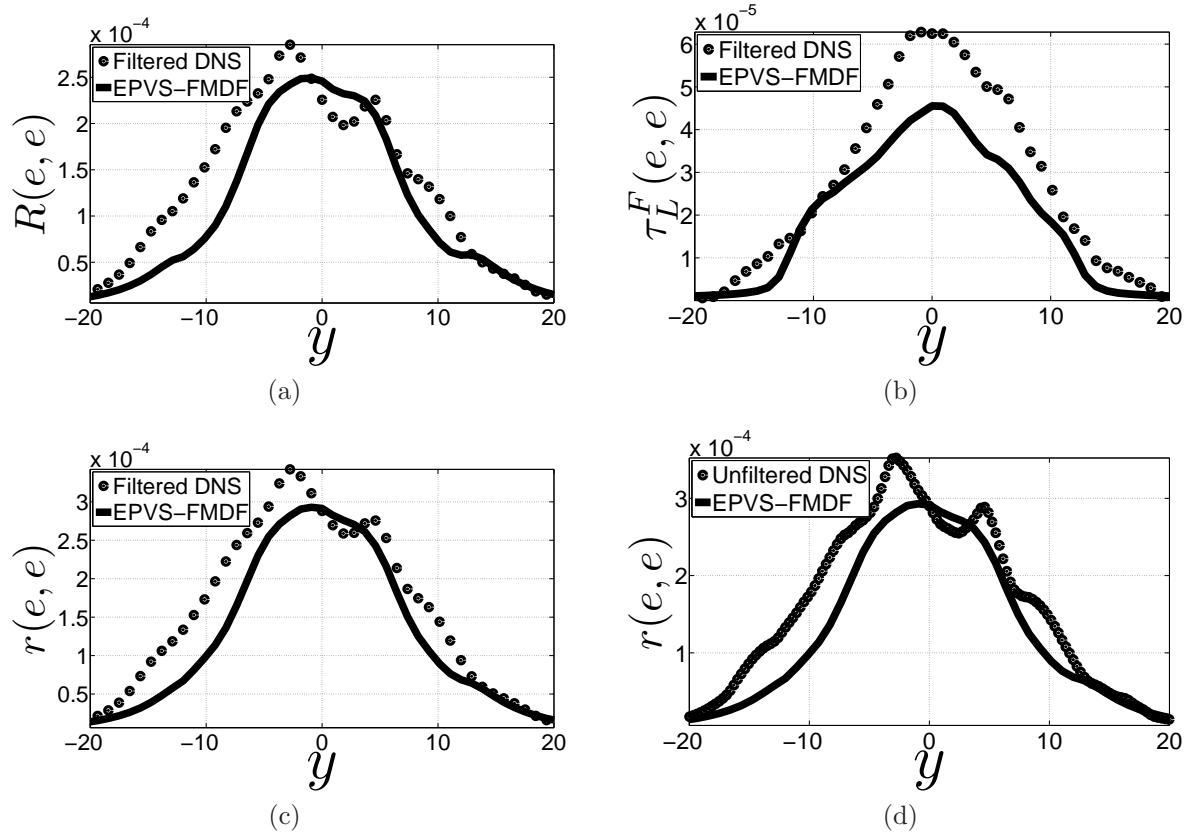
Figure 23: Cross-stream variations of (a) $R(e,e)$, (b) $\tau_L^F(e,e)$, (c) $r(e,e)$ from filtered DNS and (d) $r(e,e)$ from unfiltered DNS. The thick solid line denotes EPVS-FMDF predictions. The circles denote DNS data.

Figure 24: Cross-stream variations of (a) $R(u,e)$, (b) $\tau_L^F(u,e)$, (c) $r(u,e)$ from filtered DNS and (d) $r(u,e)$ from unfiltered DNS. The thick solid line denotes EPVS-FMDF predictions. The circles denote DNS data.
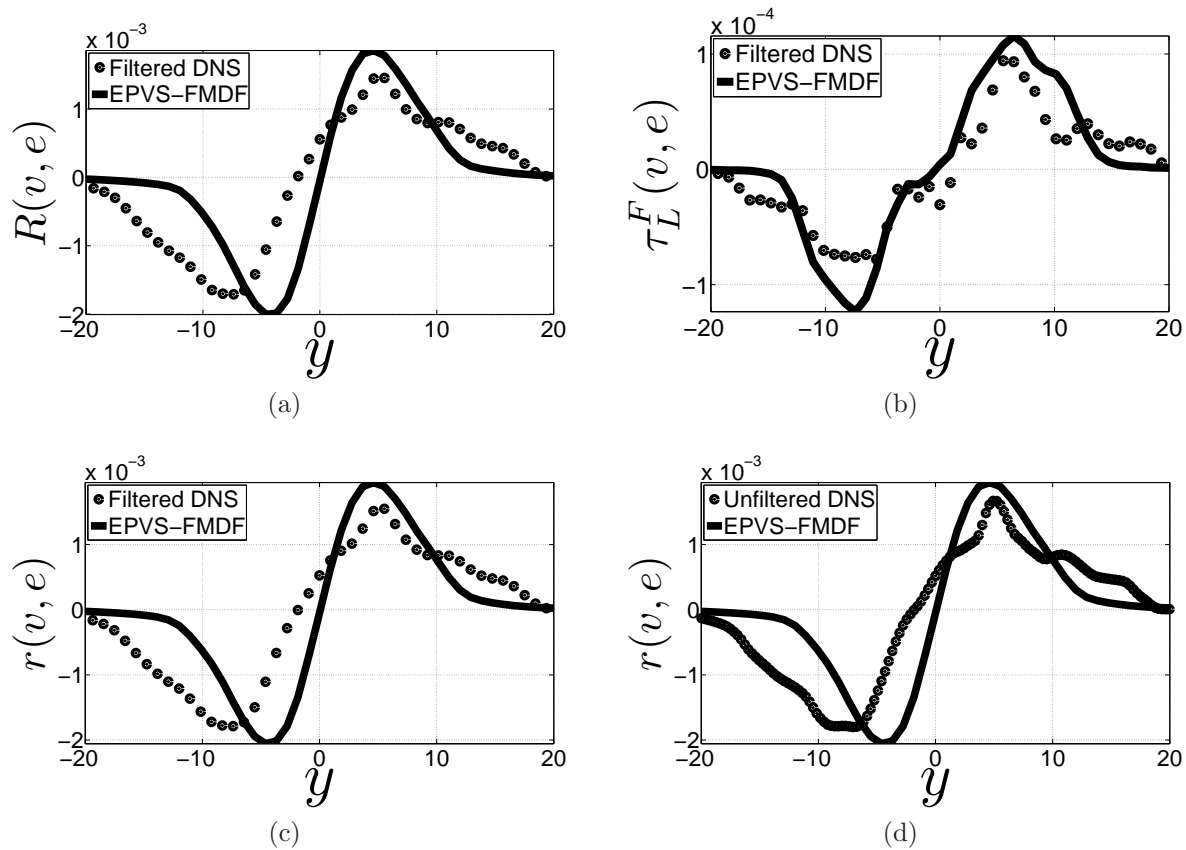
Figure 25: Cross-stream variations of (a) $R(v, e)$, (b) $\tau_L^F(v, e)$, (c) $r(v, e)$ from filtered DNS and (d) $r(v, e)$ from unfiltered DNS. The thick solid line denotes EPVS-FMDF predictions. The circles denote DNS data.

70

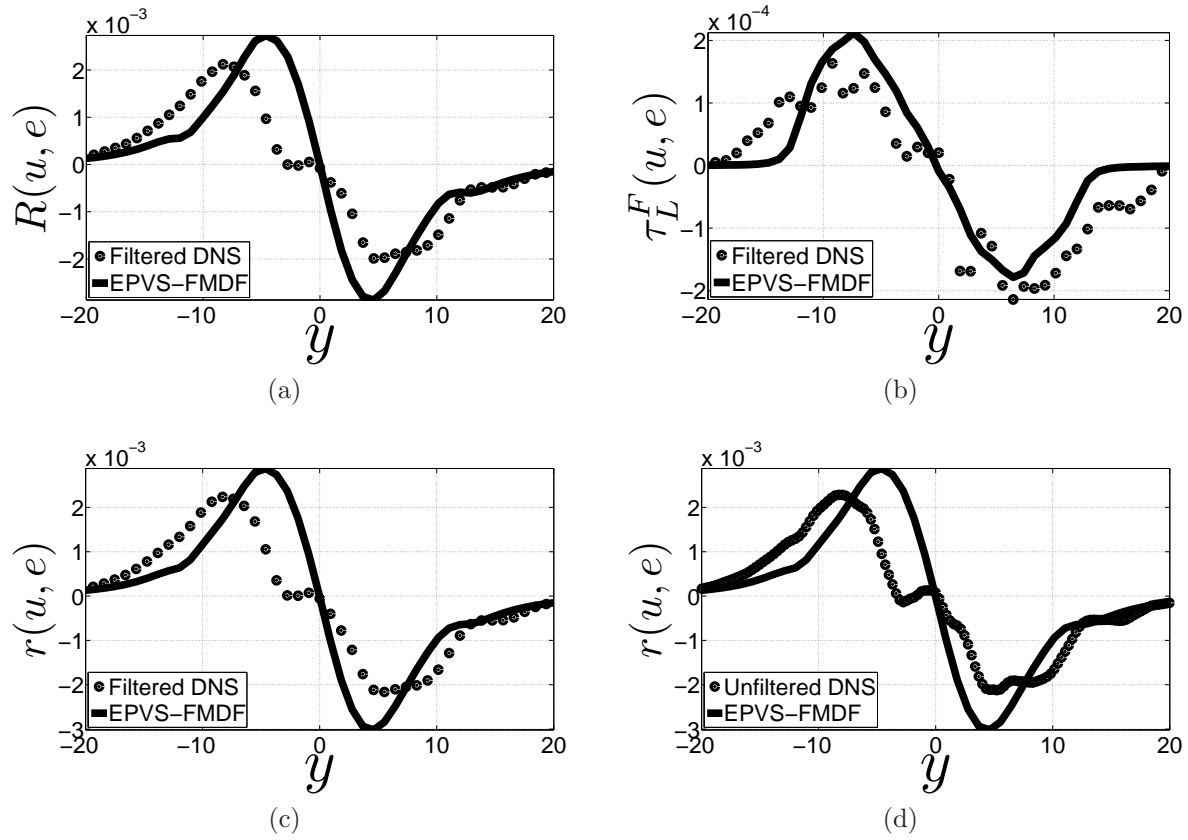Figure 26: Temporal variation of (a) scalar thickness (δ_s) and (b) momentum thickness (δ_m). The thick solid line denotes EPVS-FMDF predictions. The circles denote DNS data.

Figure 27: Temporal variation of (a) total resolved kinetic energy (E_f) and (b) SGS kinetic energy production rate (P_k). The thick solid line denotes EPVS-FMDF predictions. The circles denote DNS data.

4.0 CONCLUSIONS

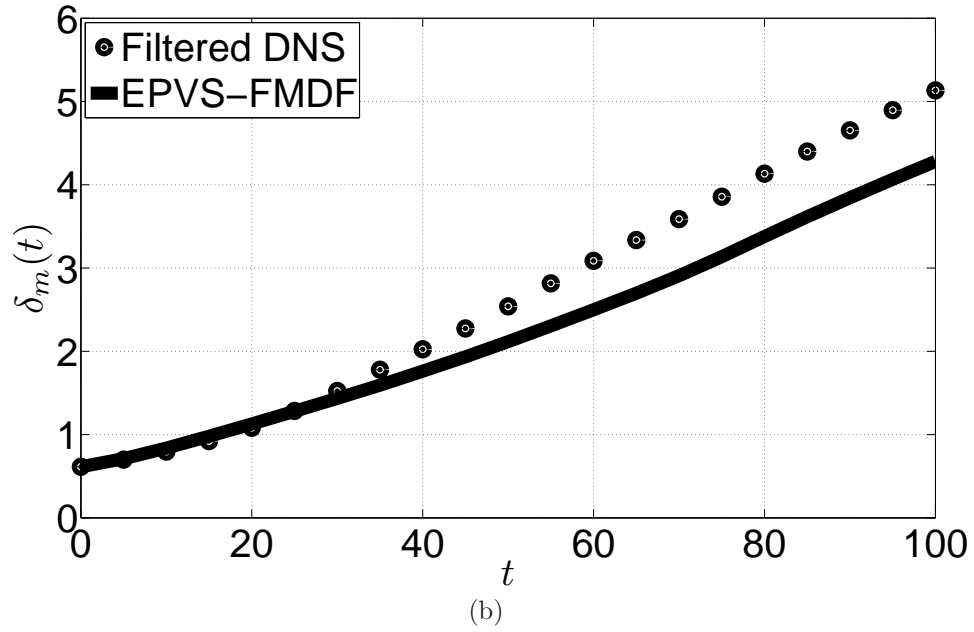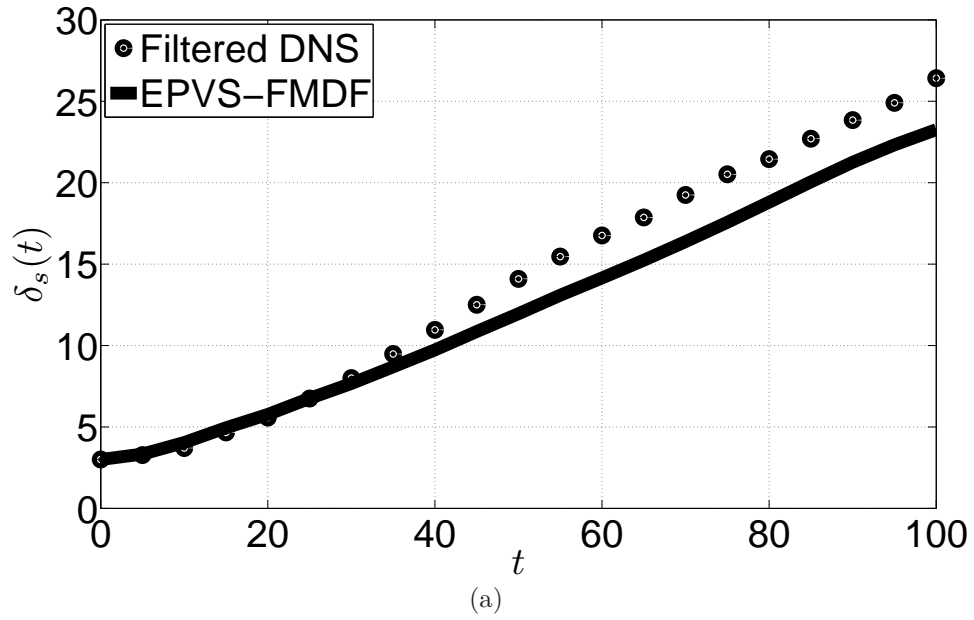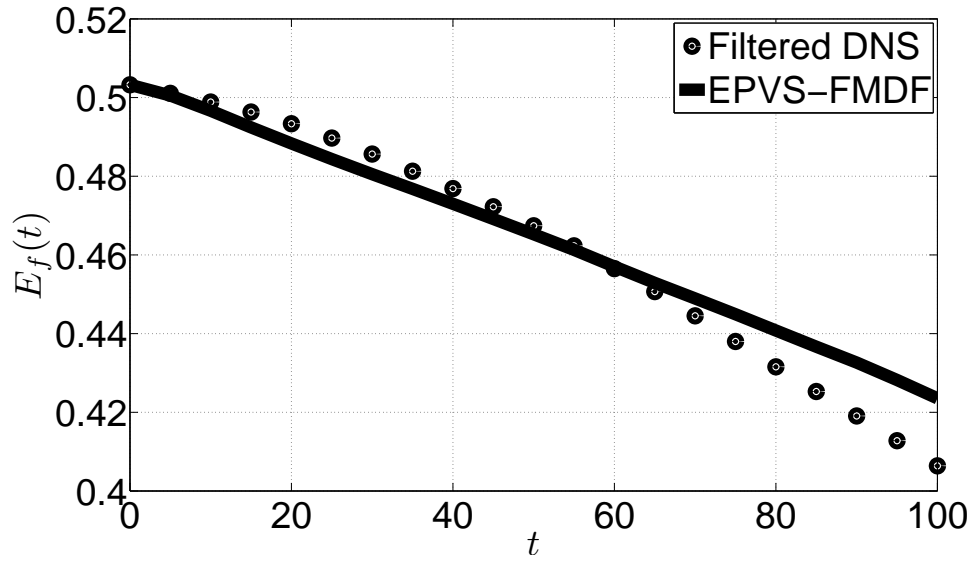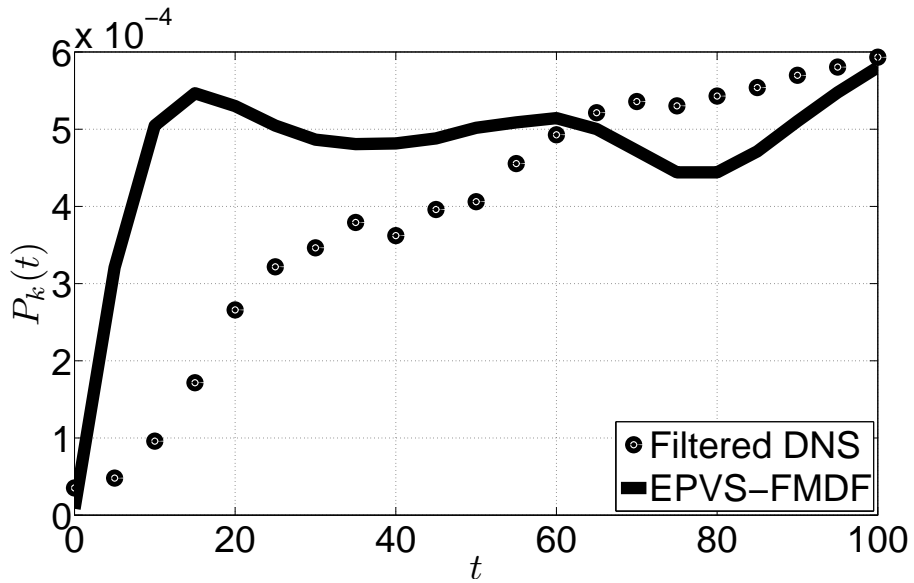Since its original conception,[1,2] the filtered density function (FDF) has become very popular for large eddy simulation (LES) of turbulent combustion. In its *stand-alone* form, the FDF must account for the joint statistics of all of the relevant physical variables. The most sophisticated FDF closure available prior to this work was the frequency-velocity-scalar FMDF (FVS-FMDF),[98] and a simpler version (VS-FMDF) which does not include the SGS frequency.[11,28] Hydrodynamic closure in incompressible, non-reacting flows has been successfully achieved via the velocity-FDF (V-FDF),[27] and the one which has been utilized the most only considers the scalar field (S-FDF and S-FMDF). This is the most elementary form of FDF when it was first introduced,[4,5] and has experienced widespread usage. Some of the subsequent contributions in FDF are in its basic implementation,[7,8,12–16,18–20,22–25,39,40,71,99–103] fine-tuning of its sub-closures,[10,104,105] and its validation via laboratory experiments.[14,106–110] See Ref.[26] for a recent review of the state of progress in FDF.

The objective of the first part of this dissertation is to employ the VS-FMDF for LES of Sandia Flame-D. It is shown that the model performs well in predicting some of the phenomena pertaining to this experiment. Most of the overall flow statistics, including the mean field, the resolved and total second order moments are in good agreements with the data. To simulate high speed turbulent flows, development of the joint "energy-pressure-velocity-scalar filtered mass density function" (EPVS-FMDF) is the objective of the second part of this dissertation. The consistency and accuracy of EPVS-FMDF transport are assessed via LES of a temporally developing mixing layers involving the transport of a passive scalar. This assessment is made by comparing the moments obtained from the Monte Carlo (MC) solver with those obtained by solving the corresponding transport equations directly by a finite-difference method (LES-FD) method. The LES-FD equations are closed by including

the moments from the MC solver. The FDF predictions are compared with direct numerical simulation (DNS) data of the same flow. It is shown that the FDF performs well in predicting some of the phenomena pertaining to the SGS transport. Most of the overall flow statistics, including the mean field, the resolved and the total second order moments are in good agreements with DNS data.

Some suggestions for possible future work are:

- Extension of the VS-FMDF for simulation of complex turbulent reacting flows with finite rate chemistry.

- Application of the VS-FMDF for LES of flows with complex geometrical configurations.

- Inclusion of the differential diffusion in EPVS-FMDF formulation.

- Application of the EPVS-FMDF for LES of complex turbulent reacting flows, including those with strong shocks.

BIBLIOGRAPHY

[1] Givi, P., Model Free Simulations of Turbulent Reactive Flows, *Prog. Energy Combust. Sci.*, **15**:1–107 (1989).

[2] Pope, S. B., Computations of Turbulent Combustion: Progress and Challenges, *Proc. Combust. Inst.*, **23**:591–612 (1990).

[3] Givi, P., Filtered Density Function for Subgrid Scale Modeling of Turbulent Combustion, *AIAA J.*, **44**(1):16–23 (2006).

[4] Colucci, P. J., Jaberi, F. A., Givi, P., and Pope, S. B., Filtered Density Function for Large Eddy Simulation of Turbulent Reacting Flows, *Phys. Fluids*, **10**(2):499–515 (1998).

[5] Jaberi, F. A., Colucci, P. J., James, S., Givi, P., and Pope, S. B., Filtered Mass Density Function for Large Eddy Simulation of Turbulent Reacting Flows, *J. Fluid Mech.*, **401**:85–121 (1999).

[6] Garrick, S. C., Jaberi, F. A., and Givi, P., Large Eddy Simulation of Scalar Transport in a Turbulent Jet Flow, in Knight, D. and Sakell, L., editors, *Recent Advances in DNS and LES*, *Fluid Mechanics and its Applications*, Vol. 54, pp. 155–166, Kluwer Academic Publishers, The Netherlands, 1999.

[7] James, S. and Jaberi, F. A., Large Scale Simulations of Two-Dimensional Nonpremixed Methane Jet Flames, *Combust. Flame*, **123**:465–487 (2000).

[8] Zhou, X. Y. and Pereira, J. C. F., Large Eddy Simulation (2D) of a Reacting Plan Mixing Layer Using Filtered Density Function, *Flow Turbul. Combust.*, **64**:279–300 (2000).

[9] Heinz, S., On Fokker-Planck Equations for Turbulent Reacting Flows. Part 2. Filter Density Function for Large Eddy Simulation, *Flow Turbul. Combust.*, **70**(1-4):153–181 (2003).

[10] Cha, C. M. and Troullet, P., A Subgrid-Scale Mixing Model for Large-Eddy Simulations of Turbulent Reacting Flows Using the Filtered Density Function, *Phys. Fluids*, **15**(6):1496–1504 (2003).

[11] Sheikhi, M. R. H., Drozda, T. G., Givi, P., and Pope, S. B., Velocity-Scalar Filtered Density Function for Large Eddy Simulation of Turbulent Flows, *Phys. Fluids*, **15**(8):2321–2337 (2003).

[12] Raman, V., Pitsch, H., and Fox, R. O., Hybrid Large-Eddy Simulation/Lagrangian Filtered Density Function Approach for Simulating Turbulent Combustion, *Combust. Flame*, **143**(1-2):56–78 (2005).

[13] Raman, V. and Pitsch, H., Large-Eddy Simulation of a Bluff-Body-Stabilized Nonpremixed Flame using a Recursive Filter-Refinement Procedure, *Combust. Flame*, **142**:329–347 (2005).

[14] van Vliet, E., Derksen, J. J., and van den Akker, H. E. A., Turbulent Mixing in a Tubular Reactor: Assessment of an FDF/LES Approach, *AIChE J.*, **51**(3):725–739 (2005).

[15] Carrara, M. D. and DesJardin, P. E., A Filtered Mass Density Function Approach to Modeling Separated Two-Phase Flows using LES I: Mathematical Formulation, *Int. J. Multiphas. Flow*, **32**:365–384 (2006).

[16] Mustata, R., Valiño, L., Jiménez, C., Jones, W. P., and Bondi, S., A Probability Density Function Eulerian Monte Carlo Field Method for Large Eddy Simulations: Application to a Turbulent Piloted Methane/Air Diffusion Flame (Sandia D), *Combust. Flame*, **145**(1-2):88–104 (2006).

[17] Drozda, T. G., Sheikhi, M. R. H., Madnia, C. K., and Givi, P., Developments in Formulation and Application of the Filtered Density Function, *Flow Turbul. Combust.*, **78**:35–67 (2007).

[18] Jones, W. P., Navarro-Martinez, S., and Röhl, O., Large Eddy Simulation of Hydrogen Auto-Ignition with a Probability Density Function Method, *Proc. Combust. Inst.*, **31**:1765–1771 (2007).

[19] Jones, W. P. and Navarro-Martinez, S., Large Eddy Simulation of Autoignition with a Subgrid Probability Density Function Method, *Combust. Flame*, **150**:170–187 (2007).

[20] James, S., Zhu, J., and Anand, M. S., Large Eddy Simulations of Turbulent Flames Using the Filtered Density Function Model, *Proc. Combust. Inst.*, **31**:1737–1745 (2007).

[21] Chen, J. Y., A Eulerian PDF Scheme for LES of Nonpremixed Turbulent Combustion with Second-Order Accurate Mixture Fraction, *Combust. Theor. Model.*, **11**(5):675–695 (2007).

[22] McDermott, R. and Pope, S. B., A Particle Formulation for Treating Differential Diffusion in Filtered Density Function Methods, *J. Comput. Phys.*, **226**(1):947–993 (2007).

[23] Raman, V. and Pitsch, H., A Consistent LES/Filtered-Density Function Formulation for the Simulation of Turbulent Flames with Detailed Chemistry, *Proc. Combust. Inst.*, **31**:1711–1719 (2007).

[24] Afshari, A., Jaberi, F. A., and Shih, T. I. P., Large-Eddy Simulations of Turbulent Flows in an Axisymmetric Dump Combustor, *AIAA J.*, **46**(7):1576–1592 (2008).

[25] Drozda, T. G., Wang, G., Sankaran, V., Mayo, J. R., Oefelein, J. C., and Barlow, R. S., Scalar Filtered Mass Density Functions in Nonpremixed Turbulent Jet Flames, *Combust. Flame*, **155**(1-2):54–69 (2008).

[26] Ansari, N., Jaberi, F. A., Sheikhi, M. R. H., and Givi, P., Filtered Density Function as a Modern CFD Tool, in Maher, A. R. S., editor, *Engineering Applications of Computational Fluid Dynamics*, chapter 1, pp. 1–22, International Energy and Environment Foundation, www.IEEFoundation.org, 2011.

[27] Gicquel, L. Y. M., Givi, P., Jaberi, F. A., and Pope, S. B., Velocity Filtered Density Function for Large Eddy Simulation of Turbulent Flows, *Phys. Fluids*, **14**(3):1196–1213 (2002).

[28] Sheikhi, M. R. H., Givi, P., and Pope, S. B., Velocity-Scalar Filtered Mass Density Function for Large Eddy Simulation of Turbulent Reacting Flows, *Phys. Fluids*, **19**(9):095196 1–21 (2007).

[29] Piomelli, U., Large-Eddy Simulation: Achievements and Challenges, *Prog. Aerosp. Sci.*, **35**:335–362 (1999).

[30] Meneveau, C. and Katz, J., Scale-Invariance and Turbulence Models for Large-Eddy Simulations, *Annu. Rev. Fluid Mech.*, **32**:1–32 (2000).

[31] Geurts, B. J., editor, *Modern Simulation Strategies for Turbulent Flow*, R. T. Edwards, Inc., Philadelphia, PA, 2001.

[32] Sagaut, P., *Large Eddy Simulation for Incompressible Flows*, Springer-Verlag, New York, NY, 3rd edition, 2005.

[33] Givi, P., Sheikhi, M. R. H., Drozda, T. G., and Madnia, C. K., Large Scale Simulation of Turbulent Combustion, *Combust. Plasma Chem.*, **6**(1):1–9 (2008).

[34] Nooren, P. A., Versiuis, M., Van der Meer, T. H., Barlow, R. S., and Frank, J. H., Raman-Rayleigh-LIF Measurements of Temperature and Species Concentrations in the Delft Piloted Turbulent Jet Diffusion Flame, *Appl. Phys.*, **B71**:95–111 (2000).

[35] Barlow, R. S., The International Workshop on Measurement and Computation of Turbulent Nonpremixed Flames. Sandia National Laboratories, `http://www.ca.sandia.gov/TNF/`, 2003.

[36] Schneider, C., Dreizler, A., Janicka, J., and Hassel, E. P., Flow Field Measurements of Stable and Locally Extinguishing Hydrocarbon-Fuelled Jet Flames, *Combust. Flame*, **135**(1):185–190 (2003).

[37] Sheikhi, M. R. H., Drozda, T. G., Givi, P., Jaberi, F. A., and Pope, S. B., Large Eddy Simulation of a Turbulent Nonpremixed Piloted Methane Jet Flame (Sandia Flame D), *Proc. Combust. Inst.*, **30**:549–556 (2005).

[38] Nik, M. B., Sheikhi, M. R. H., Givi, P., and Pope, S. B., VSFMDF for LES of Sandia's Turbulent Piloted Jet Flame, *Bull. Am. Phys. Soc.*, **52**(17):155 (2007).

[39] Nik, M. B., Yilmaz, S. L., Givi, P., Sheikhi, M. R. H., and Pope, S. B., Simulation of Sandia Flame D Using Velocity-Scalar Filtered Density Function, *AIAA J.*, **48**(7):1513–1522 (2010).

[40] Nik, M. B., Yilmaz, S. L., Sheikhi, M. R. H., and Givi, P., Grid Resolution Effects on VSFMDF/LES, *Flow Turbul. Combust.*, **85**(3-4):677–688 (2010).

[41] Nik, M. B., Givi, P., Madnia, C. K., and Pope, S. B., Energy-Pressure-Velocity Filtered Mass Density Function, *Bull. Am. Phys. Soc.*, **55**(16):138 (2010).

[42] Nik, M. B., Givi, P., Madnia, C. K., and Pope, S. B., Energy-Pressure-Velocity-Scalar Filtered Mass Density Function, *Bull. Am. Phys. Soc.*, **56**(18):195 (2011).

[43] Nik, M. B., Mohebbi, M., Sheikhi, M. R. H., and Givi, P., Progress in Large Eddy Simulation of High Speed Turbulent Mixing and Reaction, AIAA Paper 2009-0133, 2009.

[44] Nik, M. B., Givi, P., Madnia, C. K., and Pope, S. B., EPVS-FMDF for LES of High-Speed Turbulent Flows, AIAA Paper 2012-0117, 2012.

[45] Yilmaz, S. L., Ansari, N., Pisciuneri, P. H., Nik, M. B., Otis, C. C., and Givi, P., Advances in FDF Modeling and Simulation, AIAA Paper 2011-5918, 2011.

[46] Libby, P. A. and Williams, F. A., editors, *Turbulent Reacting Flows*, *Topics in Applied Physics*, Vol. 44, Springer-Verlag, Heidelberg, 1980.

[47] Pope, S. B., PDF Methods for Turbulent Reactive Flows, *Prog. Energy Combust. Sci.*, **11**:119–192 (1985).

[48] Bilger, R. W., Molecular Transport Effects in Turbulent Diffusion Flames at Moderate Reynolds Number, *AIAA J.*, **20**:962–970 (1982).

[49] Pope, S. B., *Turbulent Flows*, Cambridge University Press, Cambridge, UK, 2000.

[50] O'Brien, E. E., The Probability Density Function (PDF) Approach to Reacting Turbulent Flows, In Libby and Williams[46], chapter 5, pp. 185–218.

[51] Vreman, B., Geurts, B., and Kuerten, H., Realizability Conditions for the Turbulent Stress Tensor in Large-Eddy Simulation, *J. Fluid Mech.*, **278**:351–362 (1994).

[52] Karlin, S. and Taylor, H. M., *A Second Course in Stochastic Processes*, Academic Press, New York, NY, 1981.

[53] Haworth, D. C. and Pope, S. B., A Generalized Langevin Model for Turbulent Flows, *Phys. Fluids*, **29**(2):387–405 (1986).

[54] Dreeben, T. D. and Pope, S. B., Probability Density Function and Reynolds-Stress Modeling of Near-Wall Turbulent Flows, *Phys. Fluids*, **9**(1):154–163 (1997).

[55] Wax, N., *Selected Papers on Noise and Stochastic Processes*, Dover, 1954.

[56] Gardiner, C. W., *Handbook of Stochastic Methods*, Springer-Verlag, New York, NY, 1990.

[57] Madnia, C. K., Jaberi, F. A., and Givi, P., Large Eddy Simulation of Heat and Mass Transport in Turbulent Flows, In Minkowycz *et al.*[72], chapter 5, pp. 167–189.

[58] Gottlieb, D. and Turkel, E., Dissipative Two-Four Methods for Time Dependent Problems, *Math. Comp.*, **30**(136):703–723 (1976).

[59] Balay, S., Buschelman, K., Gropp, W. D., Kaushik, D., Knepley, M. G., McInnes, L. C., Smith, B. F., and Zhang, H., PETSc Web page, `http://www.mcs.anl.gov/petsc/`, 2009, Accessed 2 July 2010.

[60] Balay, S., Buschelman, K., Eijkhout, V., Gropp, W. D., Kaushik, D., Knepley, M. G., McInnes, L. C., Smith, B. F., and Zhang, H., PETSc Users Manual, Technical Report ANL-95/11 - Revision 2.1.5, Argonne National Laboratory, 2004.

[61] Balay, S., Gropp, W. D., McInnes, L. C., and Smith, B. F., Efficient Management of Parallelism in Object Oriented Numerical Software Libraries, in Arge, E., Bruaset, A. M., and Langtangen, H. P., editors, *Modern Software Tools in Scientific Computing*, pp. 163–202, Birkhäuser Press, 1997.

[62] Danaila, I. and Boersma, B. J., Direct Numerical Simulation of Bifurcating Jets, *Phys. Fluids*, **12**(5):1255–1257 (2000).

[63] Poinsot, T. J. and Lele, S. K., Boundary Conditions for Direct Simulations of Compressible Viscous Flows, *J. Comp. Phys.*, **101**:104–129 (1992).

[64] Peters, N., *Turbulent Combustion*, Cambridge University Press, Cambridge, UK, 2000.

[65] Smith, G. P., Golden, D. M., Frenklach, M., Moriarty, N. W., Eiteneer, B., Goldenberg, M., Bowman, C. T., Hanson, R., Song, S., Gardiner, W. C., Lissianski, V., and Qin, Z., `http://www.me.berkeley.edu/gri_mech`, Accessed 2 July 2010.

[66] Muradoglu, M., Liu, K., and Pope, S. B., PDF Modeling of a Bluff-Body Stabilized Turbulent Flame, *Combust. Flame*, **132**:115–137 (2003).

[67] Givi, P. and Riley, J. J., Some Current Issues in the Analysis of Reacting Shear Layers: Computational Challenges, in Hussaini, M. Y., Kumar, A., and Voigt, R. G., editors, *Major Research Topics in Combustion*, pp. 588–650, Springer-Verlag, New York, NY, 1992.

[68] Drummond, J. P. and Givi, P., Suppression and Enhancement of Mixing in High-Speed Reacting Flow Fields, in Buckmaster, J. D., Jackson, T. L., and Kumar, A., editors, *Combustion in High-Speed Flows*, pp. 191–229, Kluwer Academic Publishers, The Netherlands, 1994.

[69] Bilger, R. W., Future Progress in Turbulent Combustion Research, *Prog. Energy Combust. Sci.*, **26**(4-6):367–380 (2000).

[70] Fox, R. O., *Computational Models for Turbulent Reacting Flows*, Cambridge University Press, Cambridge, UK, 2003.

[71] Heinz, S., On Fokker-Planck Equations for Turbulent Reacting Flows. Part 2. Filtered Density Function for Large Eddy Simulation, *Flow Turbul. Combust.*, **70**:153–181 (2003).

[72] Minkowycz, W. J., Sparrow, E. M., and Murthy, J. Y., editors, *Handbook of Numerical Heat Transfer*, John Wiley & Sons, Inc., New York, NY, second edition, 2006.

[73] Germano, M., Turbulence: The Filtering Approach, *J. Fluid Mech.*, **238**:325–336 (1992).

[74] Dopazo, C. and O'Brien, E. E., An Approach to the Autoignition of a Turbulent Mixture, *Acta Astronaut.*, **1**(9-10):1239–1266 (1974).

[75] Delarue, B. J. and Pope, S. B., Application of PDF Methods to Compressible Turbulent Flows, *Phys. Fluids*, **9**(9):2704–2715 (1997).

[76] Delarue, B. J. and Pope, S. B., Calculations of Subsonic and Supersonic Turbulent Reacting Mixing Layers Using Probability Density Function Methods, *Phys. Fluids*, **10**(2):487–498 (1998).

[77] Martin, M. P., Piomelli, U., and Candler, G. V., Subgrid-Scale Models for Compressible Large-Eddy Simulations, *Theor. Comp. Fluid Dyn.*, **13**:361–376 (2000).

[78] Risken, H., *The Fokker-Planck Equation, Methods of Solution and Applications*, Springer-Verlag, New York, NY, 1989.

[79] Muradoglu, M., Jenny, P., Pope, S. B., and Caughey, D. A., A Consistent Hybrid-Volume/Particle Method for the PDF Equations of Turbulent Reactive Flows, *J. Comp. Phys.*, **154**(2):342–371 (1999).

[80] Muradoglu, M., Pope, S. B., and Caughey, D. A., The Hybrid Method for the PDF Equations of Turbulent Reactive Flows: Consistency Conditions and Correction Algorithms, *J. Comp. Phys.*, **172**:841–878 (2001).

[81] Kloeden, P. E., Platen, E., and Schurz, H., *Numerical Solution of Stochastic Differential Equations through Computer Experiments*, Springer-Verlag, New York, NY, corrected second printing edition, 1997.

[82] Gikhman, I. I. and Skorokhod, A. V., *Stochastic Differential Equations*, Springer-Verlag, New York, NY, 1972.

[83] Riley, J. J. and Metcalfe, R. W., Direct Numerical Simulations of a Perturbed, Turbulent Mixing Layer, AIAA Paper 80-0274, 1980.

[84] Sandham, N. D. and Reynolds, W. C., Three-Dimensional Simulations of Large Eddies in the Compressible Mixing Layer, *J. Fluid Mech.*, **224**:133–158 (1991).

[85] Moser, R. D. and Rogers, M. M., The Three-Dimensional Evolution of a Plane Mixing Layer: Pairing and Transition to Turbulence, *J. Fluid Mech.*, **247**:275–320 (1993).

[86] Vreman, B., Geurts, B., and Kuerten, H., Large-Eddy Simulation of the Turbulent Mixing Layer, *J. Fluid Mech.*, **339**:357–390 (1997).

[87] Metcalfe, R. W., Orszag, S. A., Brachet, M. E., Menon, S., and Riley, J. J., Secondary Instabilities of a Temporally Growing Mixing Layer, *J. Fluid Mech.*, **184**:207–243 (1987).

[88] Lin, S. J. and Corcos, G. M., The Mixing Layer: Deterministic Models of a Turbulent Flow. Part 3. The Effect of Plane Strain on the Dynamics of Streamwise Vortices, *J. Fluid Mech.*, **141**:139–178 (1984).

[89] Moser, R. D. and Rogers, M. M., The Three-Dimensional Evolution of a Plane Mixing Layer: The Kelvin-Helmholtz Rollup, *J. Fluid Mech.*, **243**:183–226 (1992).

[90] Moser, R. D. and Rogers, M. M., Spanwise Scale Selection in Plane Mixing Layers, *J. Fluid Mech.*, **247**:321–337 (1993).

[91] Erlebacher, G., Hussaini, M. Y., Speziale, C. G., and Zang, T. A., Toward the Large Eddy Simulation of Compressible Turbulent Flows, *J. Fluid Mech.*, **238**:155–185 (1992).

[92] Pope, S. B., Ten Questions Concerning the Large-Eddy Simulation of Turbulent Flows, *New J. Phys.*, **6**:35–58 (2004).

[93] Giridhar, J., A Framework for Large Eddy Simulation of Incompressible Flows with Error Control, Ph.D. Thesis, Sibley School of Mechanical and Aerospace Engineering, Cornell University, Ithaca, NY, 2005.

[94] Pope, S. B., On the Relation Between Stochastic Lagrangian Models of Turbulence and Second-Moment Closures, *Phys. Fluids*, **6**(2):973–985 (1994).

[95] Poinsot, T. and Veynante, D., *Theoretical and Numerical Combustion*, Poinsot, T. and Veynante, D., Bordeaux, France, third edition, 2012.

[96] Vreman, B., Direct and Large-Eddy Simulation of the Compressible Turbulent Mixing Layer, Ph.D. Thesis, University of Twente, Enschede-Noord, Netherlands, 1995.

[97] Gicquel, L. Y. M., Givi, P., Jaberi, F. A., and Pope, S. B., Velocity Filtered Density Function for Large Eddy Simulation of a Turbulent Mixing Layer, in Liu, C., Sakell, L., and Herklotz, R., editors, *DNS/LES-Progress and Challenges*, pp. 327–334, Greyden Press, Columbus, OH, 2001.

[98] Sheikhi, M. R. H., Givi, P., and Pope, S. B., Frequency-Velocity-Scalar Filtered Mass Density Function for Large Eddy Simulation of Turbulent Reacting Flows, *Phys. Fluids*, **21**(7):075102 1–14 (2009).

[99] Chen, J. Y., A Eulerian PDF Scheme for LES of Nonpremixed Turbulent Combustion with Second-Order Accurate Mixture Fraction, *Combust. Theor. Model.*, **11**(5):675–695 (2007).

[100] Pope, S. B., Self-Conditioned Fields for Large-Eddy Simulations of Turbulent Flows, *J. Fluid. Mech.*, **652**:139–169 (2010).

[101] Yilmaz, S. L., Nik, M. B., Givi, P., and Strakey, P. A., Scalar Filtered Density Function for Large Eddy Simulation of a Bunsen Burner, *J. Propul. Power*, **26**(1):84–93 (2010).

[102] Yilmaz, S. L., Nik, M. B., Sheikhi, M. R. H., Strakey, P. A., and Givi, P., An Irregularly Portioned Lagrangian Monte Carlo Method for Turbulent Flow Simulation, *J. Sci. Comput.*, **47**(1):109–125 (2011).

[103] Ansari, N., Goldin, G. M., Sheikhi, M. R. H., and Givi, P., Filtered Density Function Simulator on Unstructued Meshes, *J. Comp. Phys.*, **230**:7132–7150 (2011).

[104] Réveillon, J. and Vervisch, L., Subgrid-Scale Turbulent Micromixing: Dynamic Approach, *AIAA J.*, **36**(3):336–341 (1998).

[105] Heinz, S., Unified Turbulence Models for LES and RANS, FDF and PDF Simulations, *Theor. Comp. Fluid Dyn.*, **21**:99–118 (2007).

[106] Tong, C., Measurements of Conserved Scalar Filtered Density Function in a Turbulent Jet, *Phys. Fluids*, **13**(10):2923–2937 (2001).

[107] Wang, D. and Tong, C., Conditionally Filtered Scalar Dissipation, Scalar Diffusion, and Velocity in a Turbulent Jet, *Phys. Fluids*, **14**(7):2170–2185 (2002).

[108] Rajagopalan, A. G. and Tong, C., Experimental Investigation of Scalar-Scalar-Dissipation Filtered Joint Density Function and Its Transport Equation, *Phys. Fluids*, **15**(1):227–244 (2003).

[109] Wang, D., Tong, C., and Pope, S. B., Experimental Study of Velocity Filtered Joint Density Function For Large Eddy Simulation, *Phys. Fluids*, **16**(10):3599–3613 (2004).

[110] Wang, D. and Tong, C., Experimental Study of Velocity-Scalar Filtered Joint Density Function for LES of Turbulent Combustion, *Proc. Combust. Inst.*, **30**:567–574 (2005).